UNIVERSITY OF OKLAHOMA

GRADUATE COLLEGE

ESTIMATION OF NEAR SURFACE TORNADIC WIND SPEEDS

A DISSERTATION

SUBMITTED TO THE GRADUATE FACULTY

in partial fulfillment of the requirements for the

Degree of

DOCTOR OF PHILOSOPHY

By

SEAN MICHAEL RAY CROWELL
Norman, Oklahoma
2011

Downloaded from SHAREOK. Persistent Handle URL: https://hdl.handle.net/11244/319185

ESTIMATION OF NEAR SURFACE TORNADIC WIND SPEEDS

A DISSERTATION APPROVED FOR THE
DEPARTMENT OF MATHEMATICS

BY

_____
Dr. Luther White, Chair

_____
Dr. Louis Wicker

_____
Dr. Nikola Petrov

_____
Dr. Alan Shapiro

_____
Dr. Semion Gutman

©Copyright by Sean M. Crowell 2011
All Rights Reserved.

for April

Acknowledgements

Many thanks are due to my committee. I owe much to my advisor, Luther White, for his guidance during our time together, as well as for his knowledge of applicable mathematics to the problem at hand. His ability to walk the line joining rigorous mathematics to problems in the real world is something I aspire to develop in myself. I owe an equally large debt to Lou Wicker. In addition to funding me for the last several years, Lou introduced me to the problems faced by meteorologists, and provided me with opportunities to better understand how to qualitatively weigh uncertainties from different sources. He gave me the opportunity to work in the field, from which I gained an appreciation for the difficulties inherent in observational science. Not least of all, he is a great friend. Alan Shapiro is the very essence of the sort of scholar I would love to be, with both deep and broad understanding of many topics in fluid mechanics, numerical methods, and observational meteorology. Semion Gutman gave me the foundations necessary to pursue this work, and kept me mathematically honest throughout my education at OU. Nikola Petrov helped me to understand how basic functional analysis translates immediately to computational work. He also encouraged a broader perspective in both my professional and personal efforts. All five of these men are responsible for my academic and practical education, and I thank them all for their efforts.

I would also like to thank Catherine Mavriplis for her mentorship during

her time at NSSL. From her instruction I learned how to think about partial differential equations from a computational point of view, and was introduced to spectral methods for solving various types of PDEs. She also showed me what it means to balance our professional and home lives, for which I am grateful.

Though he is not on my committee, I would like to name S. Lakshmivarahan as an "honorary member". He has played a role in my development as a researcher equivalent to that of any member of my committee, by introducing me to the ideas about forecast model biases and observational errors, which form the basis of much of my work to this point. He freely gave his time to educate me on these topics, for which I am grateful.

The model data I used to test my methods was given to me by Vincent Wood of the National Severe Storms Laboratory. His explanations helped me to understand the important physical processes at work in the model output that I examined. In addition, his constant encouragement and enthusiasm have served as a source of inspiration.

I would also like to thank various other faculty members for their excellent teaching efforts. Dr. Paul Goodey's basic analysis course sparked a love within me for approximation and computation. Dr. Evgeni Fedorovich gave an atmospheric dynamics course tied together all of my disparate knowledge from working on numerical partial differential equations in atmospheric sciences. Dr. K. B. Lee's graduate course in topology helped me to understand that the basic tenets of analysis hold on far more general structures than Euclidean spaces. Dr. Christian Remling's functional analysis course helped me to appreciate very difficult ideas for their elegance rather than utility.

I am grateful to many graduate students in both the Mathematics de-

partment and School of Meteorology for discussions that have helped me to clarify mathematical and physical issues, including (in no particular order) Terra Thompson, Daniel Betten, Sean Bauer, Lynn Greenleaf, Daniel Dawson, Robin Tanamachi, Corey Potvin, Daniel Benton, and many many others.

Finally, the greatest debt I owe is to my family. Without their support, I could not have completed this journey. Thank you April, Kaetlyn and Amelia for all of your love and patience. Thanks also to my grandmother, who has always encouraged my educational goals, and will always be one of my best friends.

Table of Contents

1 Tornadoes and Fluid Dynamics 3

1.1 Physical Description of the Dynamics 3

1.2 The Navier-Stokes and Continuity Equations 5

1.3 The Dry Steady Axisymmetric Approximation 6

2 Modeling Tornadic Vortices 9

2.1 Analytic Solution Vortex Models 9

2.1.1 Rankine Vortex 10

2.1.2 Burgers-Rott Vortex 10

2.1.3 Sullivan's Vortex 11

2.2 Wood-White Model 12

2.2.1 A Constraint on k 13

2.2.2 Derivatives 14

2.3 Vertical Variation in the Tangential Velocity 14

3 Statement of the problem 16

3.1 Introduction 16

3.2 Physical Considerations 16

3.3 The Tangential Component of Velocity 17

3.4 Dynamical constraints for u and w 17

3.4.1 Different Types of Solutions 19
3.4.2 Variational Wind Retrievals: Standard Procedures . . . 20
3.5 Summary 23

4 Choosing v for a Given Set of Observations 25
4.1 Least-Squares Cost Functional 25
4.2 Uncertainty in Model and Observations 27

5 Strong Solutions of the Model Equations 29
5.1 Introduction 29
5.2 Solution by Method of Characteristics 30
5.2.1 Characteristic ODEs for the Streamfunction Ψ 30
5.2.2 Characteristic ODEs for u and w 32
5.2.3 Existence and Uniqueness 34
5.3 Properties of Information Voids 38
5.3.1 Tensor Product Tangential Velocity Model 40
5.4 Analysis with Wood-White Models 47
5.4.1 Characteristic ODE Solutions 48
5.4.2 Qualitative Analysis for the Case $\nu = 0$ 49
5.4.3 Information Voids 50

6 Estimation on Information Voids 54
6.1 Introduction 54
6.2 Weak Solutions for the Dirichlet Problem 55
6.3 Weak Solutions for the Neumann Problem 60
6.4 Regularity of Weak Solutions 64
6.5 Extending the Domain of the Dirichlet Problem 66

6.6 Discussion 69

7 Accounting for Uncertainty 70

7.1 Introduction 70

7.2 Smooth Dependence on Parameters 70

7.3 Consistency with Observations 72

7.3.1 Approximating the Observation Surface 73

7.3.2 Optimal Initial Conditions for Negligible Observation Errors 74

7.4 Uncertain Outer Radial Boundary Conditions 77

7.5 Probabilistic Estimation of u and w 77

7.6 Summary 80

8 Numerical Experiments 81

8.1 Introduction 81

8.2 Generation of Pseudo-Observations 81

8.3 Impacts of the Minimum Observable Height 82

8.4 Impacts of Random Errors 85

8.4.1 Estimating the Tangential Velocity 86

8.4.2 Physical Quantities of Interest 87

8.4.3 Distributions of Physical Quantities from Sampling . . 89

8.4.4 Discussion 90

8.5 Approximating Weak Solutions of the Elliptic Problem 95

8.5.1 Discretized Problem and Solutions 96

8.5.2 Discussion 99

9 Summary and Discussion 128

List of Tables

8.1 Minimum Observable Height versus Minimum Unreachable Height 85

8.2 Optimal Parameters versus h 91

8.3 Ensemble Mean Parameters versus h 92

8.4 Optimal versus Ensemble Mean Values of Physical RVs 93

List of Figures

3.1 Schematic of the Physical Domain 24

5.1 Information Void Which Does Not Intersect $\partial\Omega_h^+$ 39
5.2 Closed Curves Surrounding a Relative Maximum 44
5.3 Illustration of relationship between h and h_o 46
5.4 Schematic of Characteristic Curves with Wood-White Model . 49
5.5 Schematic of Sign Changes for $\frac{du}{dt}$ 51
5.6 Wood-White estimated radial velocity with $\frac{du}{dt} = 0$ overlaid. . . 52
5.7 Example of Wood-White Circulation and Information Void . . 53

8.1 Davies-Jones Tangential Velocity and Wood-White Model . . . 83
8.2 Streamfunction Derived from Davies-Jones Model Output . . . 83
8.3 Comparison of Davies-Jones Radial and Vertical Velocities with Streamfunction Derived Velocities 84
8.4 Random Errors and Corresponding Noisy Tangential Velocity 86
8.5 Maximum Likelihood Streamfunction Fields (Σ) 101
8.6 Maximum Likelihood Radial Velocity Fields (Σ) 102
8.7 Maximum Likelihood Vertical Velocity Fields (Σ) 103
8.8 Maximum Likelihood Streamfunction Fields (2Σ) 104
8.9 Maximum Likelihood Radial Velocity Fields (2Σ) 105
8.10 Maximum Likelihood Vertical Velocity Fields (2Σ) 106
8.11 Maximum Likelihood Streamfunction Fields (3Σ) 107
8.12 Maximum Likelihood Radial Velocity Fields (3Σ) 108
8.13 Maximum Likelihood Vertical Velocity Fields (3Σ) 109
8.14 Ensemble Distributions of u^+ (Σ) 110
8.15 Ensemble Distributions of w^+ (Σ) 111
8.16 Ensemble Distributions of $|\vec{v}|_{\max}$ (Σ) 112

8.17 Ensemble Distributions of u^+ (2Σ) 113
8.18 Ensemble Distributions of w^+ (2Σ) 114
8.19 Ensemble Distributions of $|\vec{v}|_{\max}$ (2Σ) 115
8.20 Ensemble Distributions of u^+ (3Σ) 116
8.21 Ensemble Distributions of w^+ (3Σ) 117
8.22 Ensemble Distributions of $|\vec{v}|_{\max}$ (3Σ) 118
8.23 Comparison of Strong and Weak Streamfunction Fields (Σ) . . 119
8.24 Comparison of Strong and Weak Radial Velocity Fields (Σ) . . 120
8.25 Comparison of Strong and Weak Vertical Velocity Fields (Σ) . 121
8.26 Comparison of Strong and Weak Streamfunction Fields (2Σ) . 122
8.27 Comparison of Strong and Weak Radial Velocity Fields (2Σ) . 123
8.28 Comparison of Strong and Weak Vertical Velocity Fields (2Σ) 124
8.29 Comparison of Strong and Weak Streamfunction Fields (3Σ) . 125
8.30 Comparison of Strong and Weak Radial Velocity Fields (3Σ) . 126
8.31 Comparison of Strong and Weak Vertical Velocity Fields (3Σ) 127

Abstract

Modeling studies consistently demonstrate that the most violent winds in a tornadic vortex occur in the lowest tens of meters above the surface. These velocities are unobservable by radar platforms due to line of sight considerations. In this work, a methodology is developed which utilizes parametric tangential velocity models derived from Doppler radar measurements, together with a tangential momentum and mass continuity constraint, to estimate the radial and vertical velocities in a steady axisymmetric frame. This technique is tested with a set of model output utilized as "truth . The methodology yields good estimates when the tangential vortex model is a good approximation to the actual tangential wind field, in the regions that are retrievable from the information aloft. Interestingly, there are regions of the unobservable portion of the domain that do not communicate with the region above through the dynamics we have selected. These regions are explored, and different variational procedures for estimating solutions on these regions are discussed. A probabilistic method is utilized to quantify how uncertainty in the vortex model parameters translates into the retrieved radial and vertical velocities, and the resulting improvement in estimations using ensemble statistics is discussed.

Introduction

Research on tornado dynamics has been done for over half a century, with observational studies beginning even earlier. As with all the sciences, meteorology relies on a constant interplay between observational and model studies, each suggesting improvements for the next generation of the other. In the 1970s a tornado vortex chamber (TVC) was constructed at Purdue University, and the resulting simulations led to a greater understanding of the dependence of qualitative features of the tornado on a small set of physical parameters (e.g., Church et al. (1977), Church et al. (1979)). Field experiments such as the Verification of Origin of Rotation in Tornados Experiment (VORTEX) gather observations of real severe thunderstorms, many of which generate tornadoes. In addition, theoreticians have done modeling studies in which the Navier-Stokes equations together with the continuity equation and appropriate models for the transport of heat and moisture, and the dissipation of kinetic energy due to turbulence are integrated numerically to get a sense of how idealized concentrated vortices behave under model assumptions.

Ultimately, these various methods of analyzing vortices all tell us different things about real tornados in nature. The TVC experiments and modeling studies indicate that the structure of the wind field near the ground should have a particular form, to be in agreement with the physical ideas about the interaction between rotation aloft and friction at the ground.

In this work, we develop a methodology for combining observational data with a parametric tangential velocity model and simplified equations of motion in order to retrieve the other two components of the wind field below height which is observable by a mobile radar. The questions of existence and uniqueness are mathematically interesting even for the situation where the dynamics are seemingly simple. The analysis done here should convince researchers to tread carefully when using complex sets of model equations to draw information from observations.

Chapter 1

Tornadoes and Fluid Dynamics

1.1 Physical Description of the Dynamics

Tornadoes are regions of highly concentrated vertical vorticity. The question of how the vertical vorticity becomes concentrated enough to form a tornado is referred to as the *tornadogenesis* problem. This is still an open problem in meteorology, one that experiments like VORTEX and VORTEX2 have been designed to answer. The rotations that are interesting to this field can be as large as a supercell (persistent rotating updraft), or smaller features like mesocyclones and their children, tornadoes.

Once a tornado is in existence, the reviews in Lewellen and Sheng (1980), Snow (1982) and Lewellen (1993) divide it into several sections where the dominant dynamics are different. Lewellen et al. (2000) describe the tornado as a region of elevated angular momentum, while the inflow layer near the ground can be visualized as a jet of diminished angular momentum. The diminished angular momentum is caused by friction at the ground, which retards the swirling wind and allows air to penetrate to the center of the vortex, keeping air aloft from filling in and "drowning" the vortex.

A few hundred meters above the ground is the *core* region, in which the dy-

namics are thought to be in near cyclostrophic balance, which means that the radial pressure gradient force ($\frac{1}{\rho}\frac{\partial p}{\partial r}$) is approximately balanced by the centrifugal force ($\frac{v^2}{r}$). Fiedler and Rotunno (1986) describe a method of estimating the maximum wind speed of a tornado using the equation of cyclostrophic balance and the pressure drop along the centerline of the tornado, which is called the *thermodynamic method*, and the resulting maximum tangential wind speed the *thermodynamic speed limit*. Studies have shown that if cyclostrophic balance determined the maximum wind speed, with a hydrostatic pressure field, then the maximum wind speeds would be much lower than what is estimated from damage surveys and radar analysis. Knowledge of the maximum wind speed possible is important for designing structures that are capable of withstanding tornadoes.

Near the ground, but away from the axis of rotation is the *inflow* region, where air is being drawn into the rotating column of rising air that makes up the tornado and its parent mesocyclone. Depending on the strength of the inflow, there may or may not be boundary layer separation at the ground (Snow, 1982). The inflow region is important to the maintenance of the tornado, since this is the source of mass and momentum that are feeding the rotation.

The region between the center of the vortex and the maximum radial inflow near the ground is what is referred to as the *corner flow* region, named for the fact that the flow in this region changes from primarily radial in the inflow to vertical as air passes into the updraft and up into the core. It is here that friction unbalances the cyclostrophic balance in the core by weakening the tangential velocity and allowing flow to penetrate to the center of the vortex. This can lead to much higher maximum wind speeds than those estimated from the thermodynamic method, as is described in Fiedler (1994).

1.2 The Navier-Stokes and Continuity Equations

A natural geometry for vortex motion is cylindrical coordinates, centered at the vortex axis. Taking (u, v, w) to be the radial, tangential (azimuthal), and vertical velocities of the fluid, the Navier-Stokes equations are given by (Kundu and Cohen, 2008)

$$\frac{\partial u}{\partial t} + u\frac{\partial u}{\partial r} + \frac{v}{r}\frac{\partial u}{\partial \theta} + w\frac{\partial u}{\partial z} - \frac{v^2}{r} = -\frac{1}{\rho}\frac{\partial p}{\partial r} + \nu\left(\Delta u - \frac{u}{r^2} - \frac{2}{r^2}\frac{\partial v}{\partial \theta}\right) \tag{1.1}$$

$$\frac{\partial v}{\partial t} + u\frac{\partial v}{\partial r} + \frac{v}{r}\frac{\partial v}{\partial \theta} + w\frac{\partial v}{\partial z} + \frac{uv}{r} = -\frac{1}{\rho r}\frac{\partial p}{\partial \theta} + \nu\left(\Delta v + \frac{v}{r^2} - \frac{2}{r^2}\frac{\partial u}{\partial \theta}\right) \tag{1.2}$$

$$\frac{\partial w}{\partial t} + u\frac{\partial w}{\partial r} + \frac{v}{r}\frac{\partial w}{\partial \theta} + w\frac{\partial w}{\partial z} = -\frac{1}{\rho}\frac{\partial p}{\partial z} + b + \nu\Delta w \tag{1.3}$$

where ν is the eddy viscosity, assumed constant, and ρ is the constant air density, p is the pressure, and b is the buoyancy force, which can be parameterized as a function of the temperature and moisture gradients, or obtained from a prognostic equation that follows from the First Law of Thermodynamics. The Laplacian in cylindrical coordinates is given by

$$\Delta = \frac{1}{r}\frac{\partial}{\partial r}\left(r\frac{\partial}{\partial r}\right) + \frac{1}{r^2}\frac{\partial^2}{\partial \theta^2} + \frac{\partial^2}{\partial z^2}. \tag{1.4}$$

To close the system, we take the incompressible continuity equation:

$$\frac{1}{r}\frac{\partial (ru)}{\partial r} + \frac{1}{r}\frac{\partial v}{\partial \theta} + \frac{\partial w}{\partial z} = 0. \tag{1.5}$$

Since we are interested in a swirling flow, it is useful to consider the radial,

azimuthal and axial vorticities, defined by

$$(\eta, \xi, \zeta) = \nabla \times (u, v, w),$$

or component-wise

$$\eta = \frac{1}{r}\frac{\partial w}{\partial \theta} - \frac{\partial v}{\partial z} \tag{1.6}$$

$$\xi = \frac{\partial u}{\partial z} - \frac{1}{r}\frac{\partial (rw)}{\partial r} \tag{1.7}$$

$$\zeta = \frac{1}{r}\frac{\partial (rv)}{\partial r} - \frac{1}{r}\frac{\partial u}{\partial \theta} \tag{1.8}$$

1.3 The Dry Steady Axisymmetric Approximation

Axisymmetric dynamics, where all functions are assumed to be independent of θ, have been the focus of much tornado research (e.g. (Lewellen and Sheng, 1980), (Rotunno, 1979), (Fiedler and Rotunno, 1986)). We shall begin with the simplified problem where we assume axisymmetric, steady flow, where all derivatives with respect to θ and t vanish. The steady axisymmetric equations are

$$u\frac{\partial u}{\partial r} + w\frac{\partial u}{\partial z} - \frac{v^2}{r} = -\frac{1}{\rho}\frac{\partial p}{\partial r} + \nu\left\{\frac{\partial}{\partial r}\left[\frac{1}{r}\frac{\partial (ru)}{\partial r}\right] + \frac{\partial^2 u}{\partial z^2}\right\} \tag{1.9}$$

$$u\frac{\partial v}{\partial r} + w\frac{\partial v}{\partial z} + \frac{uv}{r} = \nu\left\{\frac{\partial}{\partial r}\left[\frac{1}{r}\frac{\partial (rv)}{\partial r}\right] + \frac{\partial^2 v}{\partial z^2}\right\} \tag{1.10}$$

$$u\frac{\partial w}{\partial r} + w\frac{\partial w}{\partial z} = -\frac{1}{\rho}\frac{\partial p}{\partial z} + \nu\left\{\frac{\partial}{\partial r}\left[\frac{1}{r}\frac{\partial (rw)}{\partial r}\right] + \frac{\partial^2 w}{\partial z^2}\right\} \tag{1.11}$$

and the axisymmetric continuity equation is

$$\frac{1}{r}\frac{\partial(ru)}{\partial r} + \frac{\partial w}{\partial z} = 0. \tag{1.12}$$

The vorticities (1.6) - (1.8) simplify to

$$\eta = -\frac{\partial v}{\partial z} \tag{1.13}$$

$$\xi = \frac{\partial u}{\partial z} - \frac{1}{r}\frac{\partial(rw)}{\partial r} \tag{1.14}$$

$$\zeta = \frac{1}{r}\frac{\partial(rv)}{\partial r} \tag{1.15}$$

Equations (1.9)-(1.12) are "dry" and isothermal, since they do not contain the effects of water vapor or temperature. We are not considering the tornadogenesis problem (unlike Davies-Jones (2008)), so this approximation is reasonable, since tornado dynamics mostly occur away from the precipitating portion of the storm. Further, we are interested in near surface tornadic winds, which are far away from the cloud base, and so should be mostly independent of the effects of moisture.

A common technique for axisymmetric dynamics (e.g., see Rotunno (1979)) is to replace u and w by a single streamfunction Ψ that satisfies $u = \frac{1}{r}\Psi_z$ and $w = -\frac{1}{r}\Psi_r$. By construction, Ψ satisfies (1.12). The equation (1.14) gives a Poisson equation for Ψ in terms of ξ. We can construct a second equation for ξ by differentiating (1.9) with respect to z and (1.11) with respect to r and subtracting. Finally, (1.10) can be used as is, or multiplied by r to create an equation for the *circulation* Γ. These three equations are independent of pressure, and are the typical form used for simulation in the references listed above and Chapter 8.

The time required for a radar platform to completely sample a thunderstorm is on the order of minutes, which implies that any motions of the tornado that have a shorter time scale than this will not be visible in the measurements. Further, the axisymmetric vortex can be seen as the azimuthal average of the full asymmetric vortex, which would be the first term of a Fourier series expansion of the full flow:

$$u(r,\theta,z) = u_o(r,z) + \sum_{n=1}^{\infty} u_n(r,z)\sin(n\theta) + \widehat{u_n}(r,z)\cos(n\theta)$$

The terms which are higher frequency (spatially) can be hypothesized to be diminishing perturbations to this averaged state. Hence, estimating the average state is the obvious first step in the process of estimating the fully three dimensional wind field.

Chapter 2

Modeling Tornadic Vortices

There are several approaches to modeling tornados. Analytic solutions to the Navier-Stokes equations with simplifying assumptions were discovered before the advent of modern supercomputing. More recently, numerical explorations have explored the physical parameters that might be important, such as buoyancy and friction. Due to the inherently multiscale nature of tornados, realistic simulations are not typically feasible, and so often simple models are used in conjunction with data to improve data quality and increase understanding of observed features. In this chapter, we first review a few of the analytic vortex models, and then give a brief summary of past numerical work, leading to the development of a model of intermediate complexity that can be used in conjunction with an empirical tangential vortex model to estimate the other components of the wind field.

2.1 Analytic Solution Vortex Models

Several analytic solutions to the Navier-Stokes equations under simplifying assumptions exist (e.g. Rott (1958), Sullivan (1959) for general (steady) solutions, and Long (1958), Kuo (1967) for similarity solutions).

2.1.1 Rankine Vortex

The Rankine vortex model satisfies the steady form of the Navier-Stokes equations in two separate regions consisting of an inner domain of solid body rotation ($r < R$) and an outer domain of irrotational flow ($r > R$), which are joined at some radius of maximal tangential velocity ($r = R$), assumed to be a solid rotating boundary between the two regions:

$$u_{rk}(r, z) = w_{rk}(r, z) = 0 \tag{2.1}$$

$$v_{rk}(r) = \begin{cases} v_{\max} \frac{r}{R} & r \leq R \\ v_{\max} \frac{R}{r} & r \geq R \end{cases} \tag{2.2}$$

This model describes the structure of a simple, steady vortex quite well, and has a small set of parameters. The model is not smooth at $r = R$, and this can lead to unrealistically high maximum tangential wind speeds when modeling doppler radar velocities. Also, if we are interested in nontrivial u and w, we have to consider more possibilities.

2.1.2 Burgers-Rott Vortex

The Burgers-Rott model has nontrivial functions for all three components of wind velocity:

$$u = -ar \tag{2.3}$$

$$v = \frac{\Gamma_\infty}{2\pi r} \left(1 - e^{\frac{-ar^2}{2\nu}}\right) \tag{2.4}$$

$$w = 2az \tag{2.5}$$

This model has an updraft that increases with height, and an inflow that strengthens with radial distance from the center of the vortex. While more complex than the Rankine vortex model, there are still some features lacking. Note that there is no dependence on height for u or v, and no radial dependence for w. Typical radar data indicate a dependence in the horizontal flow on the height coordinate. For example, near the ground u should be negative as air flows in, while higher in the storm, u should be positive as air diverges from the center. In addition, Snow (1982) discusses the phenomenon of central core downdrafts for certain dynamic regimes, the so-called "two-cell" vortex, which this model cannot capture. Finally, the tangential velocity satisfies a free slip lower boundary condition, rather than a no slip condition, which leads to tangential wind velocities that are weaker than real tornados.

2.1.3 Sullivan's Vortex

The Sullivan vortex model is more complex:

$$u = -ar + 6\frac{\nu}{r}\left(1 - e^{-\frac{ar^2}{2\nu}}\right) \tag{2.6}$$

$$v = \frac{\Gamma}{2\pi r}\left[\frac{H(ar^2/2\nu)}{H(\infty)}\right] \tag{2.7}$$

$$w = 2az(1 - 3e^{-\frac{ar^2}{2\nu}}) \tag{2.8}$$

where

$$H(x) = \int_0^x \exp\left(-t + 3\int_0^t \left[\frac{1 - e^{-s}}{s}\right] ds\right) dt. \tag{2.9}$$

Sullivan's vortex exhibits the existence of a two-celled vortex for certain parameter regimes.

These models have been used for data and theoretical analyses due to their being solutions of some form of the Navier-Stokes equations. Meteorologists trust the equations of motion because they arise from very basic assumptions about the laws that govern the universe, namely conservation of mass and momentum. The drawback they all share is that the tangential wind velocity is free-slip at the ground, implying that friction does not play a role in weakening the cyclostrophic balance aloft, which is counter to our understanding of the physical mechanisms present in real tornados, as discussed in Chapter 1. As such, they are more appropriate for the tangential velocity above the lowest few hundred meters above the surface.

2.2 Wood-White Model

In the spirit of the Rankine model (2.2), Wood and White developed a more general empirical tangential velocity model in Wood and White (2011). The version of their model used here is given by

$$\phi(r; n, k, r_c) = \frac{n {r_c}^{n-k} r^k}{(n-k){r_c}^n + kr^n}. \tag{2.10}$$

This model shares many of the features of the Rankine vortex, including a single maxima at $r = r_c$ and an algebraic rate of decay for $r > r_c$. The major difference is that the vortex is smooth at $r = r_c$, and that we can control the rate of decay. Researchers (e.g. Robin Tanamachi, personal communication) have commented that the effect of the nonsmooth derivative in the Rankine

model can be seen in the analyzed radar data, when these observations are fit by a Rankine vortex using a least-squares technique, with larger tangential velocities than are physically consistent with other measurements.

2.2.1 A Constraint on k

Suppose we model the tangential velocity as $v = v_c\phi(r)\psi(z)$, where ϕ is the Wood-White (WW) function and ψ is a model for the vertical variation in v. Computing the vertical vorticity ζ for this v we get

$$\zeta = v_\infty \frac{nkr_c^{n-k}r^{k-1}}{(n-k)r_c^n + kr^n}\left[1 + \frac{1}{k} - \frac{nr^n}{(n-k)r_c^n + kr^n}\right]\psi(z). \tag{2.11}$$

Note that for $k = 1$,

$$\zeta(0, z) = \frac{2n}{(n-1)r_c}\psi(z) \neq 0$$

but for $k > 1$,

$$\zeta(0, z) = 0.$$

On the other hand, the radial derivative of vorticity, ζ_r, can be shown to satisfy

$$\zeta_r(0+, z) = \begin{cases} 0 & \text{when } k = 1 \\ +\infty & \text{when } k > 1 \end{cases} \tag{2.12}$$

Clearly the vertical vorticity should have a finite radial derivative at the vortex axis. In the case where we let $\psi \equiv 1$, the $k > 1$ case leads to infinite radial velocities at the vertical axis ($r = 0$), which is unphysical. For these reasons,

we will assume $k = 1$.

2.2.2 Derivatives

For future reference, we compute various derivatives of interest with the constraint $k = 1$.

$$\phi_{ww}(r; n, r_c) = \frac{n {r_c}^{n-1} r}{(n-1){r_c}^n + r^n} \tag{2.13}$$

$$\frac{d}{dr}\phi_{ww}(r; n, r_c) = \frac{n(n-1)r_c^{n-1}}{((n-1){r_c}^n + r^n)^2}({r_c}^n - r^n) \tag{2.14}$$

$$\frac{d^2}{dr^2}\phi_{ww}(r; n, r_c) = \frac{-n^2(n-1){r_c}^{n-1}r^{n-1}}{((n-1){r_c}^n + r^n)^3}\left((n+1){r_c}^n - r^n\right) \tag{2.15}$$

$$\frac{1}{r}\frac{d}{dr}(r\phi_{ww}(r; n, r_c)) = \frac{n{r_c}^{n-1}}{((n-1){r_c}^n + r^n)^2}\left(2(n-1){r_c}^n - (n-2)r^n\right) \tag{2.16}$$

$$\frac{d}{dr}\left(\frac{1}{r}\frac{d}{dr}(r\phi_{ww}(r; n, r_c))\right) = \frac{n^2{r_c}^{n-1}r^{n-1}}{((n-1)r_c^n + r^n)^3}\left((n-2)r^n - (n^2+n-2){r_c}^n\right) \tag{2.17}$$

2.3 Vertical Variation in the Tangential Velocity

The tornado dynamics reviews mentioned in the last chapter discuss how v changes with height. At the ground, v should be zero due to the fact that the ground has zero swirl velocity. The no slip condition has been shown to produce wind fields with statistics closer to actual tornadoes than other boundary conditions, such as a free slip condition. From the ground, v increases smoothly to a relative maximum just above the inflow layer, at the "core radius", above

which it decreases to the top of the funnel cloud. This general description can also be approximated by the WW function described in the last section. Hence, we could model the tangential velocity with $v = v_c \phi_{ww}(r; r_c, n_r)\phi_{ww}(z; z_c, n_z)$, or in the case of multiple maxima, with a linear combination of these functions.

Chapter 3

Statement of the problem

3.1 Introduction

The most violent winds in a tornado occur in the lowest tens of meters above the ground, but line of sight limitations for radar platforms make this region of the tornado, namely the inflow and corner flow regions, impossible to measure directly. Here we explore a mathematical framework for estimating the structure of the wind velocity below the radar horizon, assuming that we have measurements of the radial velocity u and tangential velocity v above the radar horizon, and that the tangential velocity's behavior below the radar horizon is predictable using empirical models.

3.2 Physical Considerations

The goal is to estimate the three velocity components u, v, and w on a physical domain $\Omega = [0, R] \times [0, H]$. Let $0 < h < H$ and define $\Omega_h = [0, R] \times [0, h]$, and assume we have measurements of u and v on $\Omega \backslash \Omega_h$, the "observable region". The domain schematic in Figure 3.1 indicates the assumptions for the problem. The green boxes represent discrete measurements $\{(u_i, v_i)\}$ of u and v, say

from two synchronized radar platforms. The blue lines represent boundary conditions that we can deduce from theory. Some numerical models (e.g. Davies-Jones (2008)) have taken $u = v = \frac{\partial w}{\partial r} = 0$ at $r = 0$ and $\frac{\partial u}{\partial z} = v = w = 0$ at $z = 0$, though these boundary conditions have been the subject of much debate in the past. The dashed red line represents an outer radial boundary along which we have no information on any of the velocity components.

3.3 The Tangential Component of Velocity

From Chapters 1 and 2, we know there are reasonable assumptions we can make about the structure of the tangential wind velocity in the tornado, whose lower portion is contained in Ω. The presence of observations of v in $\Omega \setminus \Omega_h$ indicates that we could seek an empirical parametric model for v that minimizes a cost associated to fitting the observational data within the random errors (noise) associated with the measurements. The vertical variation in v that arises from the parametric model will be entirely determined by the data in $\Omega \setminus \Omega_h$, and so we will have to rely on our intuition about how the tangential velocity should behave below the radar horizon, together with the fitting procedure, in order to say anything about the other components u and w. Procedures for selecting v will be discussed in Chapter 4.

3.4 Dynamical constraints for u and w

Given a model for v which approximates the measurements as described in the last paragraph, we can look for possible radial velocities u and vertical velocities w that are dynamically consistent with our model for v. Of course,

"dynamically consistent" implies a set of underlying dynamical assumptions. Conservation of mass is a fundamental physical requirement. Since we are in the $r-z$ plane, we take the incompressible axisymmetric continuity equation

$$\frac{1}{r}(ru)_r + w_z = 0 \tag{3.1}$$

to be the constraint which imposes conservation of mass. Clearly this constraint alone is insufficient for determining u and w, and so we need another constraint. Examining the other equations of motion (1.9)-(1.11) described in Chapter 1, we see that (1.10) does not contain a pressure term:

$$u\frac{\partial v}{\partial r} + w\frac{\partial v}{\partial z} + \frac{uv}{r} = \nu\left\{\frac{\partial}{\partial r}\left[\frac{1}{r}\frac{\partial(rv)}{\partial r}\right] + \frac{\partial^2 v}{\partial z^2}\right\}, \tag{3.2}$$

and so seems possibly to close the system, in the sense that with v chosen, we have two constraints and two unknowns u and w to be determined.

Introduce the Stokes streamfunction Ψ defined by

$$\frac{1}{r}\frac{\partial \Psi}{\partial z} = u \tag{3.3}$$

$$-\frac{1}{r}\frac{\partial \Psi}{\partial r} = w \tag{3.4}$$

Defined this way, the function Ψ satisfies (3.1) automatically. This change of variables can be seen as an equivalent way of satisfying mass conservation, and is discussed in the analysis alongside the velocity formulation.

3.4.1 Different Types of Solutions

We are interested in finding functions u and w which satisfy

$$\zeta u - \eta w = \beta \tag{3.5}$$

$$\frac{1}{r}(ru)_r + w_z = 0, \tag{3.6}$$

where $\zeta = \frac{1}{r}(rv)_r$, $\eta = -v_z$ and $\beta = \nu(\zeta_r - \eta_z)$ are known or estimated in advance. How should we require these constraints to be enforced? We can force them to hold pointwise, which is to say that we seek $u, w \in C^1(\Omega)$ which satisfy these equations at every $(r, z) \in \Omega$. We call this the *strong form* of the problem. In Chapter 5, we will analyze the strong form of the problem and discuss when we can find classical solutions. Throughout mathematics, there are many examples of problems that do not admit solutions satisfying these kinds of conditions, such as hyperbolic conservation laws, which exhibit discontinuities in finite time. The typical solution is to work with the equations in a "weak form", whose definition depends on the problem, but usually involves forcing an integrated form of the equations to be satisfied. For our case, we could look for solutions $u, w \in H^1(\Omega)$ which minimize

$$J(u, w) = \int_\Omega \lambda_v(\zeta u - \eta w - \beta)^2 + \lambda_m \left(\frac{1}{r}(ru)_r + w_z\right)^2 dA. \tag{3.7}$$

Clearly a strong solution would be a minimizer, and if the strong solution was unique, then the minimizer would be also. This would give a complete theory for the problem.

If we express the problem in terms of Ψ, then it reduces to a single equation

for the strong form:

$$\zeta \Psi_z + \eta \Psi_r = r\beta \tag{3.8}$$

and a corresponding cost function to (3.7) would be

$$J(\Psi) = \int_\Omega \lambda_v (\zeta \Psi_z + \eta \Psi_r - r\beta)^2 dA. \tag{3.9}$$

Even though the problems are equivalent, we will see that occasionally it is easier to use the velocity formulation to analyze the properties of the solutions, while the streamfunction formulation is easier to deal with mathematically and computationally.

3.4.2 Variational Wind Retrievals: Standard Procedures

The field of wind retrieval from radar measurements has utilized methodologies similar to both the strong approach and the weak approach. Dual doppler analysis papers from the past decade almost exclusively use a variational approach due to its flexibility for including different families of constraints, and the ability to choose how strongly to enforce them on a case by case basis.

Supposing we can find u and w which satisfy (3.5) and (3.6) either pointwise, or in some other form, we still have observations of u, and we would like our retrieved velocities to be consistent with these observations. If our model and data were perfect, consistency would be equivalent to finding the minimizer of (3.7). Unfortunately, real atmospheric vortices are not steady, nor are they axisymmetric, so our modelization of the problem is going to have errors. In addition, the measurements we take of the atmospheric velocities

will have random errors associated to the instrument noise, which is always present in radar measurements.

We would like our flow to satisfy the theoretical boundary conditions that are indicated in the domain schematic. This includes both homogeneous Dirichlet and Neumann conditions at the surface and at the vertical axis for u and w. We can consider the requirement that the flow match these conditions as additional constraints in our cost function. The data matching condition will provide the u boundary condition in the observable region, but we have to figure out what conditions make sense for u at the outer radial boundary below $z = h$, and for w at the top and outer radial boundaries. Where the boundary condition is unknown, the typical practice is to use the natural boundary condition arising from the Euler-Lagrange equations associated with the cost functional, typically called the "variational boundary condition", since the minimization procedure actually determines the boundary condition. The retrieved boundary values will be dependent on the first guess for the minimization.

In addition to data matching and satisfying theoretical requirements relative to each other, there is a common assumption amongst researchers that the fields they retrieve should vary smoothly over a domain, and contain no "noise" or small-scale fluctuations. Forcing the solutions to match data with random measurement errors can lead to this sort of small scale noise, as can poor spatial resolution in the discrete computational grid or use of a numerical method not suited to the physical problem. As a result, it is common practice to include "smoothing terms" as constraints in the cost functional in order to seek solutions with a minimum of small scale noise. These smoothing terms are typically the weak form of elliptic operators, such as the square of the gra-

dient (equivalent to the Laplacian operator in the Euler-Lagrange equations), or the square of the Laplacian (equivalent to the biharmonic operator), and so on.

Suppose that we have selected a tangential velocity model v, and have observations of the radial velocity u_o in the observable region $\Omega \backslash \Omega_h$ arising from a transformation from radar coordinates. A cost functional which captures the essence of the preceding discussion is given by

$$J(u,w) = J_v + J_m + J_o + J_b + J_s \tag{3.10}$$

$$J_v(u,w) = \int_\Omega \lambda_v(\zeta u - \eta w - \beta)^2 dA \tag{3.11}$$

$$J_m(u,w) = \int_\Omega \lambda_m \left(\frac{1}{r}(ru)_r + w_z\right)^2 dA \tag{3.12}$$

$$J_o(u) = \int_{\Omega\backslash\Omega_h} \lambda_o(u-u_o)^2 dA \tag{3.13}$$

$$\begin{aligned} J_b(u,w) = \int_{\partial\Omega} \big[&\lambda_{u_d}(u-u_d)^2 + \lambda_{w_d}(w-w_d)^2 + \\ &+ \lambda_{u_n}(\nabla u\cdot\vec{n} - u_n)^2 + \lambda_{w_n}(\nabla w\cdot\vec{n} - w_n)^2\big]\, ds \end{aligned} \tag{3.14}$$

$$J_s(u,w) = \int_\Omega \left[\lambda_{u_s}|\nabla u|^2 + \lambda_{w_s}|\nabla w|^2\right] dA \tag{3.15}$$

Here the quantities $\lambda_{(\cdot)}$ are weights that are taken to be measures of the confidence in each constraint. The functions u_d and u_n represent the possibly nonhomogeneous Dirichlet and Neumann boundary conditions for u, and similarly for w. The existence of a unique minimizer for this functional is not guaranteed, and our mathematical analysis for the problem would have to include the necessary conditions for such a minimizer. The difficulties involved in the mathematical analysis of such a complex cost functional motivate us to consider the simpler problem of finding classical solutions, and avoiding the

full variational procedure whenever possible.

3.5 Summary

We have a collection of observations $\{u_i, v_i\}_{i=1}^{N_{obs}}$, which we assume are taken on regular observational grid at elevations in the range $[0, R] \times [h, H]$. From these observations, we would like to reconstruct u, v, and w on $[0, R] \times [0, H]$. Our knowledge about the general characteristics of the tangential velocity in tornados seems to indicate we can estimate v on Ω using an empirical parametric model. With this model in hand, we seek u and w that are dynamically consistent with v, subject to the constraints

$$\zeta u - \eta w = \beta \tag{3.16}$$

$$\frac{1}{r}(ru)_r + w_z = 0, \tag{3.17}$$

where $\zeta = \frac{1}{r}(rv)_r$, $\eta = -v_z$ and $\beta = \nu(\zeta_r - \eta_z)$.

We seek the best possible solutions following the procedure

- Choose an appropriate model for the tangential data, via least-squares or some other fitting technique.
- Seek strong solutions to (3.5) and (3.6) where they exist and are unique.
- Seek solutions that satisfy a weaker form of (3.5) and (3.6) where strong solutions don't exist or are not unique.

Potentially sensitive parameters to investigate include errors in observations, weights for different terms in our variational formulation, and uncertain boundary conditions at $r = R$.

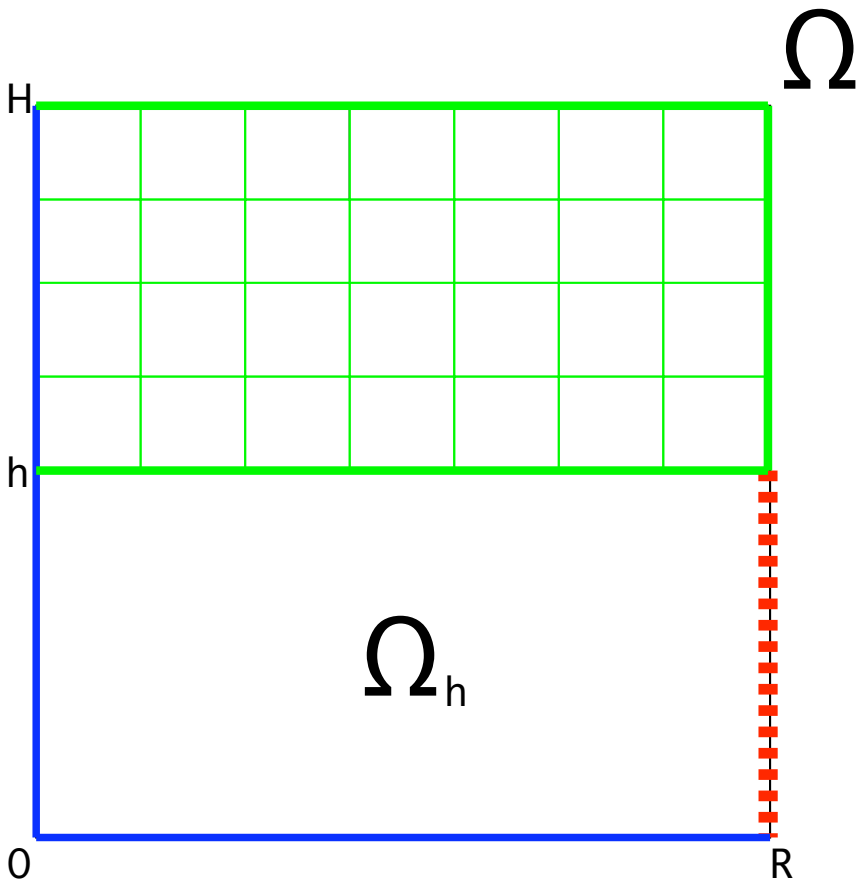


Figure 3.1: Schematic of the Physical Domain. The blue lines represent boundary conditions we can assume to be no slip or no flux. The red line is the outer radial boundary where we have no data.

Chapter 4

Choosing v for a Given Set of Observations

In this chapter, we discuss various methodologies for choosing a tangential velocity model, using ideas from the theory and practice of inverse problems, as well as information theory. We will consider different families of models, and then choose the families that fit the data well, in addition to being of minimal complexity necessary.

4.1 Least-Squares Cost Functional

Suppose that there exists a set of tangential wind speed measurements $\{\hat{v}_i\}_{i=1}^{N_{obs}}$ at spatial locations $\{(r_i, z_i)\}_{i=1}^{N_{obs}}$, and that the data can be modeled with a parametric model $v(r, z; q)$, where $q \in \mathcal{Q} \subset \mathbb{R}^p$ is the vector of model parameters. Define the least-squares data misfit functional by

$$J(q) = \frac{1}{2} \sum_{i=1}^{N_{obs}} (v(r_i, z_i; q) - \hat{v}_i)^2. \tag{4.1}$$

where we implicitly assume the data to be error free.

Proposition 4.1: *Suppose that $\mathcal{Q} \subset \mathbb{R}^p$ is compact, and that for each i, $v(r_i, z_i; q)$ is continuous on $\mathcal{Q}$. Then there exists a minimizer $q^* \in \mathcal{Q}$ of J.*

Proof. If $v(r_i, z_i; q)$ is continuous on $\mathcal{Q}$ for each i, then J is also continuous on $\mathcal{Q}$. Since $\mathcal{Q}$ is compact, the Extreme Value Theorem guarantees the existence of $q^* \in \mathcal{Q}$ such that $J(q^*) = \min_{\mathcal{Q}} J(q)$. □

If $q_n \in \mathcal{Q}$ is a minimizing sequence, $||q_n - q^*|| \to 0$, then in what topology does $v(r, z; q_n) \to v(r, z; q^*)$? The next result says that the convergence is uniform on Ω, as long as v is a smooth function of its parameters.

PROPOSITION 4.2: *Let $q_n \to q_o$ in $\mathcal{Q}$, and suppose $\Omega \subset \mathbb{R}^2$ and $\mathcal{Q}$ are convex and compact and $v \in C^1(\Omega \times \mathcal{Q})$. Then $\sup_\Omega |v(r, z; q_n) - v(r, z; q_o)| \to 0$ as $n \to \infty$.*

Proof. From the mean value theorem for functionals, for each $n \in \mathbb{N}$ there is a $t(n) \in \mathbb{R}$ so that

$$v(r, z; q_n) - v(r, z; q_o) = \nabla_q v(r, z; (1 - t(n))q_n + t(n)q_o) \cdot (q_n - q_o).$$

We know that $q_o \in \mathcal{Q}$ from Proposition 4.1. Since $v \in C^1(\Omega \times \mathcal{Q})$, and $\Omega \times \mathcal{Q}$ is compact, $\nabla_q v$ is bounded on $\Omega \times \mathcal{Q}$, say by K, and so

$$\sup_\Omega |v(r, z; q_n) - v(r, z; q^*)| \leq K||q_n - q^*|| \to 0,$$

as $n \to \infty$. □

REMARK 4.3: The same argument, with more smoothness assumptions, would give uniform convergence of the spatial derivatives of v (and hence the vorticities) to the spatial derivatives of the optimal estimate $v(r, z; q^*)$. The proof rests upon the convexity and compactness of our spatial domain Ω and the parameter space $\mathcal{Q}$. Our problem involves Cartesian products of closed intervals

for these sets, and so this assumption will be satisfied.

4.2 Uncertainty in Model and Observations

In the presence of measurement and model error, the estimation problem changes from the setting of optimization theory to that of probability theory. Although the minimization problem defined by (4.1) always has a solution, vectors $q \in \mathcal{Q}_\epsilon \subset \mathcal{Q}$ may exist such that the resulting model $v(r, z; q)$ matches the data to within the measurement error's statistics, described by the random vector ϵ. In this case, it is impossible to reject the models which are the images of each $q \in \mathcal{Q}_\epsilon$, since they have nontrivial likelihood, relative to ϵ.

Following Tarantola (2005), we can use probability distributions to describe the state of information we gain from combining our model $v(q)$ together with observations $\hat{v}$. If we postulate the existence of a true tangential velocity field v^t, then posterior distribution of model parameters in $\mathcal{Q}$ taking observations and uncertainties in D into account is given by

$$\sigma_{\mathcal{Q}}(q) = const \cdot \rho_{\mathcal{Q}}(q) \int_D \frac{\rho_d(v^t)\Theta(v^t|q)}{\mu_d(v^t)} dv^t \tag{4.2}$$

where $\rho_{\mathcal{Q}}$ is the prior distribution of uncertainty in the model parameters, ρ_D is the measurement error prior distribution, $\Theta(v^t|q)$ is the uncertainty in the error between $v(q)$ and the true velocity, and μ_D is the homogeneous distribution over the observation space D.

We can define error distributions ϵ_M and ϵ_D via $v(q) = v^t + \epsilon_M$ and $\hat{v} =$

$v^t + \epsilon_D$. Suppose both ϵ_D and ϵ_M have Gaussian distributions:

$$\Theta(v^t|q) = const. \exp\left[(v^t - v(q))^\mathsf{T} C_T^{-1}(v^t - v(q))\right] \tag{4.3}$$

$$\rho_D(v^t) = const. \exp\left[(v^t - \hat{v})^\mathsf{T} C_D^{-1}(v^t - \hat{v})\right] \tag{4.4}$$

Tarantola shows that the by simplifying the product of these two, the posterior $\sigma_\mathcal{Q}(q)$ is given as

$$\sigma_\mathcal{Q}(q) = const \cdot \rho_\mathcal{Q}(q) \exp\left[(v(q) - \hat{v})^\mathsf{T} C^{-1}(v(q) - \hat{v})\right], \tag{4.5}$$

where $C = C_T + C_D$. Note that v^t disappears from our considerations, which is essential, since v^t is unknown.

REMARK 4.4: The Gaussian assumption for ϵ_D is a common one. Assuming that the parametric model $v(q)$ is a reasonable representation of what we expect v^t to be, the Gaussian assumption is a fair one as well. Since the separate covariance matrices combine into a single covariance, we can model the combined uncertainty by choosing C to represent the covariance present in the data values, and perhaps inflate it by a reasonable factor.

REMARK 4.5: The image of $q \in \mathcal{Q}$ in velocity space is Gaussian, as is seen from (4.5). The density will still have a MLE at some vector q^*, because the weighted least-squares cost functional $J = (v(q) - \hat{v})^\mathsf{T} C^{-1}(v(q) - \hat{v})$ with symmetric positive definite C will have a global minimum, using the same continuity and compactness argument of Proposition 4.1.

Chapter 5

Strong Solutions of the Model Equations

5.1 Introduction

In this chapter, we explore a methodology for finding solutions of our model equations, both in the velocity form

$$\zeta u - \eta w = \beta \tag{5.1}$$

$$\frac{\partial (ru)}{\partial r} + r w_z = 0 \tag{5.2}$$

and in the streamfunction form

$$\zeta \Psi_z + \eta \Psi_r = r\beta \tag{5.3}$$

in the strong sense, meaning that we seek a pair of functions $u, w \in C^1(\Omega)$ (or $\Psi \in C^2(\Omega)$) that satisfy the equations pointwise on Ω. In the sections that follow, we explore the impact of the assumptions of limited observability on the mathematical questions about our system.

5.2 Solution by Method of Characteristics

Below we deduce the requirements for strong solutions, first in the streamfunction formulation, and then in the velocity formulation.

5.2.1 Characteristic ODEs for the Streamfunction Ψ

A classical method of solution for axisymmetric fluid flow is the introduction of a streamfunction Ψ, which is defined implicitly for incompressible flows as $\frac{1}{r}\frac{\partial \Psi}{\partial z} = u$ and $-\frac{1}{r}\frac{\partial \Psi}{\partial r} = w$. Note that this definition automatically satisfies the mass conservation constraint (5.2). Further, if we plug in these expressions for u and w in (5.1), the streamfunction must satisfy (5.3). This is a first-order, hyperbolic partial differential equation, with corresponding characteristic equations

$$\frac{dr}{dt} = \eta \tag{5.4}$$

$$\frac{dz}{dt} = \zeta \tag{5.5}$$

$$\frac{d\Psi}{dt} = \nu r \beta \tag{5.6}$$

where t denotes motion along the characteristic curve $(r(t), z(t))$. Below we will develop the mathematical theory for solutions of (5.4) and (5.5). For now, simply note that if r and z along the characteristic curves are known, then

$$\Psi(t) = \Psi(r_o, z_o) + \int_0^t r(\tau)\beta(r(\tau), z(\tau))d\tau \tag{5.7}$$

where $(r_o, z_o) = (r(t = 0), z(t = 0))$ are Cauchy data for the r and z equations.

The difficulty in posing the problem in terms of Ψ is that of converting

data about u and w into data about Ψ. In order to satisfy the axial boundary condition $u(0,z)=0$, we must have that $\frac{1}{r}\Psi_z(r,z)\to 0$ as $r\to 0$ for every z. Thus $\Psi(0,z)$ must actually be constant. Similarly, if we assume that $w=0$ at $z=0$, this gives $\frac{1}{r}\Psi_r(r,0)=0$ for every r, and so $\Psi(r,0)$ must be constant. In order that we keep the velocities finite at the origin, we must have $\Psi\equiv$ const on the bottom and axial boundaries, and sowe take $\Psi=0$ for simplicity. For the purposes of providing (5.6) with initial data at (r_o,z_o), we can use either of the definions of Ψ and integrate, since

$$\Psi(r_o,z_o)=\int_0^{r_o}-rw(r,z_o)dr=r_o\int_{z_o}^{b}u(r_o,z)dz \tag{5.8}$$

Each of these integrals involves some uncertainty for our problem, because we cannot measure w directly, and the second integral either requires us to start at $z=0$ (where $\Psi=0$) and know the structure of u in Ω_h (which is our goal), or to know Ψ at some upper limit b.

In the special case where $\nu=0$, we see that Ψ is constant on characteristic curves. This constant is in general dependent on the characteristic curve, and hence there must exist a function F such that $\Psi=F(\Gamma)$. By definition, this implies that

$$u=\frac{1}{r}\frac{\partial F}{\partial\Gamma}\frac{\partial\Gamma}{\partial z} \tag{5.9}$$

$$w=-\frac{1}{r}\frac{\partial F}{\partial\Gamma}\frac{\partial\Gamma}{\partial r} \tag{5.10}$$

Removing the viscosity reduces the unknowns down to the univariate function F. The question that remains is how to estimate this function. Without more information, the functional relationship F is arbitrary, meaning that any F

will satisfy the requirements of (5.3) with $\nu = 0$. The boundary conditions imply that $F(0) = 0$.

5.2.2 Characteristic ODEs for u and w

For all (r, z) where $\zeta(r, z) \neq 0$, we can solve for u in (5.1) and substitute the resulting expression into (5.2), which yields a first order hyperbolic equation in w

$$\eta \frac{\partial w}{\partial r} + \zeta \frac{\partial w}{\partial z} + \frac{\zeta}{r} \frac{\partial}{\partial r} \left(r \frac{\eta}{\zeta} \right) w = -\frac{\nu \zeta}{r} \frac{\partial}{\partial r} \left(\frac{r}{\zeta} \left(\frac{\partial \zeta}{\partial r} - \frac{\partial \eta}{\partial z} \right) \right) \tag{5.11}$$

with corresponding characteristic ordinary differential equations

$$\frac{dr}{dt} = \eta \tag{5.12}$$

$$\frac{dz}{dt} = \zeta \tag{5.13}$$

$$\frac{dw}{dt} + \frac{\zeta}{r} \frac{\partial}{\partial r} \left(r \frac{\eta}{\zeta} \right) w = -\frac{\nu \zeta}{r} \frac{\partial}{\partial r} \left(\frac{r}{\zeta} \left(\frac{\partial \zeta}{\partial r} - \frac{\partial \eta}{\partial z} \right) \right). \tag{5.14}$$

Similarly, when $\eta(r, z) \neq 0$, we can solve for w and obtain a first order hyperbolic equation for u,

$$\eta \frac{\partial u}{\partial r} + \zeta \frac{\partial u}{\partial z} + \eta \left(\frac{1}{r} + \frac{\partial}{\partial z} \frac{\zeta}{\eta} \right) u = \nu \eta \frac{\partial}{\partial z} \left(\frac{1}{\eta} \left(\frac{\partial \zeta}{\partial r} - \frac{\partial \eta}{\partial z} \right) \right) \tag{5.15}$$

with characteristic ordinary differential equations

$$\frac{dr}{dt} = \eta \tag{5.16}$$

$$\frac{dz}{dt} = \zeta \tag{5.17}$$

$$\frac{du}{dt} + \left(\frac{\eta}{r} + \eta\frac{\partial}{\partial z}\left(\frac{\zeta}{\eta}\right)\right)u = \nu\eta\frac{\partial}{\partial z}\left(\frac{1}{\eta}\left(\frac{\partial\zeta}{\partial r} - \frac{\partial\eta}{\partial z}\right)\right). \tag{5.18}$$

REMARK 5.1: Note that the characteristic curves $(r(t,s), z(t,s))$ are the same for both sets of equations in the velocity formulation, as well as in the stream-function formulation, and depend only on v, its derivatives, and the starting point parameterized by s. Hence the ODEs for u, w, and Ψ are valid on the same curves. Thus, for u and w to be solutions of our initial pair of equations, both (5.14) and (5.18) have to hold everywhere that $\zeta \neq 0$ and $\eta \neq 0$.

REMARK 5.2: These are linear ordinary differential equations for u and w in t, and as such can be solved through the use of integrating factors. Define $f_u(r,z) = \frac{\eta}{r} + \eta\frac{\partial}{\partial z}\left(\frac{\zeta}{\eta}\right)$ and $g_u(r,z) = \nu\eta\frac{\partial}{\partial z}\left(\frac{\zeta_r - \eta_z}{\eta}\right)$, and $f_w(r,z) = r^{-1}\zeta\frac{\partial}{\partial r}(r\frac{\eta}{\zeta})$ and $g_w(r,z) = -\nu r^{-1}\zeta\frac{\partial}{\partial r}(r\frac{\zeta_r - \eta_z}{\zeta})$. Once r and z have been found as functions of t and s, u and w can be written explicitly along the characteristic curves as

$$u(t) = u_o \exp\left[-\int_0^t f_u(\tau)d\tau\right] + \int_0^t g_u(\tau)\exp\left[-\int_\tau^t f_u(\sigma)d\sigma\right]d\tau \tag{5.19}$$

$$w(t) = w_o \exp\left[-\int_0^t f_w(\tau)d\tau\right] + \int_0^t g_w(\tau)\exp\left[-\int_\tau^t f_w(\sigma)d\sigma\right]d\tau \tag{5.20}$$

where $u_o = u(r_o, z_o)$ and $w_o = w(r_o, z_o)$ are initial conditions. Qualitatively, f_u and f_w are the inviscid parts of the solutions, and g_u and g_w capture the effects of viscosity on the solutions.

5.2.3 Existence and Uniqueness

We consider the question of existence and uniqueness of solutions to the characteristic ordinary differential equations (5.4) and(5.5). These two equations appear in each set of characteristic differential equations, implying that the characteristic curves in the plane are the same for each system. The formal solutions given by (5.7), (5.19), and(5.20) assume knowledge of r and z along each characteristic curve. Further, in order for us to have a unique solution on Ω_h, every point of Ω_h must have a characteristic curve passing through it, which also passes through the observable region $\Omega \setminus \Omega_h$.

LEMMA 5.3: *Let $v \in C^1(\Omega)$ such that the circulation $\Gamma = rv$ satisfies $\nabla\Gamma \neq 0$ on every open subset of Ω. Then*

(1) The solutions, $(r(t), z(t))$, of (5.4)-(5.5), are the largest connected subset of Ω which satisfy $\Gamma(r(t), z(t)) = \Gamma(r_o, z_o)$ for all t, where $(r_o, z_o) := (r(0), z(0))$ are initial conditions.

(2) If $\zeta(r, z) \neq 0$ or $\eta(r, z) \neq 0$, then there is a unique characteristic curve passing through (r, z).

(3) If $\zeta(r, z) = 0$ and $\eta(r, z) = 0$ then (r, z) corresponds to a critical point of Γ.

Proof. (1) When $\eta \neq 0$, we can write the solution curves as $(r, z(r))$ by considering

$$\frac{dz}{dr} = \frac{\zeta}{\eta} \tag{5.21}$$

and when $\zeta \neq 0$ as $(r(z), z)$ from

$$\frac{dr}{dz} = \frac{\eta}{\zeta}. \tag{5.22}$$

Note that

$$\frac{\zeta}{\eta} = \frac{(rv)_r}{-rv_z} = -\frac{\Gamma_r}{\Gamma_z}$$

which implies that the characteristic curves are everywhere tangent to the level curves of Γ, which is proportional to the circulation on circles of radius r about the center of the vortex.

Any point in the largest connected subset that contains the level curve containing (r_o, z_o) is a point on the trajectory $(r(t), z(t))$, simply by taking large (or small) enough values for t. Likewise, any point on the trajectory is in this connected subset, else the mapping $t \mapsto (r(t), z(t))$ would fail to be continuous, which contradicts the theory of ordinary differential equations.

(2) Note that $\nabla\Gamma = [(rv)_r, rv_z]^\mathsf{T} = [r\zeta, -r\eta]^\mathsf{T}$, and so if one of the vorticities is nonzero at (r_o, z_o), then $\nabla\Gamma \neq 0$, and the implicit function theorem guarantees the existence of a nontrivial curve $(r(t), z(t))$ for t near zero, on which $\Gamma(r(t), z(t)) = \Gamma(r_o, z_o)$. Since the circulation function is continuously differentiable, we know the sets $\{(r, z) \in \Omega : \Gamma(r, z) = C_1\} \cap \{(r, z) \in \Omega : \Gamma(r, z) = C_2\} = \emptyset$ for $C_1 \neq C_2$, and so the curve is unique.

(3) If both vorticities are zero at (r_o, z_o), then $\nabla\Gamma(r_o, z_o) = \vec{0}$, and since Γ

is nonconstant on every open subset of Ω, we have a critical point at (r_o, z_o).

□

REMARK 5.4: Defining "level curve" as a connected component of the set $\{(r,z) \in \Omega : \Gamma(r,z) = \Gamma_o\}$, this lemma says that as long as Γ is nonconstant on open sets, every point (r_o, z_o) will have a unique level curve of Γ passing through it, and that this level curve is actually the trajectory of the dynamical system (5.4)-(5.5) with initial value $(r(0), z(0)) = (r_o, z_o)$.

REMARK 5.5: We can traverse the level curves of Γ in the t direction, or the $-t$ direction. If we traverse in the positive t direction, motion along the curve follows the signs of the vorticities. In the negative t direction, motion along the curve moves in the direction opposite to the signs of the vorticities.

DEFINITION (Characteristic Curves and Information Voids): *Suppose that* $v \in C^1(\Omega)$, *and* $\nabla\Gamma \neq 0$ *on open sets.*

(a) Define the map $c(\cdot, r_o, z_o) : \mathbb{R} \to \Omega$ *by* $(r,z) = c(t, r_o, z_o)$, *where* (r,z) *is the forward solution of* (5.4)-(5.5) *at time* t, *with initial condition* (r_o, z_o).

(b) For $(r_o, z_o) \in \Omega^o$, *define* $C(r_o, z_o)$ *to be the orbit of* (r_o, z_o) *under the dynamical system* (5.4)-(5.5), *which is the image of* $\mathbb{R}$ *under* $c(\cdot, r_o, z_o)$.

(c) If there exists a T *such that* $c(T, r_o, z_o) = (r_o, z_o)$, *then* $C(r_o, z_o)$ *is called closed.*

(d) Define the set $K_h = \{(r,z) \in \Omega_h : C(r,z) \cap (\Omega \setminus \Omega_h) = \emptyset\}$. *We call* K_h *the* information void *associated with* h*, since the data in the observable region do not communicate with* K_h *along characteristic curves.*

REMARK 5.6: Ω is a bounded set, and so $\overline{K_h}$ is compact. This means that for each $(r,z) \in \Omega$, there is a point $(r^*,z^*) \in \overline{K_h}$ such that $d_{K_h}(r,z) = ||(r^*,z^*) - (r,z)||_2$.

THEOREM 5.7: *Suppose* $v \in C^2(\Omega)$ *and* Γ *is nonconstant on all open subsets* $U \subset \Omega$. *Then* Ψ *is the solution of* (5.3) *if and only if* Ψ *satisfies* (5.6) *on the curves which are solutions of* (5.4) *and* (5.5)*, and hence there is a unique solution at every* $(r,z) \in \Omega \setminus K_h$.

Proof. If $(r,z) \notin K_h$, then the characteristic curve $C(r,z)$ intersects the observable region $\Omega \setminus \Omega_h$, and so we have an observation $\Psi(r_o,z_o)$ at some point $(r_o,z_o) \in \Omega \setminus \Omega_h$. Hence there is a $t \geq 0$ so that $\Psi(r,z) = \Psi(r_o,z_o) + \int_0^t r(\tau)\beta(\tau)d\tau$. □

THEOREM 5.8: *Suppose* $v \in C^2(\Omega)$ *and* Γ *is nonconstant on all open subsets* $U \subset \Omega$. *Then* u *and* w *are solutions of* (5.1) *and* (5.2) *if and only if they satisfy* (5.14) *on* $\Omega \setminus (\{(r,z) \in \Omega : \zeta(r,z) = 0\} \cup K_h)$*, and* (5.18) *on* $\Omega \setminus (\{(r,z) \in \Omega : \zeta(r,z) = 0\} \cup K_h)$.

Proof. This follows from Lemma 5.3, Remark 5.4 and (5.19)-(5.20). □

REMARK 5.9: Theorems 5.7 and 5.8 give a unique strong solution on every characteristic where we have data for u, w, or Ψ, and so they connect the "local" characteristic ODE theory with the "global" PDE theory. It states that

information aloft tells us about the dynamics below, at the physical locations that lie on characteristics emanating from $\Omega \backslash \Omega_h$.

5.3 Properties of Information Voids

ASSUMPTION 5.10: *For this section we will always assume that* $v \in C^1(\Omega)$ *and that* Γ *is nonconstant on open subsets of* Ω*, so that Lemma 5.3 applies.*

PROPOSITION 5.11: *Suppose that* $\Gamma(r_o, z_o) \neq \Gamma(r, z)$ *for all* $(r, z) \in \Omega \setminus \Omega_h$. *Then* $(r_o, z_o) \in K_h$.

Proof. Lemma 5.3 implies that $C(r_o, z_o)$ is a level curve of Γ. Hence, if $\Gamma(r_o, z_o) \neq \Gamma(r, z)$ for all $(r, z) \in \Omega \setminus \Omega_h$, then $C(r_o, z_o) \cap (\Omega \setminus \Omega_h) = \emptyset$. □

REMARK 5.12: This condition is sufficient, but not necessary. Consider a tangential velocity model

$$v(r, z) = \phi_{ww}(r, n_r, r_c)(a\phi_{ww}(z, n_z, z_c) + b\phi_{ww}(z, \widetilde{n_z}, \widetilde{z_c})) \tag{5.23}$$

with more than one maximum at the same radius, as in Figure 5.1. Note that there are closed characteristic curves surrounding the maximum which occurs at $z = 100m$, though the circulation maximum value there is the same as the one which occurs on $\partial\Omega_h^+$. Hence this implies that attaining the absolute max of Γ on $z = h$ does not guarantee a lack of voids in Ω_h.

PROPOSITION 5.13: *If* v *vanishes on the axes, then no characteristic curve may intersect the axes* $r = 0$ *or* $z = 0$.

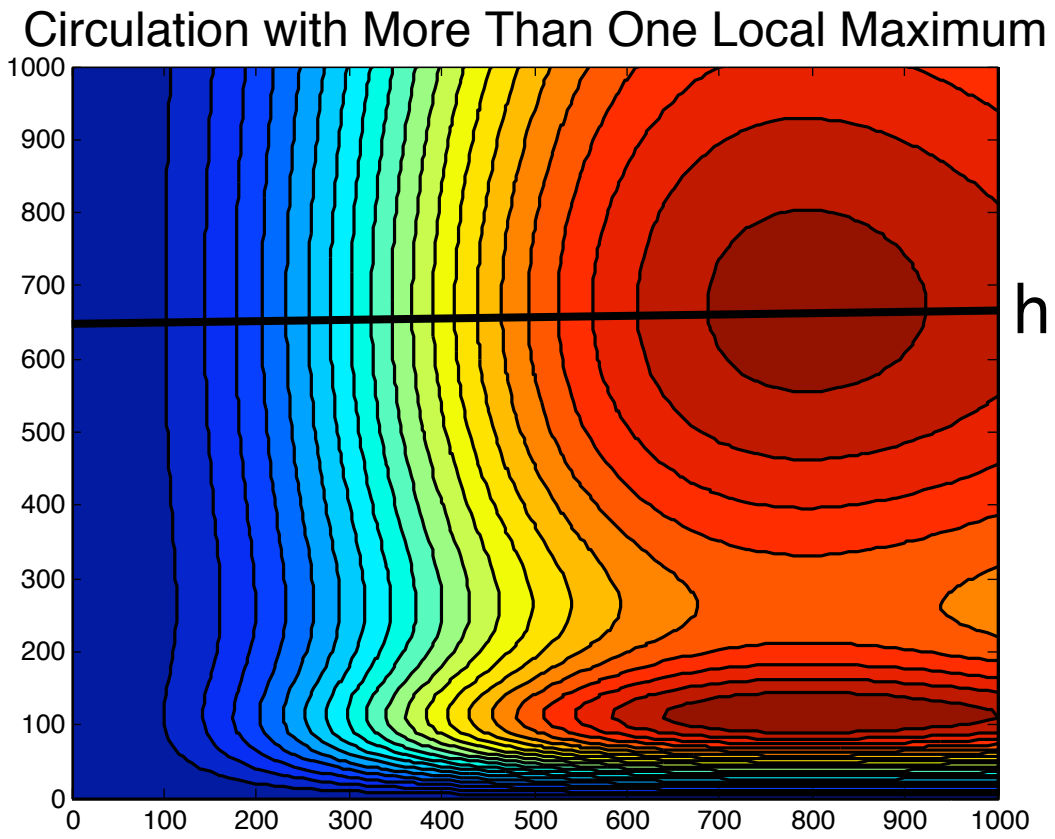


Figure 5.1: An example of the circulation function yielding information voids which are disconnected from $\partial\Omega_h^+$ $(z = h)$, though Γ attains its maximum on $\partial\Omega_h^+$.

Proof. Note that $v(r,0) = 0$ implies that $\Gamma(r,0) = 0$, and similarly on the vertical axis. Hence, the axes are characteristic curves. Further, since Γ is differentiable, its level curves may not intersect. Thus, no other characteristic curve may cross the axes. □

5.3.1 Tensor Product Tangential Velocity Model

We can prove more specific results when we assume that the tangential velocity can be modeled by a tensor product of one dimensional functions.

ASSUMPTION 5.14 (Tensor Product Form of v): *Suppose that*

$$v(r,z,q) = \phi(r;q_r)\psi(z;q_z) \tag{5.24}$$

$$\zeta(r,z,q) = \frac{1}{r}\frac{d}{dr}(r\phi(r;q_r))\psi(z;q_z) \tag{5.25}$$

$$\eta(r,z,q) = -\phi(r;q_r)\frac{d}{dz}\psi(z;q_z) \tag{5.26}$$

(1) ϕ *and* ψ *are smooth enough to satisfy the requirements for well-posedness of the problem,*

(2) $\phi(0) = \psi(0) = 0$*,*

(3) $\phi(r) > 0$ *on* $(0,R)$ *and* $\psi(z) > 0$ *on* $(0,H)$*.*

(4) ϕ *and* ψ *are nonconstant on open intervals.*

REMARK 5.15: Condition (2) enforces the requirement that v vanish on the axes. Condition (3) is needed to keep the flow from aloft from being separated from the flow below. Condition (4) is needed so that Γ is nonconstant on open sets, which was a key assumption that led to a unique characteristic

curve passing through every point. This also prevents $\partial\Omega_h^+$ from being itself a characteristic curve, except possibly at isolated points, where the gradient is

PROPOSITION 5.16 (Fixed Points): *The fixed points of* (5.4)-(5.5) *consist of the set*

$$F_v = \left\{ \{0\} \cup \left\{ r \in (0,R) : \frac{d}{dr}(r\phi(r;q_r)) = 0 \right\} \right\} \times \\ \times \left\{ \{0\} \cup \left\{ z \in (0,H) : \frac{d}{dz}(\psi(z;q_z)) = 0 \right\} \right\}.$$

Proof. Clearly if $(r,z) \in F_v$, then $\zeta(r,z) = \eta(r,z) = 0$. Conversely, assume $\zeta(r,z) = \eta(r,z) = 0$. If $r \neq 0$ and $z \neq 0$, then both $\psi(0) \neq 0$ and $\phi(0) \neq 0$, and so $\frac{d}{dr}(r\phi(r)) = \frac{d\psi}{dz}(z) = 0$. If $\frac{d}{dr}(r\phi(r)) \neq 0$, then $\phi(r) = 0$, which implies $r = 0$. Similarly, if $\frac{d\psi}{dz} \neq 0$, then $z = 0$. □

COROLLARY 5.17: *Suppose that* $\frac{d}{dr}r\phi(r)$ *has a finite collection of zeros* $r_1 < r_2 < ... < r_n$, *and that* $\frac{d\psi}{dz}$ *also has a finite collection of zeros* $z_1 < z_2 < ... < z_m$. *Then each of these, viewed as a horizontal (vertical) line, is a nullcline for* (5.4)-(5.5).

REMARK 5.18: Corollary 5.17 implies that the characteristic curves can only change direction when crossing the horizontal or vertical lines determined by the zeros of the component models. With this knowledge, we can easily divide the domain into sections bounded by the nullclines and consider the direction of the trajectories in each section as t increases. If we want to traverse the characteristic in the opposite direction, we take t to be decreasing.

PROPOSITION 5.19: *Suppose that* $\frac{d}{dr}(r\phi(r)) = 0$ *at* $r = r_o$*, and* $\frac{d\psi}{dz} = 0$ *at* $z = z_o$*. Then* $C(r_o, z_1)$ *is tangent to the horizonal line* $z = z_1$ *at* (r_o, z_1)*, and* $C(r_1, z_o)$ *is tangent to the vertical line* $r = r_1$ *at* (r_1, z_o)*.*

Proof. The slope $\frac{dz}{dr}$ of characteristic curve is zero at $r = r_o$ since $\frac{dz}{dt} = \zeta(r_o, z) = 0$. In addition, the point (r_o, z_o) is on the line $z = z_o$, which also has slope 0. Hence $C(r_o, z_o)$ is tangent to $z = z_o$. Although $\frac{dz}{dr}$ at (r_1, z_o) is undefined, we can clearly see that $C(r_1, z_o)$ and $r = r_1$ intersect, and that $\frac{dr}{dt}$ at (r_1, z_o) is 0. □

REMARK 5.20: Proposition 5.19 says that the zeros of the vertical vorticity in the radial direction correspond to constrained maxima or minima of Γ along horizontal lines, and the zeros of the radial vorticity correspond to constrained maxima or minima of Γ along vertical lines.

PROPOSITION 5.21: *Suppose that* $\Gamma = r\phi(r)\psi(z)$ *has a relative maximum at the point* $(r_o, z_o) \in \Omega^o$*, and that* $\nabla\Gamma \neq 0$ *on* $\Omega^o \setminus \{(r_o, z_o)\}$*. If* $0 < z_1 < H$ *satisfies* $C(r_o, z_1) \subset \Omega^o$*, then* $C(r_o, z)$ *is a closed curve.*

Proof. Let $z_1 > z_o$. Since Γ has only a single relative maximum, we must have that $\frac{\partial\Gamma}{\partial r} > 0$ for $r < r_o$ and $\frac{\partial\Gamma}{\partial r} < 0$ for $r > r_o$, and similarly for the vertical gradient of Γ. Consider the characteristic curve which passes through (r_o, z_1), and first traverse in the positive t direction. Since $\Gamma_z(r_o, z_1) < 0$, $\eta > 0$, and so the characteristic curve moves to the right. For $r > r_o$ and $z > z_o$, $\eta > 0$ and $\zeta < 0$, and so the characteristic curve moves to the right and down. Since we assumed that $C(r_0, z_1) \subset \Omega^o$, there must be an r_1 with $r_o < r_1 < R$ such that $(r_1, z_o) \in C(r_o, z_1)$, else $C(r_o, z_1)$ would cross the line $r = R$. Similarly,

since for $r > r_o$ and $z < z_o$, $\eta < 0$ and $\zeta < 0$, there must be a $0 < z_2 < z_0$ such that $(r_o, z_2) \in C(r_o, z_1)$. Otherwise $C(r_o, z_1)$ would intersect the lower axis $z = 0$, which would contradict Proposition 5.13. Thus $C(r_o, z_1)$ intersects the line $r = r_o$ at (r_o, z_2). By traversing $C(r_o, z_1)$ in the negative t direction starting from (r_o, z_1), and using similar arguments, there is a $0 < z_3 < z_o$ such that $(r_o, z_3) \in C(r_o, z_1)$.

Suppose $z_2 < z_3$. Then there is a z^* with $z_2 < z^* < z_3$, and since $\Gamma_z > 0$, we must have that

$$\Gamma(r_o, z_2) < \Gamma(r_o, z^*) < \Gamma(r_o, z_3). \tag{5.27}$$

But this is a contradiction, since $\Gamma(r_o, z_2) = \Gamma(r_o, z_3)$.

Let t_2 such that $c(t_2, r_o, z_1) = (r_o, z_2)$ and t_3 such that $c(-t_3, r_o, z_1) = (r_o, z_3)$. Then $c(t_2 + t_3, r_o, z_1) = (r_o, z_1)$ and $C(r_o, z_1)$ is closed. □

REMARK 5.22: Figure 5.2 gives a schematic representation of the characteristic curves when the assumptions of Proposition 5.21 are satisfied.

PROPOSITION 5.23: *Suppose that* $\Gamma = r\phi(r)\psi(z)$ *has a relative maximum at the point* $(r_o, z_o) \in \Omega^o$*, and that* $\nabla\Gamma \neq 0$ *on* $\Omega^o \setminus \{(r_o, z_o)\}$*. If* $h < z_0$*, then* $K_h = \emptyset$*.*

Proof. There are two cases. For $r \leq r_o$, $\eta < 0$ and $\zeta \geq 0$. Hence if we traverse $C(r, z)$ in the positive t direction, the curve must eventually cross $z = h$, since $C(r, z)$ cannot intersect the vertical axis. For $r > r_o$, $\eta < 0$ and $\zeta < 0$. Since $C(r, z)$ cannot intersect the horizontal axis, there must be a z_1 such that $(r_o, z_1) \in C(r, z)$, and now we can apply the argument from the

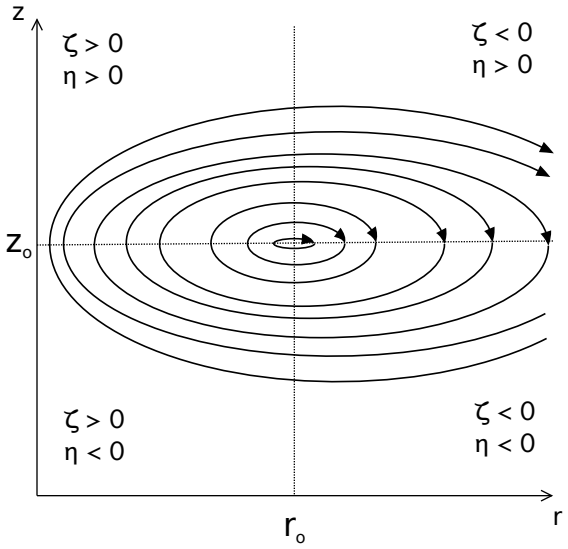


Figure 5.2: Closed curves surrounding the relative maximum at (r_o, z_o). Arrows are pointing in the positive t direction.

first case, using our (r_o, z_1) as our initial point. Hence, for any $(r, z) \in \Omega_h$, $C(r, z) \cap (\Omega \setminus \Omega_h) \neq \emptyset$, which implies $K_h = \emptyset$. □

REMARK 5.24: Proposition 5.23 implies that if we have observations below the maximum tangential velocity, then we can retrieve the wind fields everywhere in Ω using the characteristic methodology.

PROPOSITION 5.25: *Suppose that $\Gamma = r\phi(r)\psi(z)$ has a relative maximum at the point $(r_o, z_o) \in \Omega^o$, and that $\nabla\Gamma \neq 0$ on $\Omega^o \setminus \{(r_o, z_o)\}$, and $z_o < h$. Then one and only one of the following statements holds:*

(1) $C(r_o, h)$ is a closed curve, and K_h is the interior of the region enclosed by $C(r_o, h)$.

(2) $C(r_o, h)$ intersects the outer radial boundary at (R, z_1) and (R, z_2), and K_h is the interior of the region enclosed by $C(r_o, h)$ and the segment $\{(R, z) : z_1 \leq z \leq z_2\}$

Proof. First, if $C(r_o, h)$ is not a closed curve, then if we traverse in the negative t direction, we must cross the line $z = z_o$, and then the line $r = r_o$, because $C(r_o, h)$ cannot intersect the axes. This implies that there is a t such that $c(-t, r_o, h) = (r^*, z^*)$ with $r^* > r_o$ and $z^* < z_o$. If $C(r_o, h)$ were to cross the line $z = z_o$ again, then the signs of the vorticities would force $C(r_o, h)$ to intersect $r = r_o$, and at the point (r_o, h) by the argument in Proposition 5.21. Similarly, if we traverse $C(r_o, h)$ in the positive t direction, $C(r_o, h)$ cannot cross the line $z = z_o$, or else $C(r_o, h)$ would be a closed curve. Thus, either $C(r_o, h)$ is a closed curve, or $C(r_o, h)$ intersects the outer radial boundary at two distinct points (R, z_1) and (R, z_2), where $z_1 < z_o < z_2$. In either case, denote the set enclosed by $C(r_o, h)$ (and possibly $\{R\} \times [z_1, z_2]$) by K_o.

If $(r, z) \in \Omega_h \setminus K_o$, proceed as before by traversing $C(r, z)$ either in the positive ($r < r_o$ or $z < z_o$) or negative ($r > r_o$ and $z > z_o$) t direction. We know that $c(t, r, z) \notin K_o$ for all $t \in \mathbb{R}$ because $\partial K_o = C(r_o, h)$ (possibly plus the outer boundary), and characteristic curves may not intersect. Since $c(t, r, z)$ also cannot intersect the axes, there must be a t such that $c(t, r, z) \in (\Omega \setminus \Omega_h)$. Thus $K \subset K_o$.

If $(r_1, z_1) \in K_o$, we have that $\Gamma(r_1, z_1) > \Gamma(r, z)$ for all $(r, z) \in \Omega \setminus \Omega_h$. Thus $C(r_1, z_1) \cap (\Omega \setminus \Omega_h) = \emptyset$ and so $(r_1, z_1) \in K$. Hence $K_o \subset K$, and $K = K_o$. □

PROPOSITION 5.26: *Suppose that $\Gamma = r\phi(r)\psi(z)$ has a relative maximum at the point $(r_o, z_o) \in \Omega^o$, and that $\nabla\Gamma \neq 0$ on $\Omega^o \setminus \{(r_o, z_o)\}$. Then there is an h_o such that if $z < h_o$, $C(r, z) \cap (\Omega \setminus \Omega_h) \neq \emptyset$.*

Proof. Since $C(r_o, h) \subset \Omega$ is closed, it is also compact. Hence the map $(r, z) \mapsto z$ has a minimizer at some point h_o. Thus, if $z < h_o$, $(r, z) \notin K_o$, and so $C(r, z) \cap (\Omega \setminus \Omega_h) \neq \emptyset$ by Proposition 5.25. □

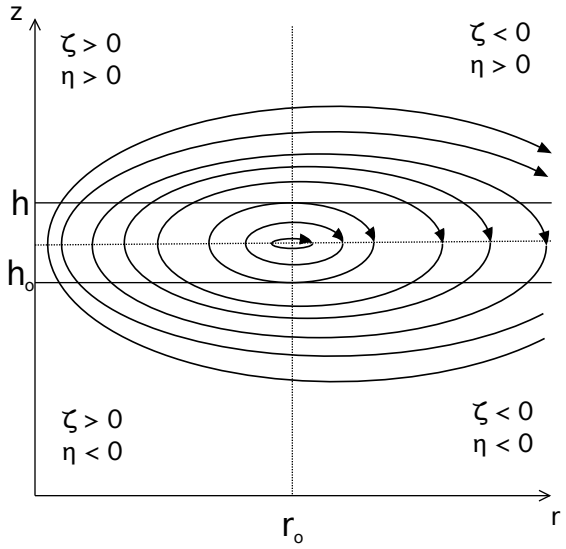


Figure 5.3: Illustration of relationship between h and h_o

REMARK 5.27: Figure 5.3 illustrates the nontrivial region below h_o where the wind fields are retrievable.

COROLLARY 5.28: *The h_o which is given by Proposition 5.26 is the solution of $\psi(z) = \psi(h)$.*

Proof. By examining the signs of the vorticities for our assumptions, this point has to be on the vertical line $r = r_o$, since $\frac{dz}{dr} \neq 0$ when $r \neq r_o$. Hence, h_o is just the solution of the equation $\psi(z) = \psi(h)$. □

COROLLARY 5.29: *If h_1 and h_2 are two minimum observable heights for the same tangential velocity model that satisfies the assumptions of Proposition 5.26 with $z_o < h_1 < h_2$, then the two heights h_{o1} and h_{o2} guaranteed by Proposition 5.26 satisfy $h_{o1} > h_{o2}$.*

Proof. Since Γ has a relative max at (r_o, z_o), and $\Gamma_z < 0$ for $z > z_o$, we must have that $\Gamma(r_o, h_1) > \Gamma(r_o, h_2)$. By Proposition 5.25, this implies that $K_{h_1} \subset$

K_{h_2} and $C(r_o, h_1)$ is contained in K_{h_2}. Hence the minimum of the mapping $(r, z) \mapsto z$ restricted to $C(r_o, h_1)$, which we denoted h_{o1}, must be no smaller than when restricted to $C(r_o, h_2)$, denoted h_{o2}. In fact, the inequality must be strict, or else we would have that $C(r_o, h_2) = C(r_o, h_1)$, which contradicts $h_1 < h_2$. □

REMARK 5.30: The interpretation of Corollary 5.29 is that if we have a given set of observations above h, and the corresponding h_o below which we can retrieve the wind fields, and are able to augment these observations somehow to decrease h to $\widehat{h}$, then we will be able to retrieve information further above the ground, at a new height $\widehat{h_o}$. This leads to an observation strategy, since we can determine in advance how low to scan in order to retrieve wind fields at heights of interest.

5.4 Analysis with Wood-White Models

Following Snow (1982), the vertical variation in the tangential wind field in the lowest vertical levels of the tornado can be modeled by the Wood-White function, with the same caveat about forcing $k = 1$, only this time so that w will be zero at $z = 0$, and of course choosing a different n parameter. Hence, let

$$v(r, z) = v_{\max}\phi_{ww}(r; n_r, r_c)\phi_{ww}(z; n_z, z_c) \tag{5.28}$$

$$\zeta(r, z) = v_{\max}\frac{1}{r}\frac{d}{dr}(r\phi_{ww}(r; n_r, r_c))\phi_{ww}(z; n_z, z_c) \tag{5.29}$$

$$\eta(r, z) = -v_{\max}\phi_{ww}(r; n_r, r_c)\frac{d}{dz}\phi_{ww}(z; n_z, z_c) \tag{5.30}$$

5.4.1 Characteristic ODE Solutions

PROPOSITION 5.31 (Wood-White Characteristic Curves): *Let v be as in* (5.28). *Then*

(1) The set of fixed points $F_v = \{0, r_\zeta\} \times \{0, z_c\}$, where

$$r_\zeta = \left(\frac{2(n_r - 1)}{n_r - 2}\right)^{1/n_r} r_c. \tag{5.31}$$

(2) $\zeta(r, z)$ is positive for $r < r_\zeta$ and negative for $r > r_\zeta$.

(3) $\eta(r, z)$ is negative for $z < z_c$ and positive for $z > z_c$.

(4) Γ has a single relative and absolute maximum at (r_ζ, z_c), and $\nabla\Gamma(r, z) = 0$ on $\Omega \setminus \{r_\zeta, z_c\}$.

Proof. (1) From Proposition 5.16, we need to find the zeros of $\frac{d}{dr}(r\phi(r; n_r, r_c))$ and $\frac{d}{dz}\phi(z; n_z, z_c)$. These formulas are given by (2.14) and (2.16), and imply that $\frac{d}{dr}(r\phi(r; n_r, r_c)) = 0$ at $r = r_\zeta$, and $\frac{d}{dz}\phi(z; n_z, z_c) = 0$ when $z = z_c$.

(2) Equation (2.16) implies this immediately, since the factor $2(n_r - 1){r_c}^{n_r} - (n_r - 2)r^{n_r}$ is positive for $r < r_c$ and negative for $r > r_c$.

(3) This follows from (2.14).

(4) This is an immediate consequence of (2) and (3), and the fact that $\nabla\Gamma = [r\zeta, -r\eta]^\mathsf{T}$.

□

REMARK 5.32: This divides Ω into four regions, with the behavior of the characteristic curves depending on which region the curve is passing through.

Figure 5.4 is a schematic drawing of the behavior. The arrows are pointing in the direction that the values of $(r(t), z(t))$ move as t increases, starting from the filled dot.

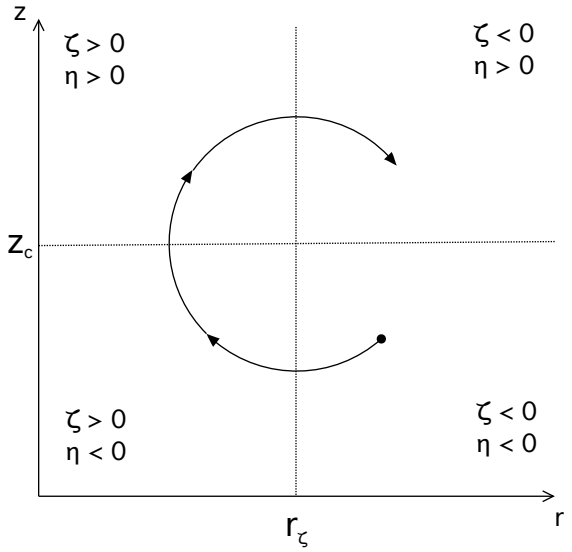


Figure 5.4: Schematic of Characteristic Curves with Wood-White Model

5.4.2 Qualitative Analysis for the Case $\nu = 0$

When $\nu = 0$, we can use the differential equations for u and w to gain further insight.

PROPOSITION 5.33: *Let v be as in* (5.28)*, and $\nu = 0$. Then horizontal line $z = z_c$ and the curve described implicitly by*

$$\frac{r\phi_r(r)}{(r\phi(r))_r} = \frac{\phi(z)\phi_{zz}(z)}{(\phi_z(z))^2} \tag{5.32}$$

divide Ω into regions on which the rate of change of u along characteristics does not change sign.

Proof. In the inviscid case, (5.19) simplifies to

$$u(t) = u_o \exp\left[-\int_o^t f_u(\tau)d\tau\right] \tag{5.33}$$

Clearly, when f_u is positive, u is decreasing, and vice versa. The integrand can be written in terms of component models, and simplified to

$$\frac{\eta}{r} + \frac{\zeta_z\eta - \zeta\eta_z}{\eta} = -\frac{\left[-\phi_r(r)(\phi_z(z))^2 + \frac{1}{r}(r\phi(r))_r\phi(z)\phi_{zz}(z)\right]}{\phi_z(z)}. \tag{5.34}$$

Since the integrand is a quotient, it can only change sign at the zeros of the factors. Clearly one of these is $z = z_c$. If we set the interior of the numerator equal to zero, we end up with

$$\frac{r\phi_r(r)}{(r\phi(r))_r} = \frac{\phi(z)\phi_{zz}(z)}{(\phi_z(z))^2}, \tag{5.35}$$

which is the curve in the statement of the Proposition. □

REMARK 5.34: Note that $(r_c, 0)$ and (r_ζ, z_c) both satisfy the equation. Figure 5.5 shows an example of qualitative schematic of where u is increasing and decreasing, with its curve along which $\frac{du}{dt} = 0$, and implies that we will find the minimum values of u along this curve. The symbol Z^* is the value of z where $\phi_{zz}(z)$ changes sign. Figure 5.6 shows an example retrieved Wood-White radial velocity with a numerical approximation of the corresponding curve overlaid.

5.4.3 Information Voids

Since our model satisfies Assumption 5.14, the results from Section 5.3.1 apply to this example. Thus for a given $h > z_c$, K_h is the region bounded by $C(r_\zeta, z_c)$

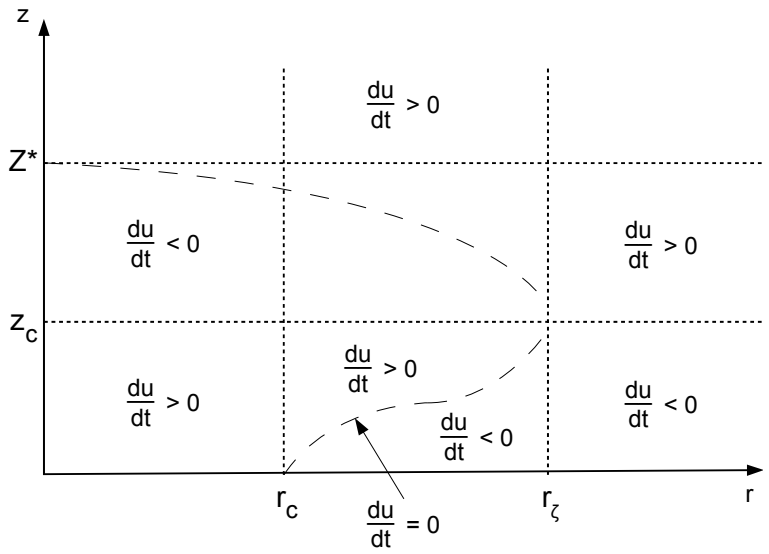


Figure 5.5: Schematic of Sign Changes for $\frac{du}{dt}$

(and possibly the outer boundary).

Figure 5.7 illustrates an example for $n_r = 3$, $n_z = 2$, $r_c = 462$, $z_c = 504$, and $h = 630$. The white area indicates the information void for this particular example. Note that for z values beneath K_h, characteristic curves connect the point (r, z) to the observable region.

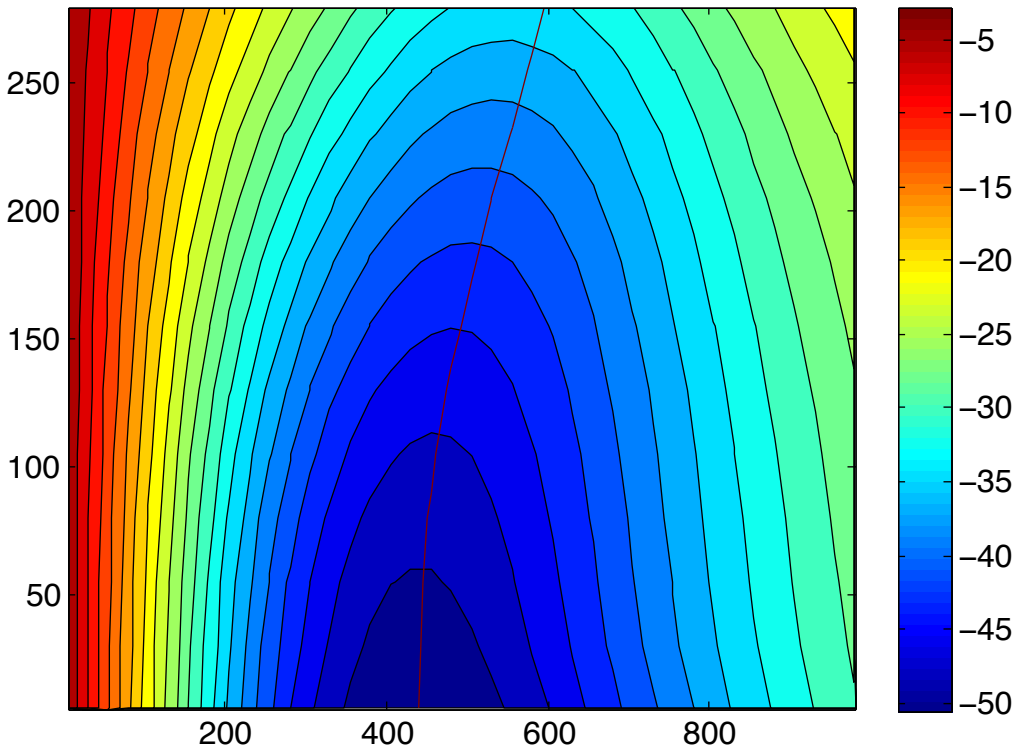


Figure 5.6: Wood-White estimated radial velocity with $\frac{du}{dt} = 0$ overlaid.

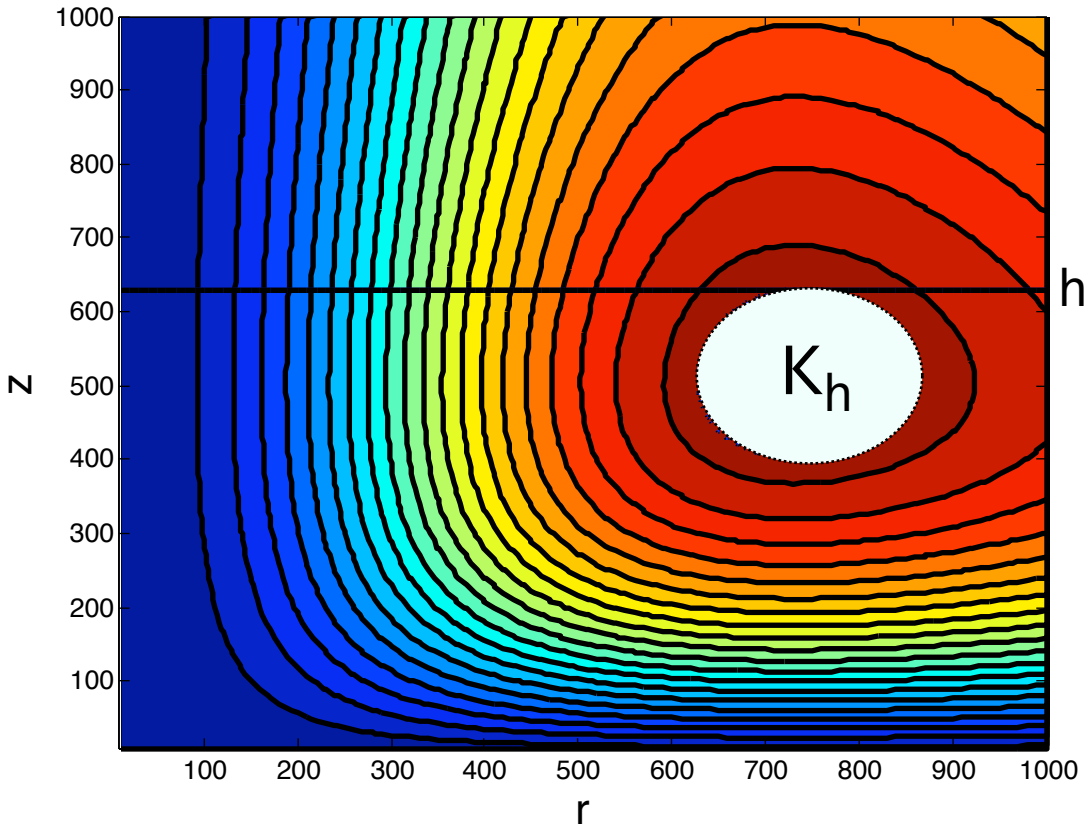


Figure 5.7: Wood-White circulation with maximum at $z_c = 504$, minimum observable height $h = 630$, and resulting information void K_h.

Chapter 6

Estimation on Information Voids

6.1 Introduction

We saw in Chapter 5 that there are conditions that imply the existence of regions of the domain called information voids, for which our model equations (5.1) and (5.2) together with observations above the minimum observable height line $z = h$ do not have a unique solution. This means that the model and data don't contain enough information to uniquely define the flow in these regions. In this chapter we explore methods to define a unique solution to the problem in these regions, in a way that is consistent with strong solutions of the problem outside these sets.

For tractability, we will make the following assumptions.

Assumption 6.1: *Γ has a single relative and absolute maximum at (r_o, z_o), and $\nabla\Gamma \neq 0$ on $\Omega \setminus \{(r_o, z_o)\}$,*

Assumption 6.2: *R is sufficiently large that $\overline{K_h} \subset \Omega^o$,*

Assumption 6.3: *The strong solutions u, w, and Ψ are known on $\Omega \setminus K_h$.*

6.2 Weak Solutions for the Dirichlet Problem

In an attempt to better determine the behavior of solutions in the information voids, we consider (5.3) with the addition of a small diffusive term:

$$-\epsilon\Delta\Psi + \zeta\frac{\partial\Psi}{\partial z} + \eta\frac{\partial\Psi}{\partial r} = \nu r\beta. \tag{6.1}$$

Denote $A_\epsilon\Psi := \epsilon\Delta\Psi + \zeta\frac{\partial\Psi}{\partial z} + \eta\frac{\partial\Psi}{\partial r}$. This modified problem is a steady advection-diffusion problem, with the radial and vertical vorticities playing the role of advection velocities, and the small constant ϵ the diffusivity. This problem is well-known in fluid mechanics to be a singular perturbation problem, in that the character of the solutions changes dramatically as $\epsilon \to 0$.

We are interested in solving (6.1) on K_h with boundary condition $\Psi_b(t)$ on ∂K_h from the characteristic solutions described in Chapter 5. We can "homogenize" the problem by defining $\tilde{\Psi} = \Psi - \widehat{\Psi}$, where $\widehat{\Psi}|_{\partial K_h} = \Psi_b$, and moving the boundary terms to the right hand side as forcing terms:

$$A_\epsilon\tilde{\Psi} = \nu r\beta + A_\epsilon\widehat{\Psi} =: f \tag{6.2}$$

This allows us to consider the problem on the space $H_0^1(K_h)$, which gives use of the Poincare inequality. For simplicity, we will use Ψ in place of $\tilde{\Psi}$ in the discussion that follows, but with the assumption that we are taking homogeneous boundary conditions on ∂K_h.

Let $\varphi \in H_0^1(K_h)$, multiply both sides of (6.1) by φ, and integrate over K_h.

After integrating the Laplacian term by parts, we have

$$a_\epsilon(\Psi, \varphi) := \int_{K_h} \epsilon \nabla\Psi \cdot \nabla\varphi + \zeta\Psi_z\varphi + \eta\Psi_r\varphi dA = \int_{K_h} f\varphi dA \qquad (6.3)$$

Note that $a_\epsilon : H_0^1(K_h) \times H_0^1(K_h) \to \mathbb{R}$ is a bilinear form. We need two fundamental results to proceed with existence considerations. The first is a special case of the Sobolev inequalities for $H_0^1(K_h)$.

THEOREM 6.4 (Poincaré Inequality): *Suppose Ω is an open, bounded set in $\mathbb{R}^n$ for some n. Then there exists a $\gamma(\Omega) > 0$ such that for all $u \in H_0^1(\Omega)$,*

$$||u||_{L^2(\Omega)} \leq \gamma ||\nabla u||_{L^2(\Omega)} \qquad (6.4)$$

REMARK 6.5: This theorem implies that the $||\cdot||_{H^1}$ and $||\cdot||_{H_0^1}$ are equivalent on $H_0^1(\Omega)$, since we have that

$$||u||_{H_0^1(\Omega)} \leq ||u||_{H^1(\Omega)} \leq (1+\gamma)||u||_{H_0^1(\Omega)} \qquad \forall u \in H_0^1(\Omega). \qquad (6.5)$$

The result can be extended to a more general case, in which Ω is bounded in one coordinate direction, since the proof follows from integration by parts and the fact that functions in $H_0^1(\Omega)$ vanish on the boundary.

The second result is the basic theorem regarding problems involving bilinear forms on Hilbert spaces.

THEOREM 6.6 (Lax-Milgram): *Let H be a Hilbert space, and $B : H \times H \to \mathbb{R}$ be a bilinear mapping, for which there exist constants $\alpha, \beta > 0$ such that*

$$|B(u,v)| \leq \alpha ||u||_H ||v||_H \qquad \forall u, v \in H \qquad (6.6)$$

and

$$\beta||u||_H^2 \leq B(u,u) \qquad \forall u \in H \tag{6.7}$$

Then if f is a bounded linear functional on H, there exists a unique element $u \in H$ such that

$$B(u,v) = f(v) \tag{6.8}$$

for every $v \in H$.

REMARK 6.7: For a proof of this theorem, see Evans (1998). The first condition (6.6) is simply that the bilinear form is bounded. The second condition (6.7) is referred to as *coercivity*.

REMARK 6.8: Note if we assume that ζ is bounded, then

$$-||\zeta||_\infty|\Psi\Psi_z| \leq -|\zeta\Psi\Psi_z| \leq \zeta\Psi\Psi_z \leq |\zeta\Psi\Psi_z| \leq ||\zeta||_\infty|\Psi\Psi_z| \tag{6.9}$$

and similarly for the first order term containing η. For simplicity, define

$$\omega_\infty = \omega_\infty(K_h) = \max\{||\zeta||_{L^\infty(K_h)}, ||\eta||_{L^\infty(K_h)}\}. \tag{6.10}$$

LEMMA 6.9 (Boundedness of a_ϵ): *Suppose $\zeta, \eta \in L^\infty(K_h)$. Then a_ϵ is bounded for every $\epsilon \geq 0$.*

Proof. Let $\Psi, \varphi \in H_0^1(K_h)$. Then

$$\begin{aligned}\int_{K_h} \epsilon|\nabla\Psi \cdot \nabla\varphi|dA &\leq \int_{K_h} \epsilon|\nabla\Psi||\nabla\varphi|dA \leq \epsilon||\nabla\Psi||_{L^2(K_h)}||\nabla\varphi||_{L^2(K_h)} \\ &= \epsilon||\Psi||_{H_0^1(K_h)}||\varphi||_{H_0^1(K_h)}\end{aligned}$$

where the first inequality follows from the Cauchy-Schwarz inequality for $\mathbb{R}^2$, and the second inequality from the Cauchy-Scharz inequality for $H_0^1(K_h)$. Further,

$$\begin{aligned}\int_{K_h} |\zeta\Psi_z\varphi + \eta\Psi_r\varphi|dA &\leq \omega_\infty||\varphi||_{L^2(K_h)} \left(||\Psi_z||_{L^2(K_h)} + ||\Psi_r||_{L^2(K_h)}\right) \\ &\leq 2\gamma\omega_\infty||\Psi||_{H_0^1(K_h)}||\varphi||_{H_0^1(K_h)}\end{aligned}$$

where $\gamma = \gamma(K_h)$ is given by the Poincare Inequality. Thus we have

$$a_\epsilon(\Psi, \varphi) \leq (\epsilon + 2\omega_\infty\gamma)||\Psi||_{H_0^1(K_h)}||\varphi||_{H_0^1(K_h)} \tag{6.11}$$

and a_ϵ is bounded. □

LEMMA 6.10 (Coercivity Criterion for a_ϵ): *Suppose that $\zeta, \eta \in L^\infty(K_h)$, and that $\gamma(K_h)$ is the Poincare constant. If $\epsilon > \omega_\infty\left(\gamma + \frac{1}{2}\right)$, then a_ϵ is coercive.*

Proof. Equation (6.9) implies

$$\begin{aligned} a_\epsilon(\Psi,\Psi) &\geq \int_{K_h} \epsilon|\nabla\Psi|^2 dA - \omega_\infty \left(\int_{K_h} |\Psi\Psi_r| + |\Psi\Psi_z| dA \right) \\ &\geq \epsilon||\nabla\Psi||^2_{L^2(K_h)} - \omega_\infty \left(||\Psi||^2_{L^2(K_h)} + \frac{1}{2}||\Psi_r||^2_{L^2(K_h)} + \frac{1}{2}||\Psi_z||^2_{L^2(K_h)} \right) \\ &\geq \epsilon||\nabla\Psi||^2_{L^2(K_h)} - \omega_\infty \left(\gamma + \frac{1}{2} \right) ||\nabla\Psi||^2_{L^2(K_h)} \\ &= \left(\epsilon - \omega_\infty \left(\gamma + \frac{1}{2} \right) \right) ||\Psi||^2_{H^1_0(K_h)} \end{aligned} \tag{6.12}$$

Thus, coercivity follows if $\epsilon > \omega_\infty \left(\gamma + \frac{1}{2}\right)$. □

REMARK 6.11: Since the size of ϵ determines how much the solution departs from the strong solution outside of K_h, this result allows us to use a minimum amount of "smoothing" to achieve a consistent solution with the strong solution outside K_h.

LEMMA 6.12: *The functional*

$$F(\varphi) = \int_{K_h} f\varphi dA \tag{6.13}$$

is bounded and linear.

Proof. By definition, and the assumption that $\widehat{\Psi} \in H^1(K_h)$,

$$\begin{aligned} |F(\varphi)| \leq \int_{K_h} |f\varphi| dA &= \int_{K_h} \left| \nu r\beta\varphi + \epsilon\nabla\widehat{\Psi}\cdot\nabla\varphi + (\zeta\widehat{\Psi}_z + \eta\widehat{\Psi}_r)\varphi \right| dA \\ &\leq \left(||\nu r\beta||_\infty + (\epsilon + \gamma\omega_\infty)||\widehat{\Psi}||_{H^1(K_h)} \right) ||\varphi||_{H^1_0(K_h)}. \end{aligned} \tag{6.14}$$

Since F is clearly linear, we have that F is a bounded linear functional on $H^1_0(K_h)$. □

THEOREM 6.13 (Existence and Uniqueness of Solutions for Dirichlet Problem): *Let a_ϵ be defined as in (6.3), and let $\Psi_b \in C^1(\partial K_h)$ with $\widehat{\Psi} \in H^1(K_h)$ such that the trace of $\widehat{\Psi}$ is Ψ_b. Further, assume that ζ, η, and β are essentially bounded, and that*

$$\epsilon > \left(\gamma + \frac{1}{2}\right)\omega_\infty \tag{6.15}$$

Then there exists a unique function $\Psi \in H_0^1(K_h)$ such that

$$a_\epsilon(\Psi, \varphi) = F(\varphi) \qquad \forall \varphi \in H_0^1(K_h) \tag{6.16}$$

Proof. This follows immediately from Lemmas 6.9, 6.10, 6.12, and the Lax-Milgram Theorem. □

REMARK 6.14: Since we know ζ and η *a priori*, we can choose ϵ in advance to be no larger than necessary for well-posedness of the problem. This will ensure minimal departure from the advective flow present outside of the information void.

In addition, since we are enforcing the Dirichlet boundary condition Ψ_b, we will have a continuous joining of the streamfunction inside the information void and outside it as well. This does not imply that the velocities are continuous across the interface, since they are components of the gradient of Ψ.

6.3 Weak Solutions for the Neumann Problem

The theoretical considerations for (6.3) imply continuity of Ψ on ∂K_h, but not smoothness. Since u and w are components of the gradient of Ψ, continuity of

Ψ is not enough to ensure that the velocities will be continuous over the entire domain. After applying the characteristic method, we know the velocities u and w on $\Omega \setminus K_h$, which are only incorporated into the Dirichlet problem in an integral sense, since Ψ is an antiderivative of u and w.

Since ∂K_h is a characteristic curve, it is also a level curve of Γ. This means that the normal vector to ∂K_h is parallel to $\nabla\Gamma$. Since we know that Γ has an absolute maximum at $(r_o, z_o) \in K_h$, $\nabla\Gamma$ will be pointing inward toward (r_o, z_o). Thus the normal derivative of Ψ is given by

$$\frac{\partial\Psi}{\partial n} = \nabla\Psi \cdot -\frac{\nabla\Gamma}{|\nabla\Gamma|} = -\frac{\frac{\partial\Psi}{\partial r}\frac{\partial\Gamma}{\partial r} + \frac{\partial\Psi}{\partial z}\frac{\partial\Gamma}{\partial z}}{\sqrt{\left(\frac{\partial\Gamma}{\partial r}\right)^2 + \left(\frac{\partial\Gamma}{\partial z}\right)^2}} = -r\frac{\zeta w - \eta u}{\zeta^2 + \eta^2} \tag{6.17}$$

A Neumann formulation, rather than the Dirichlet formulation discussed in Section 6.2, would utilize the information about u and w on ∂K_h.

In deriving (6.3), we assumed that $\Psi \in H_0^1(K_h)$. For the Neumann problem, this assumption no longer holds. Define

$$g_b(t) = -r(t)\frac{\zeta(t)w_b(t) - \eta(t)u_b(t)}{\zeta^2(t) + \eta^2(t)} \tag{6.18}$$

to be the desired inhomogeneous Neumann boundary condition. If we multiply (6.1) by $\varphi \in H^1(K_h)$, integrate over K_h, the resulting expression is

$$\int_{K_h} \left[\epsilon\nabla\Psi \cdot \nabla\varphi + \zeta\Psi_z\varphi + \eta\Psi_r\varphi\right] dA = \int_{K_h} r\beta\varphi dA + \int_{\partial K_h} \epsilon g_b\varphi dt. \tag{6.19}$$

Note that the left hand side of (6.19) is a_ϵ as we defined it in Section 6.2, except that the domain of a_ϵ is now $H^1(K_h) \times H^1(K_h)$, and so we cannot use the Poincarè inequality to verify the requirements of the Lax-Milgram theorem.

REMARK 6.15: If $\Psi \in H^1(K_h)$ satisfies (6.19) for every φ, then so does $\Psi + C$, where $C \in \mathbb{R}$ is any constant, since the equation involves only the derivatives of Ψ. Since weak solutions are not unique, a_ϵ cannot be coercive on $H^1(K_h)$. This implies that we need to augment our weak formulation if we want a unique solution.

With the interests of existence and uniqueness in mind, we consider (6.1) with the addition of a small zeroth order term,

$$\epsilon \Delta \Psi + \zeta \Psi_z + \eta \Psi_r + \epsilon \Psi = r\beta. \tag{6.20}$$

and employ the same method as we used in Section 6.2. We now seek $\Psi \in H^1(K_h)$ which satisfies the weak form of this equation with Neumann conditions, given by

$$\int_{K_h} \left[\epsilon \nabla \Psi \cdot \nabla \varphi + \zeta \Psi_z \varphi + \eta \Psi_r \varphi + \epsilon \Psi \varphi\right] dA = \int_{K_h} r\beta \varphi dA + \int_{\partial K_h} \epsilon g_b \varphi dt. \tag{6.21}$$

Denote $\tilde{a}_\epsilon(\Psi, \varphi) := \int_{K_h} \left[\epsilon \nabla \Psi \cdot \nabla \varphi + \zeta \Psi_z \varphi + \eta \Psi_r \varphi + \epsilon \Psi \varphi\right] dA$. The next two propositions show that the problems of existence and uniqueness are solved with the addition of the small zeroth order term.

LEMMA 6.16 (Boundedness of $\tilde{a}_\epsilon$): *Suppose $\zeta, \eta \in L^\infty(K_h)$. Then the bilinear form $\tilde{a}_\epsilon : H^1(K_h) \times H^1(K_h) \to \mathbb{R}$ is bounded for every $\epsilon > 0$.*

Proof. Referring to the proof of Proposition 6.9, we can use the same estimates (without the Poincarè constant γ), together with the fact that if $\Psi \in H^1(K_h)$, then $\Psi, \Psi_r, \Psi_z \in L^2(K_h)$, and $||\Psi||_{L^2(K_h)} \leq ||\Psi||_{H^1(K_h)}$ (and similarly for the

spatial derivatives), and so

$$\tilde{a}_\epsilon(\Psi,\varphi) \leq (\epsilon + \frac{\omega_\infty}{2})||\Psi||_{H^1(K_h)}||\varphi||_{H^1(K_h)}. \tag{6.22}$$

Thus $\tilde{a}_\epsilon$ is bounded on $H^1(K_h) \times H^1(K_h)$. □

LEMMA 6.17 (Coercivity Criterion for $\tilde{a}_\epsilon$): *Suppose that $\zeta, \eta \in L^\infty(K_h)$. If $\epsilon > \omega_\infty$, then $\tilde{a}_\epsilon$ is coercive.*

Proof. Note that

$$\begin{aligned}
\tilde{a}_\epsilon(\Psi,\Psi) &\geq \epsilon \int_{K_h} \left(|\nabla\Psi|^2 + \Psi^2\right) dA - \omega_\infty \int_{K_h} |\Psi|(|\Psi_r| + |\Psi_z|)dA \\
&\geq \epsilon \int_{K_h} \left(|\nabla\Psi|^2 + \Psi^2\right) dA - \frac{\omega_\infty}{2} \int_{K_h} \left(2\Psi^2 + |\nabla\Psi|^2\right) dA \\
&\geq \int_{K_h} (\epsilon - \omega_\infty) \left(|\nabla\Psi|^2 + \Psi^2\right) dA \\
&= (\epsilon - \omega_\infty)||\Psi||_{H^1(K_h)}
\end{aligned}$$

Thus for $\epsilon > \omega_\infty$, $\tilde{a}_\epsilon$ is coercive. □

THEOREM 6.18 (Existence and Uniqueness of Solutions for the Neumann Problem): *Let $\tilde{a}_\epsilon$ be defined as in* (6.21)*. Further, assume that ζ, η, and β are essentially bounded, and that*

$$\epsilon > \omega_\infty \tag{6.23}$$

Then there exists a unique function $\Psi \in H^1(K_h)$ such that

$$a_\epsilon(\Psi,\varphi) = \int_{K_h} r\beta\varphi dA + \int_{\partial K_h} g_b\varphi dt \qquad \forall\varphi \in H^1(K_h) \tag{6.24}$$

Proof. The result follows from Lemmas 6.16, 6.17 and the Lax-Milgram theorem. □

REMARK 6.19: While Theorem 6.18 ensures continuity of the normal derivative of Ψ across ∂K_h, this is still not sufficient to enforce continuity of u and w between $\Omega \setminus K_h$ and K_h. The linear combination of the two velocities indicated by (6.18) will be continuous on ∂K_h (in the trace sense), but the velocities themselves may not be. That is, if we denote the solution of the Neumann problem by Ψ_ϵ, and the corresponding velocities by u_ϵ and w_ϵ, then we expect Ψ_ϵ to satisfy (6.18) where u_b and w_b will be the traces of u_ϵ and w_ϵ on ∂K_h. It does not follow that $u_\epsilon \to u_b$ or $w_\epsilon \to w_b$ as interior points approach the boundary ∂K_h. However, the continuity of this normal derivative is an improvement over the result of the Dirichlet problem, where we only had continuity of Ψ at the boundary.

6.4 Regularity of Weak Solutions

Evans (1998) contains several useful theorems that apply directly to the elliptic forms a_ϵ and $\tilde{a}_\epsilon$. Denote the generic second order elliptic partial differential operator on an open, bounded domain $U \subset \mathbb{R}^n$ by

$$Lu := -\sum_{i,j=1}^{n} a^{ij}(x) u_{x_i} u_{x_j} + \sum_{i=1}^{n} b^i(x) u_{x_i} + c(x)u \tag{6.25}$$

and the weak form associated to $Lu = f$ by

$$\alpha(u,v) = \int_U \left[\sum_{i,j=1}^{n} a^{ij}(x) u_{x_i} v_{x_j} + \sum_{i=1}^{n} b^i(x) u_{x_i} v + c(x) uv \right] dx = \int_U f v dx. \tag{6.26}$$

Then the following results hold.

PROPOSITION 6.20 (Smoothness of Solutions): *Suppose* $a^{ij}, b^i, c \in C^{m+1}(U)$, *and* $f \in H^{m+1}(U)$. *If* $u \in H^1(U)$ *satisfies* (6.26), *then* $u \in H^{m+2}_{loc}(U)$, *and for any strict subset* $V \subset\subset U$,

$$||u||_{H^{m+2}(V)} \leq C \left(||f||_{H^m(U)} + ||u||_{L^2(U)} \right) \tag{6.27}$$

Proof. See Evans (1998). □

COROLLARY 6.21: *Suppose* $a^{ij}, b^i, c \in C^\infty(U)$, *and* $f \in C^\infty(U)$. *If* $u \in H^1(U)$ *satisfies* (6.26), *then* $u \in C^\infty(U)$.

Proof. See Evans (1998). The proof uses the previous proposition, together with a particular case of the Sobolev inequalities. □

REMARK 6.22: These two results make no assumptions about boundary conditions, and so they will hold for either the Dirichlet or Neumann problems. They say that smoothness in v implies smoothness in Ψ, and hence in u and w. This implies that the velocities are smooth in the interior of K_H.

6.5 Extending the Domain of the Dirichlet Problem

Sections 6.2 and 6.3 detail different methods of attempting to seek a solution that deviates from the strong solutions as little as possible using an elliptic smoother of the form (6.1) or (6.20). Under assumptions on ϵ, the weak form of these problems have unique solutions on the interior of K_h. The solution of the Dirichlet problem agrees with the boundary data Ψ_b on ∂K_h, while the solution of the Neumann problem has a normal derivative (to ∂K_h) which agrees with the characteristic data, composed of a linear combination of u and w. Neither of these formulations ensures continuity of u and w across ∂K_h.

Assumption 6.2 says that R is large enough that $K_h \subset\subset \Omega$, and so by Assumption 6.1 there must be a $\delta > 0$ so that the set U_δ enclosed by the characteristic curve $\{(r,z) \in \Omega : \Gamma(r,z) = \Gamma(r_\zeta, h) - \delta\}$ is contained within the interior of Ω. The boundedness and coercivity results from Section 6.2 will hold for U_δ, with the replacement of the norms for functions defined on K_h by norms for functions defined on U_δ, and the Poincare constant $\gamma_\delta = \gamma(U_\delta)$. Thus we can assert the Lax-Milgram theorem to achieve well-posedness of the Dirichlet problem for (6.3) with data Ψ_b on ∂U_δ.

From Assumption 6.3 and the results in Chapter 5, we know that the set $U_\delta \setminus K_h$ is reachable by characteristics passing through $\partial\Omega_h^+$. This means that there is a function $\Psi_c \in C^1(U_\delta \setminus K_h)$ that agrees with the characteristic solution on the exterior of K_h, and which we can extend in a smooth fashion to Ψ_δ

defined on all of U_δ. Consider the functional given by

$$J_\delta(\Psi) = \frac{1}{2}||\Psi - \Psi_\delta||^2_{H^1(U_\delta)} \tag{6.28}$$

We calculate the first variation of J_δ. Let $\varphi \in H^1_0(U_\delta)$, and compute

$$i(t) = J_\delta(\Psi + t\varphi) = \frac{1}{2}\int_{U_\delta} \left[(\Psi + t\varphi - \Psi_\delta)^2 + |\nabla(\Psi - \Psi_\delta) + t\nabla\varphi|^2\right] dA, \tag{6.29}$$

from which it follows that

$$i'(t) = \int_{U_\delta} \left[(\Psi - \Psi_\delta - t\varphi)\varphi + (\nabla(\Psi - \Psi_\delta) + t\nabla\varphi)\cdot\nabla\varphi\right] dA. \tag{6.30}$$

Assuming that J_δ has a minimizer at Ψ we must have the $i'(0) = 0$, whence

$$\int_{U_\delta} \left[(\Psi - \Psi_\delta)\varphi + \nabla(\Psi - \Psi_\delta)\cdot\nabla\varphi\right] dA = 0, \tag{6.31}$$

which must be satisfied if Ψ is to be a minimizer of J_δ. With this in mind, we seek a function $\Psi \in H^1_0(U_\delta)$ which satisfies

$$a_\epsilon(\Psi, \varphi) + \left\langle \Psi 1_{U_\delta \setminus K_h}, \varphi \right\rangle_{H^1(U_\delta)} = \int_{U_\delta} f\varphi dA + \left\langle \Psi_\delta 1_{U_\delta \setminus K_h}, \varphi \right\rangle_{H^1(U_\delta)} \tag{6.32}$$

for all $\varphi \in H^1_0(U_\delta)$, where $1_{U_\delta \setminus K_h}$ is the indicator function for the region on which we have characteristic solutions. Denote $a_\delta(\Psi, \varphi) := a_\epsilon(\Psi, \varphi) + \left\langle \Psi 1_{U_\delta \setminus K_h}, \varphi \right\rangle_{H^1(U_\delta)}$.

THEOREM 6.23: *Let* $\zeta, \eta \in L^\infty(U_\delta)$, $\epsilon > \omega_\infty\left(\gamma_\delta + \frac{1}{2}\right) - 1$, *and* $\Psi_\delta \in H^1_0(U_\delta)$.

Then there exists a Ψ *such that*

$$a_\delta(\Psi, \varphi) = \int_{U_\delta} f\varphi dA + \left\langle \Psi_\delta 1_{U_\delta \setminus K_h}, \varphi \right\rangle_{H^1(U_\delta)} \tag{6.33}$$

for all $\varphi \in H_0^1(U_\delta)$.

Proof. Note that

$$\left\langle \Psi 1_{U_\delta \setminus K_h}, \Psi \right\rangle \geq ||\Psi||^2_{H^1(U_\delta)} \geq ||\Psi||^2_{H_0^1(U_\delta)} \tag{6.34}$$

which implies that

$$a_\delta(\Psi, \Psi) \geq \left(\epsilon - \omega_\infty \left(\gamma_\delta + \frac{1}{2} \right) + 1 \right) ||\Psi||^2_{H_0^1(U_\delta)}. \tag{6.35}$$

Hence a_δ is coercive, and the estimate in Lemma 6.9 together with the Poincare inequality imply that

$$a_\delta(\Psi, \varphi) \leq (\epsilon + (2\omega_\infty(U_\delta) + 1)\gamma_\delta + 1)||\Psi||_{H_0^1(U_\delta)}||\varphi||_{H_0^1(U_\delta)} \tag{6.36}$$

Thus a_δ is bounded. The operator

$$F_\delta(\varphi) = \int_{U_\delta} \left(f + \Psi_\delta 1_{U_\delta \setminus K_h} \right) \varphi dA \tag{6.37}$$

is clearly linear in φ, and is bounded since $f, \Psi_\delta, \varphi \in L^2(U_\delta)$ and $\Psi_\delta, \varphi \in L^2(U_\delta \setminus K_h)$. Therefore, the Lax-Milgram theorem provides the existence of $\Psi \in H_0^1(U_\delta)$ which satisfies (6.33). □

6.6 Discussion

The methods detailed in this chapter are elliptic "smoothers", meaning that they attempt to smoothly interpolate the boundary data into the interior of the information voids. The theory above discusses the existence and uniqueness theory relevant to each of these methods. Implementation of any of these methods is a complex problem due to the geometry of the region, which is an irregular closed curve. Generating finite elements for sets like K_h in an efficient and accurate manner is a topic of open research in the community that researches numerical methods for partial differential equations. One way that we could approach this is to use the locally orthogonal coordinate system that arises from the unit vectors proportional to $\nabla\Gamma$ and the vector tangent to the level curves of Γ.

Chapter 7

Accounting for Uncertainty

7.1 Introduction

In the previous chapters, we developed of a methodology for estimating the wind fields below a minimum observable height, using observations above this height to estimate parameters for a tangential velocity model, and then using the model equations (5.1) and (5.2) to extrapolate into the unobservable region in a dynamically consistent manner. All of the development has assumed a perfect model and perfect data. In this chapter, we discuss methods of minimizing the effects of both modelization error and measurement error in our data.

7.2 Smooth Dependence on Parameters

When the modelization of the problem is imperfect, or the data have errors which lead to a suboptimal choice of v, continuity of the solution map $v \mapsto (u, w)$ implies that small errors in v yield small errors in u and w. The results in Section 5.2.3 imply that we can consider the dependence of u and w on v using the characteristic differential equations, since the spatial dependence of

u and w are also determined by v, according to Lemma 5.3. We can adapt Theorems 10.7.1 and 10.7.2 of Dieudonne (1960), which discuss these systems of the form $\dot{x} = f(t, x, z)$, where z is a parameter vector. We are assuming $v \equiv v(q)$, and so the question is really whether the characteristic curves vary smoothly with q, and whether u and w are smooth functions of q along these curves. These results answer both questions in the affirmative, as long as v and its spatial derivatives are smooth on the space of parameters $\mathcal{Q}$.

THEOREM 7.1 (Dieudonne): *Let E be a Banach space over $\mathbb{R}$, $I \subset \mathbb{R}$ and $H \subset E$ be open subsets, $\mathcal{Q}$ a metric space, and f a mapping from $I \times H \times \mathcal{Q}$ into E. Suppose that*

(1) for any $q \in \mathcal{Q}$, $(t, x) \mapsto f(t, x, q)$ is continuously differentiable from $I \times H$ into E and

(2) f and $D_2 f$ are continuous in $I \times H \times \mathcal{Q}$.

Then for any point $(t_o, x_o, q_o) \in I \times H \times \mathcal{Q}$, there is an open $J \subset I$ centered at t_0 and $T \subset \mathcal{Q}$ centered at q_0 such that for each $q \in T$, there is a unique solution $t \mapsto x(t, q)$ of $\dot{x} = f(t, x, q)$ on J such that $x(t_0, q) = x_0$. Further, the mapping $(t, q) \mapsto x(t, q)$ is bounded and continuous in $J \times T$.

REMARK 7.2: For our case, the function f is the vector composed of the right hand sides of (5.4),(5.5), and one of (5.6),(5.18), and (5.14). For Theorem 7.1 to hold, we need ζ, η and their first and second order partial derivatives with respect to r and z to be continuously differentiable with respect to the parameters over $\mathcal{Q}$ for the entire spatial domain Ω. Since the distribution of characteristic curves $(r(q), z(q))$ are solutions of differential equations that satisfy the assumptions of the Theorem 7.1, these results apply to the global

solutions of the equations, in those regions where the characteristic solutions are uniquely defined. Hence there is a set $\widehat{\mathcal{Q}} \subset \mathcal{Q}$ such that the solution mapping $q \mapsto (u(r,z), w(r,z))$ restricted to $\widehat{\mathcal{Q}}$ is continuous.

Similar theorems of Dieudonne say that more smoothness in f with respect to the parameters yields more smoothness in u with respect to the parameters, up to analyticity.

7.3 Consistency with Observations

Recall that we have observations of the radial velocity u in the region $\Omega \setminus \Omega_h$. These observations contain random measurement errors, which together with our modelization errors imply the need for an "analysis" state which represents an optimal combination of the observations with the model constraints, weighted by their error characteristics.

First, assume that our tangential model for v has a single maximum at (r_o, z_o), and that $\nabla\Gamma \neq 0$ on $\Omega^o \setminus \{(r_o, z_o)\}$. Since we have characteristics passing through every point in $\Omega \setminus \Omega_h$, we can seek values of the radial velocity along $\partial\Omega_h^+$ so that when we solve for $u(t)$ along each characteristic curve (passing through $\Omega \setminus \Omega_h$) we attain a minimum value of some weighted combination of modelization and observation errors. This is precisely the data assimilation problem, though somewhat simplified, since initial conditions at different locations on $\Omega \setminus \Omega_h$ are completely independent of each other, since characteristic curves cannot cross.

7.3.1 Approximating the Observation Surface

Since our measurements are in the form of discrete volume averages of radial velocity, $\hat{u}_i$, at locations (r_i, z_i) for $i = 1, ..., N_{obs}$, we must construct an approximating function $u_o(r, z)$ for our observational data so that we can compare the observations with model solutions along characteristic curves.

Given a two dimensional array, there are many different ways we can approximate the surface which generated those points. In meteorology, this topic is known as "objective analysis". If we assume that the data are regularly spaced, then we can approximate the observation surface using tensor products of one dimensional functions, which leads to a tremendous speedup of the algorithms needed to compute the surface.

Interpolants exactly match the function values at the spatial locations of the data. One example which is pertinent to the discussion at hand is the bilinear interpolant, which is the tensor product of two sets of piecewise linear functions. This interpolant is monotone, meaning that the spatial derivatives of the interpolant are the same as the finite difference approximations from the data, and no spurious extrema are created. A bicubic interpolant is a tensor product of cubic splines, such as hermite splines, or cubic b-splines. These are not monotone interpolants, but they are smoother than the bilinear interpolant, and theoretical results assert that the L^2 approximation error is smaller than that of the bilinear interpolant.

We can apply regression techniques using a least-squares fit (or some other criterion) of data using a predetermined set of functions. The resulting approximation will not match the data at the spatial points, but is more robust with respect to errors in the data. If we select a Fourier (or Chebyshev) series

truncated at some $N << N_{obs}$, and then choose the coefficients of the series using least squares or some other criteria, then the resulting approximation will be a regression approximation of the data.

7.3.2 Optimal Initial Conditions for Negligible Observation Errors

Suppose that the errors in the data are negligible relative to the modelization errors. This amounts to choosing the initial values $u(0,s)$ or $\Psi(0,s)$ which most closely approximate the raw observations. Since $u(0,s_1)$ and $u(0,s_2)$ are independent for $s_1 \neq s_2$, we can find the minimizer for each s, and the result will be a global minimum.

PROPOSITION 7.3: *Assume that $\eta > 0$ on $\Omega \setminus \Omega_h$. Given $(s,h) \in \partial\Omega_h^+$, and $T(s) > 0$ the smallest value of t such that $c(T(s),s,h) \in \partial(\Omega \setminus \Omega_h)$, the value of $u(0,s)$ which minimizes the objective functional*

$$J_u(u(0,s)) = \frac{1}{2}\int_0^{T(s)} \left(u_o(r(t,s),z(t,s)) - u(t,s)\right)^2 dt \tag{7.1}$$

is given by

$$u(0,s) = \frac{\int_0^{T(s)} \left(u_o(r(t,s),z(t,s)) - \int_0^t g_u \exp\left[-\int_\tau^t f_u d\sigma\right] d\tau\right) \exp\left[-\int_0^t f_u d\tau\right] dt}{\int_0^{T(s)} \exp\left[-2\int_0^t f_u d\tau\right] dt}. \tag{7.2}$$

.

Proof. Assuming that $\eta > 0$ (so that (5.18) is valid), we can write the solution

of (5.18) as (5.19). Omitting s for simplicity, the objective functional is

$$\begin{aligned} J_u(u(0)) &= \frac{1}{2}\int_0^T \left(u_o(r(t),z(t)) - u(0)\exp\left[-\int_0^t f_u d\tau\right] - \right. \\ &\qquad \left. \int_0^t g_u \exp\left[-\int_\tau^t f_u d\sigma\right] d\tau \right)^2 dt \\ &= \frac{1}{2}\int_0^T \left(u_o(r(t),z(t)) - \int_0^t g_u \exp\left[-\int_\tau^t f_u d\sigma\right] d\tau \right)^2 dt - \\ &u(0)\int_0^T \left(u_o(r(t),z(t)) - \int_0^t g_u \exp\left[-\int_\tau^t f_u d\sigma\right] d\tau \right) \times \\ &\times \exp\left[-\int_0^t f_u d\tau\right] dt + (u(0))^2 \int_0^T \exp\left[-2\int_0^t f_u d\tau\right] dt \end{aligned}$$

The derivative of J with respect to $u(0,s)$ is

$$\begin{aligned} \frac{dJ}{du(0)} = -\int_0^T &\left(u_o(r(t),z(t)) - \int_0^t g_u \exp\left[-\int_\tau^t f_u d\sigma\right] d\tau \right) \times \\ &\times \exp\left[-\int_0^t f_u d\tau\right] dt + u(0)\int_0^T \exp\left[-2\int_0^t f_u d\tau\right] dt. \end{aligned}$$

Setting this to 0 and solving for $u(0,s)$, we get (7.2). This value of $u(0,s)$ is a minimum because J_u is quadratic in $u(0,s)$, and $\frac{d^2J}{du(0,s)^2} > 0$, since $\exp\left[-\int_0^t f_u d\tau\right] > 0$ for every t. □

REMARK 7.4: Since we know the characteristic curves in advance, we can calculate the optimal initial conditions *a priori* for each s using (7.2).

REMARK 7.5: We can discretize (7.2) by choosing a partition $\{t_o, t_1, ..., t_m\}$ of the interval $[0, T(s)]$, upon which the outer integrals become sums, and the

optimizer is given by

$$u(0,s) = \frac{\sum_{i=0}^{m} \left(u_o(r(t_i,s), z(t_i,s)) - \int_0^{t_i} g_u \exp\left[-\int_\tau^{t_i} f_u d\sigma \right] d\tau \right) \exp\left[-\int_0^{t_i} f_u d\tau \right] dt}{\sum_{i=0}^{m} \exp\left[-2\int_0^{t_i} f_u d\tau \right] dt}. \tag{7.3}$$

The inner integrals can be approximated using trapezoidal quadrature methods, in order to provide the most efficient calculation, since $t_i < t_j$ implies $[0, t_i] \subset [0, t_j]$.

REMARK 7.6: Similarly, $\Psi(t,s) = \Psi(0,t) + \int_0^t r\beta d\tau$, and our objective functional would be given by

$$J_\Psi(\Psi(0,s)) = \frac{1}{2} \int_0^{T(s)} \left(\Psi(0,s) + \int_0^t r\beta d\tau - \Psi_o(r(t,s), z(t,s)) \right)^2 dt. \tag{7.4}$$

Differentiating with respect to $\Psi(0,s)$, setting the derivative to 0, and solving for $\Psi(0,s)$, we see that

$$\Psi(0,s) = \frac{1}{T(s)} \int_0^{T(s)} \left(\Psi_o(r(t_i,s), z(t_i,s)) - \int_0^t r\beta d\tau \right) dt \tag{7.5}$$

which says that the optimal initial value for the streamfunction problem is the mean of the deviations of the predictions from the observation interpolant, which is exactly what we would expect, since $\Psi(0,s)$ plays the role of an "intercept", with the rest of the behavior of Ψ being totally determined by v and its derivatives.

REMARK 7.7: We could extend this technique to the case where the observations are not considered error free using either uncorrelated error variances for

each observation, or an observation error covariance matrix which contains the quantified correlations between the observations' errors. The resulting minimum will be similar in spirit to the solutions presented above, and a more general discussion of this topic can be found in Lakshmivarahan et al. (2006).

7.4 Uncertain Outer Radial Boundary Conditions

From the results in Chapters 5 and 6, for a specified h, we can find a unique u, v, and w which satisfy the model equations and approximately match the observations (using the results in Section 7.3), if we assume that K is bounded by a characteristic curve. This means that if $K_h \cap \{(R, z) : 0 < z < h\}$ is a set of positive measure, then the problem is not completely solved.

One solution is take a Neumann condition at this outer radial boundary. Since the normal is the radial unit vector $\vec{i_r}$, this is equivalent to assuming the $\frac{\partial \Psi}{\partial r} = 0$, and hence that $w(R, z) = 0$, which may not be physically realistic if the tornado in embedded in a larger scale storm updraft. We could also take a nonzero Neumann condition that we believe to represent the strength of the storm scale updraft, perhaps estimated from aloft and assuming a linear decrease to the ground level.

7.5 Probabilistic Estimation of u and w

Recall we denoted the space of admissible parameters $\mathcal{Q}$. We now consider this as a space of random vectors q that take their values in $\mathbb{R}^p$. The sampling method is discussed in Tarantola (2005). The posterior pdf $\sigma_{\mathcal{Q}}(q)$ is given by

the formula (4.5). From Chapter 5, we know that each choice of q maps to a unique set of characteristic curves that are the level curves of the circulation $\Gamma(r, z, q)$. In addition, every characteristic which passes through the MOH line will have data that can be used to find u and w. Denote this mapping $A : \mathcal{Q} \to H^2(\Omega_h) \times H^2(\Omega_h)$. If we compute $A(q) = (u(q), w(q))$ for every $q \in \mathcal{Q}$, we have a collection of velocity fields that represent the range of the map $q \mapsto (u, w)$. Each of these realizations (u_o, w_o) also can be attached to the density value $\sigma_{\mathcal{Q}}(q_o)$ of its preimage $A^{-1}(u, w) \in \mathcal{Q}$. In this case we can define a density $\sigma(u, w) = \sigma_{\mathcal{Q}}(A^{-1}(u, w))$, and compute statistics for the collection of velocity fields (u, v, w) associated to this distribution using the moments derived from this density.

Of course we cannot examine the velocity field for each parameter vector q. With a limited set of computational resources, the best we can hope for is a large, finite sample of parameter vectors that capture the characteristics of the density $\sigma_{\mathcal{Q}}$, such as its maximum likelihood estimator, mean and variance. If our set $\mathcal{Q}$ is compact, then a uniformly spaced sample will capture these properties if the resolution of the sample is fine enough. Partition the space $\mathcal{Q} = \bigcup_{i=1}^{m} Q_i$, where $Q_i \bigcap Q_j = \emptyset$ when $i \neq j$, and denote the volume of Q_i by $V(Q_i)$. Then we can replace our continuous density with a discrete one:

$$\sigma_{\mathcal{Q}}(q) \approx \sum_{i=1}^{N_q} \sigma_{\mathcal{Q}}(q_i)\chi_{Q_i}(q) \tag{7.6}$$

With this discretization, our probability density function becomes a probability mass function (pmf), with the interpretation that $\mathcal{P}\{q = q_i\} = \sigma_{\mathcal{Q}}(q_i)V(Q_i)$, and $\mathcal{P}\{u(q) = u(q_i), w(q) = w(q_i)\} = \sigma_{\mathcal{Q}}(q_i)V(Q_i)$. Using this pmf, we can calculate the moments of the distribution of the velocities. This approach is

similar to the way that the ensemble Kalman filter (EnKF) approximates the error covariance necessary to assimilate the next time period of observations with the model forecast, though we are using agreement with the observations as a weighting, so that we don't use a uniform pmf to calculate the covariance.

Once we have discretized the pdf, we have to consider how much computational cost we can afford for calculating the forward solutions of the characteristic ODEs for a given resolution. If we denote the discretized sample space as $\mathcal{Q}^{N_q}$, the computation of the range of $A(\mathcal{Q}^{N_q})$ is a "perfectly parallel" problem, since for each realization q, the wind field $(u(q), w(q))$ can be computed independently of all of the others. Further, since $\mathcal{Q}^{N_q}$ is a finite set, we can rank these vectors by the corresponding pmf values, and choose the n_q most likely (largest pmf values) for which to compute the image wind fields (u, v, w). In this way, we can estimate how much of the variability we are capturing by summing the corresponding probabilities.

From Chapter 5, we know that for the case that we have extrema in the circulation below the MOH line, we will have information voids such that the points within these sets will not have a unique solution flowing from observational data above. Without the addition of more information or techniques, this makes quantities like the mean and variance of the velocity fields less meaningful, since they will not be directly comparable at all grid points. A comparison on the gridpoints all of the realizations share is meaningful, but likely will leave out interesting features. For this reason, it makes sense to compare random variables without spatial dependence defined on the velocities, such as maximum absolute wind speed. We can assign any such random variable $F(u, v, w)$ the distribution $\sigma_{\mathcal{Q}}(q)$ in the same way that we assigned the distribution to the velocities, and in this way calculate statistics. These

statistics are a way of distilling the information contained in each realization of the parameter space into a useful quantity.

7.6 Summary

The topics in this chapter were chosen for their relevance to the topic at hand, and more generally to any situation where data and models are being used in conjunction with one another. The results about continuity of the solution map $q \mapsto (u, v, w)$ limits the sensitivity of the solutions to small errors in the selection of the optimal parameter vector. The discussion in Section 7.3.2 demonstrates a simple algorithm for maximizing the ability of our method to make predictions in agreement with the observations. Section 7.4 points out a few difficulties when $K_h \cap \partial\Omega_h \neq \emptyset$. Finally, Section 7.5 provides a framework for estimating how the uncertainty in the optimal choice of parameter vector q translates to uncertainty in the estimated wind fields u and w, by way of the probability density function $\sigma_{\mathcal{Q}}(q)$ on $\mathcal{Q}$. Certainly more could be discussed, but these topics give a brief overview of the types of issues we must face with random errors in our data.

Chapter 8

Numerical Experiments

8.1 Introduction

In this chapter, we examine the performance of the retrieval methodology described in the previous chapters. The experiments we will perform will test how the methodology responds with respect to changes in the height h that dictates what features of the wind field we can see, as well as how the retrieval quality varies with different amounts of noise added to the data. In the first section, we will discuss the generation of pseudo-observations with which to test the method. The second section will demonstrate the results proved in Chapter 5 regarding information voids and near surface observability. The third section will explore the effects of errors in the observations on the retrieval, and will include the estimation of random variables defined on the wind fields.

8.2 Generation of Pseudo-Observations

As a first test of the methodology, a set of pseudo-observations was generated using a "snapshot" of model output of the Davies-Jones axisymmet-

ric thunderstorm model, which is described in Davies-Jones (2008). The relative maximum in the tangential wind velocity of $v_c = 75.129\frac{m}{s}$ occurs at $(r_c, z_c) = (462m, 504m)$, and the model fields were all made nondimensional by dividing the fields by v_c. A Wood-White tangential wind field $v = \phi_{ww}(r, n_r, 1)\phi_{ww}(z, n_z, 1)$ was fit to the cross sections of the model data lying on the lines $r = r_c$ (for n_z) and $z = z_c$ (for n_r). The resulting parameters are $n_r = 3.2$ and $n_z = 2.5$, when the data to be fit are taken to be the lowest square kilometer. The tangential wind velocity v and corresponding circulation Γ are shown in Figure 8.1. Taking $\nu = 0$, the streamfunction Ψ was computed on the domain $\Omega = [0, 4] \times [0, 4]$ by integrating the model output values for the vertical velocities along the height where the tangential velocity achieved its relative maximum to calculate Ψ along this line, and then by finding the point on this line with identical circulation to the point of interest. Since $\nu = 0$, the results in Chapter 5 show that Ψ is constant on characteristics. The corresponding radial and vertical velocities were estimated by using second order centered finite differences to estimate the partial derivatives of Ψ. The resulting velocity fields are depicted in Figure 8.3. Notice that in sign and in magnitude, the retrieved u and w approximate the model fields to a fair degree. The inflow location and strength are approximately the same as that of the Davies-Jones model data, and the size and strength of the updraft are also very similar to the model data.

8.3 Impacts of the Minimum Observable Height

We are interested in examining the performance of the methodology for strong solutions when the minimum observable height h is varied from 1 to 4. The

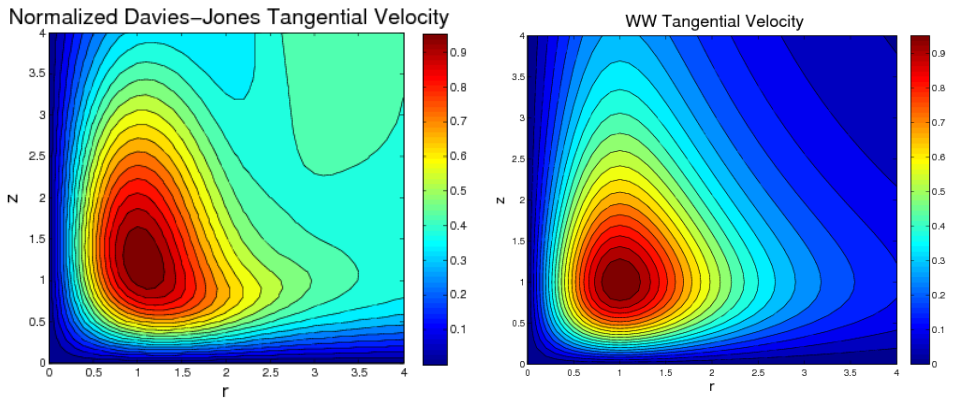


Figure 8.1: Normalized Davies-Jones tangential velocity and Wood-White tangential velocity model.

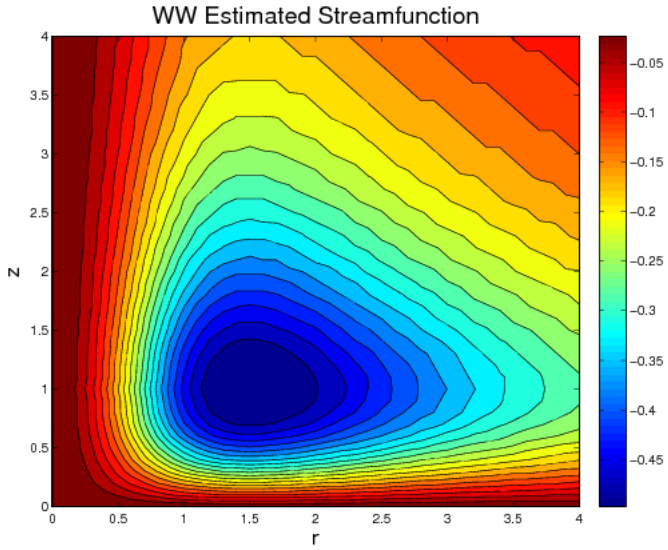


Figure 8.2: Pseudo-observations of streamfunction derived from the Davies-Jones model data

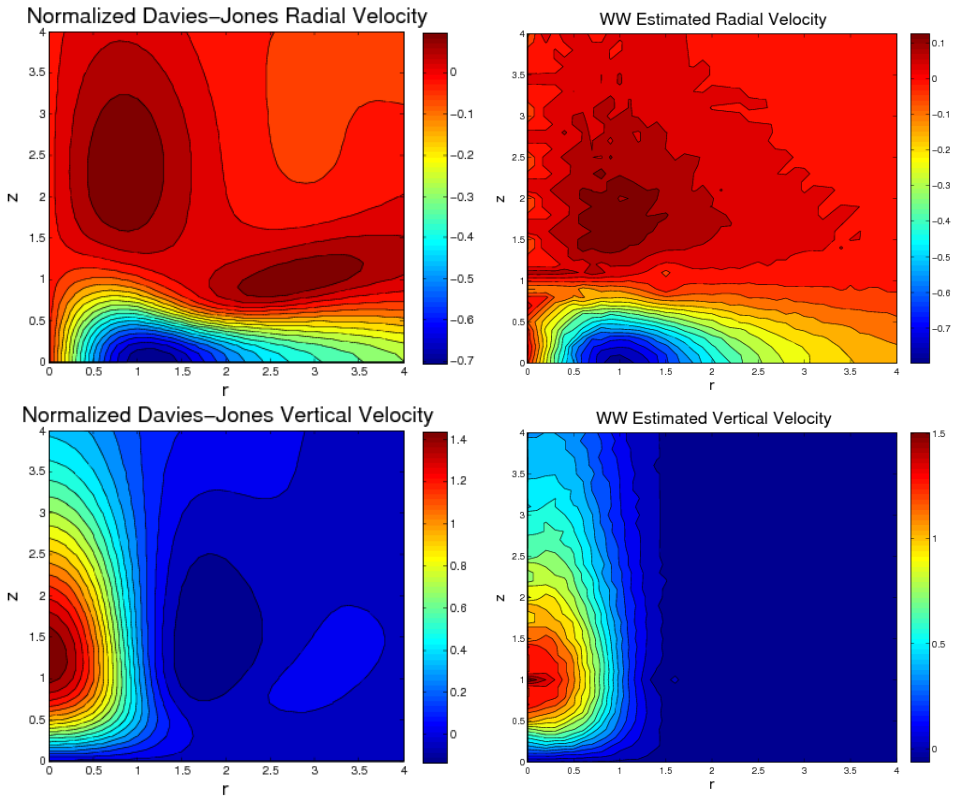


Figure 8.3: Normalized Davies-Jones radial and vertical velocities (left) and pseudo-observations of radial and vertical velocities derived from the stream-function in Figure 8.2.

normalized h	normalized h_o	$100m$ h_o
1.25	0.793	79.3
1.50	0.648	64.8
1.75	0.541	54.1
2.00	0.459	45.9
3.00	0.270	27.0
4.00	0.181	18.1

Table 8.1: Pairing of minimum observable height h and minimum unreachable height h_o. Normalized h_o is in units of z_c, while $100m$ h_o is for $z_c = 100m$.

height h_o below which everything is retrievable using the characteristic methodology can be calculated *a priori* using the equation

$$\phi_{ww}(h_o, n_z, z_c) = \phi_{ww}(h, n_z, z_c). \tag{8.1}$$

This computation was performed for values of h, and the results are presented in Table 8.1. As the relevant theoretical work states, a larger value for h corresponds to a smaller value for h_o, and so when we have less observational data, we cannot retrieve as high above the ground with the characteristic method.

8.4 Impacts of Random Errors

We are interested in the effects of measurement errors on all aspects of wind field estimation. The initial problem of estimating v in the presence of errors was discussed in Chapter 4, while the problem of estimating the resulting distribution of radial and vertical velocities via sampling was discussed in Chapter 7. Supposing that our observational error has a standard deviation of $1\frac{m}{s}$, which after rescaling by v_c corresponds to 0.013, we can calculate the wind fields we retrieve that arise from parameter vectors that yield tangential

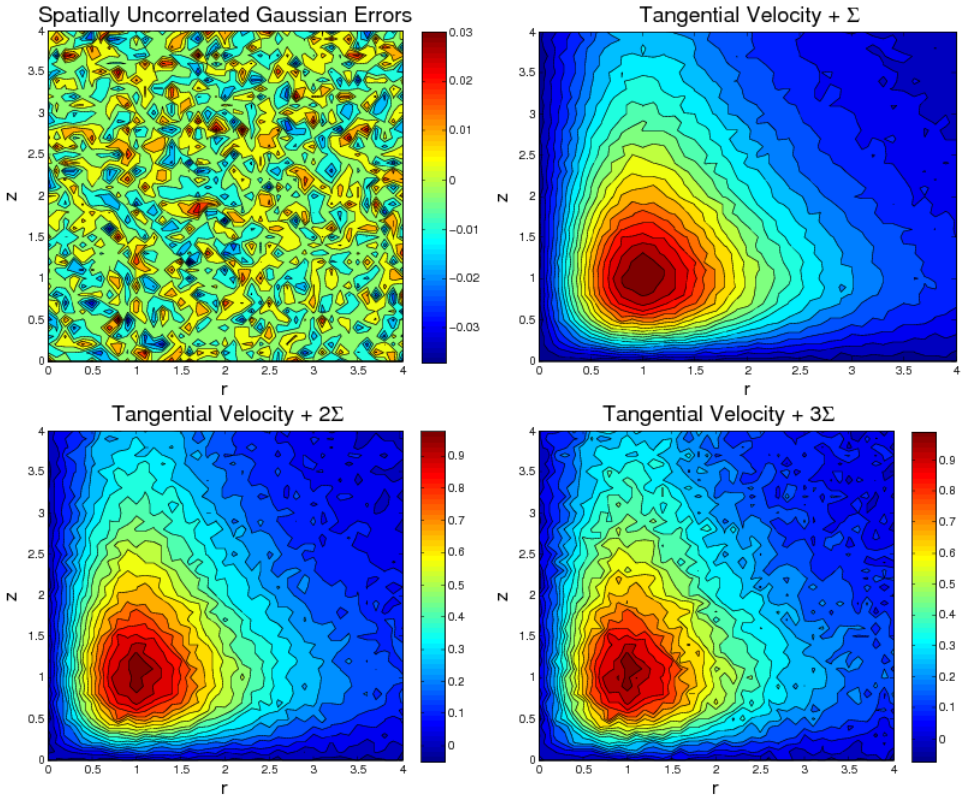


Figure 8.4: A realization Σ of an uncorrelated discretized Gaussian error distribution with covariance $\sigma^2 I$ ($\sigma = 0.103$), and the sum of the Wood-White v from Figure 8.1 with Σ, 2Σ, and 3Σ.

velocities that lie within this tolerance in an L^2 sense or an L^∞ sense. Figure 8.4 shows a realization of an uncorrelated Gaussian error distribution with standard deviation 0.013 and the sum of our idealized tangential velocity with multiples of this random error.

8.4.1 Estimating the Tangential Velocity

First, we determine how well the least-squares fitting procedure can recover the tangential velocity parameters, assuming different minimum observable heights h. This minimization is done in via the sampling method, meaning we sample a discretized version of the sample space $\mathcal{Q}$ which is the Cartesian

product of intervals which represent reasonable ranges for each parameter. Table 8.2 shows the variability of estimating the five parameters when we vary the minimum observable height and the amount of random error in the tangential velocity observations.

8.4.2 Physical Quantities of Interest

The sampling procedure for estimating u, v and w as random variables over $\mathcal{Q}$ is a useful means of determining the impacts of random observation error on the solutions. Unfortunately, we know that the information voids K_h are intimately linked to the parameters for v, and so the location and size of K_h will vary with each choice of $q \in \mathcal{Q}$. To remedy this, we can distill the information contained in the strong solutions u, v, and w into real valued random variables that depend on the velocities, but not on the spatial variables directly.

One quantity of interest is the *maximum inflow speed*, defined as

$$u^+ = \min_{z \leq z_c} u(r, z) \tag{8.2}$$

and the physical location where this occurs, denoted $x_{mif} = (r_{mif}, z_{mif})$, where $u(r_{mif}, z_{mif}) = u^+$. It might occur that x_{mif} is not unique. These quantities tell us where we should expect the air flowing into the tornado near the surface to be the strongest, since the literature tells us that radial flow will dominate the energy budget in this part of the vortex.

Another quantity we are interested in is the *maximum updraft speed*, defined

as

$$w^+ = \max_{r \leq r_c} w(r, z) \tag{8.3}$$

and x_{mud}, which is where the vertical velocity achieves its maximum. We expect this maximum to occur along the axis of the tornado, above the corner flow region for our test case, since we are working with a single-celled vortex (Snow (1982)).

A third random variable of interest to structural engineers is the *maximum absolute wind speed*, given by

$$|\vec{v}|_{\max} = \max_{(r,z)\in\Omega} \sqrt{u^2 + v^2 + w^2} \tag{8.4}$$

together with its maximizer x_{maw}. This quantity is equivalent to the maximum kinetic energy per unit mass in the physical domain. Kinetic energy is a part of Bernoulli's constant, which is conserved for our (inviscid) problem on streamlines. If we neglect gravitational effects, and assume a constant density, we can estimate the maximum pressure drop near the surface using pressure and velocity measurements aloft and the equation

$$\frac{1}{2}\sqrt{u^2 + v^2 + w^2} + \frac{p}{\rho} = Const \tag{8.5}$$

where the the constant depends on the streamline.

8.4.3 Distributions of Physical Quantities from Sampling

We examine here the effect of different sizes of random error, as measured by the standard deviation of the normal distribution from which it is drawn, on real valued random variables defined on the velocities, such as maximum absolute wind speed. For the purposes of these tests, we will consider only strong solutions, and hence not include the effects of the void filling techniques discussed in Chapter 6 on the solutions. This is reasonable, since the elliptic formulations will achieve their extrema on the boundaries of K_h, and hence will not alter distributions for the random variables such as maximum absolute wind speeds.

The results detailed in the tables below were computed as follows. The set $\mathcal{Q} = \mathcal{Q}_{v_c} \times \mathcal{Q}_{n_r} \times \mathcal{Q}_{n_z} \times \mathcal{Q}_{r_c} \times \mathcal{Q}_{z_c}$, where

$$\mathcal{Q}_{v_c} = [0.3, 2], \tag{8.6}$$

$$\mathcal{Q}_{n_r} = [1.5, 4.5], \tag{8.7}$$

$$\mathcal{Q}_{n_z} = [1.5, 4.5], \tag{8.8}$$

$$\mathcal{Q}_{r_c} = [0.3, 2], \text{and} \tag{8.9}$$

$$\mathcal{Q}_{z_c} = [0.3, 2]. \tag{8.10}$$

$\mathcal{Q}$ was sampled uniformly with a spacing of 0.1 in each component space, and the resulting collection of vectors $\{\vec{q}_i\}_{i=1}^{N_q}$ ($N_q > 5.5 \cdot 10^6$ for each h) were used to specify a set of admissible tangential velocities $\{v_i(r,z)\}_{i=1}^{N_q}$. The observable

domain $\Omega \setminus \Omega_h$ was discretized with a grid $\{(r_j, z_j)\}_{j=1}^{N_g}$, and the cost functional

$$J_h(v_i) = \sum_{i=1}^{N_g} (v_i(r_j, z_j) - v_o(r_i, z_j))^2 \tag{8.11}$$

was evaluated for each v_i, where v_o is the true v plus some multiple of Σ. Following Tarantola (2005), we define a probability distribution on the admissible velocities via

$$p_h(v_i) = \exp\left[-J(v_i)\right] \tag{8.12}$$

which allows us to discuss the outcomes of our retrievals in probabilistic language. We view the minimizer $\hat{v}$ of J_h as the *maximum likelihood estimator* of p_h. Since v_o contains errors, $\hat{v}$ will not necessarily represent the "true" tangential velocity. Since the space of admissible velocities is finite, we can rank them in order of descending likelihood $p_h(v_i)$, and use this distribution to weight the retrieved velocities u_i and w_i. Using these weights we can compute means and standard deviations for u^+, w^+ and $|\vec{v}|_{\max}$ and compare for different error standard deviations and values of h. Results for $h = 1, 1.2, 1.5, 1.7, 2, 2.5, 3, 3.5$ and for uncorrelated Gaussian errors with standard deviation σ, 2σ and 3σ ($\sigma = 0.103$) are given below. Table 8.3 shows the ensemble mean parameters for different values of h and errors, to compare with Table 8.2.

8.4.4 Discussion

The conclusions of the theoretical results in Chapter 5 are demonstrated in Figures 8.5-8.13, where in general, increasing h increases the volume of the information void K_h, represented in white. The relationship in the figures isn't

Optimal Parameters							
σ							
h	v_c	n_r	n_z	r_c	z_c	$\Omega \setminus \Omega_h$ error	Ω error
1	1	3.2	2.5	1	1	2.93e-5	0.00003
1.2	1	3.2	2.5	1	1	2.96e-5	0.00003
1.5	1	3.2	2.5	1	1	2.95e-5	0.00003
1.7	1	3.2	2.5	1	1	3.00e-5	0.00003
2	1	3.2	2.5	1	1	2.95e-5	0.00003
2.5	1	3.2	2.5	1	1	3.01e-5	0.00003
3	1	3.2	2.5	1	1	2.92e-5	0.00003
3.5	1.1	3.2	2.6	1	1	3.60e-5	0.0004
2σ							
h	v_c	n_r	n_z	r_c	z_c	$\Omega \setminus \Omega_h$ error	Ω error
1	1	3.2	2.5	1	1	2.29e-4	0.0002
1.2	1	3.2	2.5	1	1	2.31e-4	0.0002
1.5	1	3.2	2.5	1	1	2.31e-4	0.0002
1.7	1	3.2	2.5	1	1	2.34e-4	0.0002
2.0	0.9	3.2	2.5	1	1.1	4.22e-4	0.0012
2.5	1.8	3.2	2.4	1	0.6	2.34e-4	0.045
3.0	0.8	3.3	2.5	1	1.2	2.25e-4	0.0043
3.5	1.9	3.2	2.6	1	0.7	2.81e-4	0.0559
3σ							
h	v_c	n_r	n_z	r_c	z_c	$\Omega \setminus \Omega_h$ error	Ω error
1	1	3.2	2.5	1	1	5.16e-4	0.0005
1.2	1	3.2	2.5	1	1	5.21e-4	0.0005
1.5	1	3.2	2.5	1	1	5.14e-4	0.0005
1.7	1	3.1	2.5	1	1	5.36e-4	0.0005
2.0	1.6	3.2	2.3	1	0.6	5.28e-4	0.0288
2.5	0.7	3.2	2.8	1	1.5	5.25e-4	0.0119
3.0	0.7	3.2	2.8	1	1.5	5.14e-4	0.0119
3.5	1.2	3.2	2.1	1	0.6	6.52e-4	0.0084

Table 8.2: Optimal parameters versus h for error with standard deviation σ, 2σ and 3σ.

Ensemble Mean Parameters							
σ							
h	v_c	n_r	n_z	r_c	z_c	$\Omega \setminus \Omega_h$ error	Ω error
1	1	3.2	2.5	1	1	3.00e-5	0.00004
1.2	1.1	3.2	2.4	1	0.9	4.53e-5	0.0002
1.5	1.2	3.2	2.4	1	0.9	1.88e-4	0.0014
1.7	1.2	3.2	2.5	1	0.9	2.73e-4	0.0017
2	1.1	3.2	2.6	1	1	3.85e-4	0.0009
2.5	1.1	3.2	2.7	1	1.1	4.42e-4	0.0007
3	1	3.2	2.6	1	1.2	4.50e-4	0.0007
3.5	1	3.2	2.7	1	1.2	3.13e-4	0.0009
2σ							
h	v_c	n_r	n_z	r_c	z_c	$\Omega \setminus \Omega_h$ error	Ω error
1	1.1	3.3	2.4	1	0.9	1.17e-4	0.00009
1.2	1.1	3.2	2.4	1	0.9	4.35e-4	0.0021
1.5	1.2	3.2	2.5	1	0.9	6.25e-4	0.0022
1.7	1.1	3.2	2.6	1	1	8.13e-4	0.0016
2.0	1	3.2	2.7	1	1.1	8.59e-4	0.001
2.5	1	3.2	2.7	1	1.2	9.03e-4	0.0014
3.0	1	3.2	2.6	1	1.2	9.41e-4	0.0016
3.5	1	3	2.8	1	1.2	7.11e-4	0.003
3σ							
h	v_c	n_r	n_z	r_c	z_c	$\Omega \setminus \Omega_h$ error	Ω error
1	1.1	3.1	2.5	1	0.9	4.31e-4	0.0009
1.2	1.1	3.1	2.6	1	1	4.81e-4	0.0006
1.5	1	3	2.7	1.1	1	5.09e-4	0.0006
1.7	1	3	2.6	1	1.1	5.05e-4	0.0006
2.0	1	3	2.6	1	1	5.27e-4	0.0006
2.5	1	2.9	2.6	1	1.1	5.01e-4	0.0008
3.0	1	2.9	2.7	1.1	1.1	4.93e-4	0.0012
3.5	1	2.9	2.7	1.1	1.1	5.07e-4	0.0017

Table 8.3: Ensemble mean parameters versus h for error with standard deviation σ, 2σ, and 3σ.

Optimal and Ensemble Mean Values of u^+, w^+, and $\|\vec{v}\|_{\max}$						
σ						
	u^+		w^+		$\|\vec{v}\|_{\max}$	
h	MLE	Ens Mean	MLE	Ens Mean	MLE	Ens Mean
1	-0.810	-0.829	1.652	1.653	1.653	1.654
1.5	-0.766	-1.228	1.336	1.576	1.338	1.678
2	-0.473	-1.086	1.111	1.564	1.158	1.642
2.5	-0.454	-0.957	1.074	1.444	1.125	1.542
3	-2.261	-0.947	2.400	1.398	2.400	1.522
3.5	-2.196	-0.915	2.459	1.388	2.459	1.538
2σ						
	u^+		w^+		$\|\vec{v}\|_{\max}$	
h	MLE	Ens Mean	MLE	Ens Mean	MLE	Ens Mean
1	-0.810	-0.978	1.653	1.671	1.653	1.703
1.5	-0.766	-1.279	1.336	1.598	1.337	1.724
2	-0.755	-1.080	1.400	1.514	1.428	1.600
2.5	-0.455	-0.961	1.074	1.431	1.125	1.535
3	-0.383	-0.943	0.963	1.373	1.051	1.512
3.5	-0.324	-0.883	0.899	1.402	1.034	1.541
3σ						
	u^+		w^+		$\|\vec{v}\|_{\max}$	
h	MLE	Ens Mean	MLE	Ens Mean	MLE	Ens Mean
1	-0.777	-1.038	1.653	1.680	1.653	1.722
1.5	-0.762	-1.035	1.336	1.498	1.337	1.552
2	-0.755	-0.973	1.398	1.471	1.428	1.522
2.5	-2.066	-0.930	2.237	1.396	2.238	1.486
3	-0.516	-0.908	1.123	1.371	1.148	1.478
3.5	-0.981	-1.025	1.219	1.235	1.256	1.457

Table 8.4: Comparison of Maximum Likelihood Estimator (MLE) and Ensemble Mean values of u^+, w^+ and $|\vec{v}|_{\max}$.

exactly comparable, since we are using the maximum likelihood estimator parameter values for each subset of observations, which are different for different values of h. Also, note that even though it appears that the voids reach to the surface, this is merely an artifact of solving the problem on a grid with a particular resolution. Were we to increase the resolution of the spatial grid, the retrievable heights h_o would become apparent.

The numerical experiments support the logical conclusion that fewer observations (larger h) and more error (larger standard deviation) both lead to degraded results. A more interesting result is that the ensembles with less a priori information (larger h) predict weaker velocities near the surface than do the ensembles closer to the relative maximum of the tangential velocity. Examining Table 8.2, there seems to be a tradeoff between the maximum core velocity v_c and the core height z_c, which is to say that these two values move in opposite directions along a contour of our cost functional. For example, when the error level is 3σ, spikes in the v_c parameter are accompanied by decreases in the z_c parameter, and vice versa. There is also some correlation with the n_z parameter and these other two, indicating some sensitivity in the results to the selection of these parameters. Certainly, v_c and z_c play a role, which can be seen using a heuristic argument involving Bernoulli's principle, since z_c alters the width of the "channel" through which the inflow is squeezed. Looking at the distributions of u^+, w^+ and $|\vec{v}|_{\max}$, we see that the mode of these three parameters moves closer to zero as h increases. The cause of this behavior is unclear, though we could speculate that this weakening is due to predicting larger core heights z_c than the true z_c, which by Bernoulli's principle would lead to a weaker inflow and a correspondingly weaker updraft.

Examining the differences between maximum likelihood estimator results

and ensemble mean results, we can see that the ensemble mean for both estimated model parameters and for wind speed maxima are less sensitive to errors in the data than than the corresponding maximum likelihood estimator values. For example, in the 3σ error portion of Table 8.4, when $h = 2.5$, the MLE wind maxima are greatly overestimated due to some strong random error present in the observation field for this level, while the ensemble means are about the same as for the other heights and error levels. In addition, the observable domain $(\Omega \setminus \Omega_h)$ errors in the tangential wind field are of the same order of magnitude for both the MLE and ensemble mean, but when we compare errors over the entire domain Ω, we see that not only are the errors at individual heights h improved when we use ensemble mean parameters, but the progression of errors as h increases makes more logical sense, that is, the errors increase as h increases, while the optimal parameter errors show no discernible pattern. This is evidence that in a situation utilizing real data, using ensemble mean parameters might help us to better hedge against uncertainty due to errors in both modelization and observations.

8.5 Approximating Weak Solutions of the Elliptic Problem

For completeness, we consider the perturbed elliptic problem from Section 6.5, with the domain extended to $U_h \supset K_h$, and Ψ_c defined to be the characteristic solution on $U_h \setminus K_h$. We choose U_h to be the smallest rectangle in the discretized space that properly contains K_h, so that we can use a simple tensor product finite element basis. Under the assumptions in this chapter, the boundary

values at $r = R$ are given by the characteristic solutions, and so with a proper choice of ϵ, (6.32) has a unique solution.

8.5.1 Discretized Problem and Solutions

Discretize the solution $\hat{\Psi}_\epsilon(r,z) \approx \sum_{i=1}^{N_e} \beta_i b_i(r,z)$, the characteristic data as $\hat{\Psi}_c(r,z) \approx \sum_{i=1}^{N_e} \beta_i^c b_i(r,z)$ and define

$$\hat{a}_\epsilon(\hat{\Psi}_\epsilon, b_j) = \sum_{i=1}^{N_e} \beta_i \int_{U_h} \left[\epsilon \nabla b_i \cdot \nabla b_j + b_j(\eta,\zeta) \cdot \nabla b_i\right] dA \tag{8.13}$$

$$\hat{a}_\delta(\hat{\Psi}_\epsilon, b_j) = \hat{a}_\epsilon(\hat{\Psi}_\epsilon, b_j) + \sum_{i=1}^{N_e} \int_{U_h} \left[b_i b_j + \nabla b_i \cdot \nabla b_j\right] 1_{U_h \setminus K_h} dA \tag{8.14}$$

$$\hat{F}(\varphi) = \int_{U_h} r\nu(\zeta_r - \eta_z) b_j dA + \sum_{i=1}^{N_e} \beta_i^c \int_{U_h} \left[b_i b_j + \nabla b_i \cdot \nabla b_j\right] 1_{U_h \setminus K_h} dA. \tag{8.15}$$

Note that this places the requirement for enforcing the boundary conditions on the characteristic solution Ψ_c, since there are no terms in $\hat{F}$ corresponding to boundary conditions. Since we assumed that $K_h \subset U_h^o$, our problem will be equivalent to the one where we include these terms, since they are present in the characteristic solution.

For our problem all of these operators can be written in terms of tensor products, since both the vorticities and solution basis functions are products

of one dimensional functions:

$$\zeta(r,z) = \left(\partial_r\phi(r) + \frac{1}{r}\phi(r)\right)\psi(z) \tag{8.16}$$

$$\eta(r,z) = -\phi(r)\partial_z\psi(z) \tag{8.17}$$

$$b_i(r,z) = \ell_i(r)\tilde{\ell}_i(z) \tag{8.18}$$

With this in mind, define the following matrices:

$$A_{ji} = \int_0^R \frac{d\ell_i}{dr}\frac{d\ell_j}{dr}dr \int_0^H \tilde{\ell}_i\tilde{\ell}_j dz + \int_0^R \ell_i\ell_j dr \int_0^H \frac{d\tilde{\ell}_i}{dz}\frac{d\tilde{\ell}_j}{dz}dz \tag{8.19}$$

$$\begin{aligned} B_{ji} = &-\int_0^R \phi(r)\ell_j\frac{d\ell_i}{dr}dr \int_0^H \frac{d\psi}{dz}\tilde{\ell}_i\tilde{\ell}_j dz + \\ &+\int_0^R \left(\frac{d\phi}{dr} + \frac{1}{r}\phi(r)\right)\ell_i\ell_j dr \int_0^H \psi(z)\tilde{\ell}_j\frac{d\tilde{\ell}_i}{dz}dz \end{aligned} \tag{8.20}$$

These are the operators that correspond to $\hat{a}_\epsilon$. For the penalization terms, we have to be careful not to include contributions that arise from the information void K_h. Since we anticipate a uniform spatial grid (Δr and Δz constant) with N_r and N_z spatial gridpoints in each direction, and piecewise linear basis functions centered on these grid points, we can simply "tag" the basis functions whose centers that lie within $U_h \setminus K_h$, and compute an operator C consisting only of contributions from this tagged set of basis functions, associated with the function $\mathcal{T}(b_i, b_j)$, which is zero when either basis function is centered inside K_h and one otherwise. We can compute C with our tag

function via

$$C_{ji} = \int_{U_h} \left[\frac{d\ell_i}{dr}\frac{d\ell_j}{dr}\tilde{\ell}_i\tilde{\ell}_j + \ell_i\ell_j\frac{d\tilde{\ell}_i}{dz}\frac{d\tilde{\ell}_j}{dz} + \ell_i(r)\tilde{\ell}_i(z)\ell_j(r)\tilde{\ell}_j(z) \right] \mathcal{T}(\ell_i\tilde{\ell}_i, \ell_j\tilde{\ell}_j)dA \tag{8.21}$$

This is a simple way to enforce agreement over a set which approximates $U_h \setminus K_h$, and converges to $U_h \setminus K_h$ as the mesh size converges to zero.

For this initial test, we will take $\nu = 0$. This implies that the right hand side linear forcing is given by

$$\vartheta_j = \sum_{i=1}^{N_e} C_{ji}\beta_i^c + d_j. \tag{8.22}$$

where d_j is the term that arises from making the problem homogeneous. This case, it consists of the contributions of piecewise linear basis functions centered on the boundary grid points to the operators A and B for the entries of their neighbors on the interior of the domain, but transferred to the right side of the equation. Putting it all together, we are seeking $\vec{\beta} \in \mathbb{R}^{N_e}$ which arises from

$$(\epsilon A + B + C)\vec{\beta} = \vartheta. \tag{8.23}$$

The invertibility of the operator on the right is guaranteed so long as ϵ satisfies the coercivity criterion holds. In practice, computing $\gamma(\Omega)$ may be difficult. A search of the literature provides an estimate $\gamma(U) \leq \frac{D}{\pi}$ where D is the diameter of U, so long as U is convex (Bebendorf, 2003). For our special case, the suprema of ζ and η are easily calculated using the derivative formulas (2.14)-(2.17). Setting the second derivatives to zero, we get $||\zeta||_\infty = |\zeta(r^*, z_c)|$,

where $r^* = \left(\frac{n_r^2+n_r-2}{n_r-2}\right)^{1/n_r} r_c$ and $||\eta||_\infty = |\eta(r_c, z^*)|$, where $z^* = \left(\frac{1}{n_z+1}\right)^{1/n_z} z_c$. Choosing ϵ appropriately with respect to these constants should yield a unique solution.

8.5.2 Discussion

Figures 8.23-8.31 show some sample results, with U_h to be taken as the rectangle which is one grid point wider in each direction than K_h. The figures show the characteristic solutions on the left, and the weak solutions arising from the extended domain problem on the right, in each case for the maximum likelihood streamfunctions whose information voids were contained within Ω^o.

The smoothed solutions are not particularly accurate in the information voids, but rather appear to be the boundary values "smeared" into a neighboring region of the void. While the solution is now defined over all of Ω, there is no reason to place a large amount of confidence in this weak solution, since it bears little resemblance to a physical flow once we take derivatives to compute u and w. The small scale fluctuations in Ψ_ϵ are amplified in u and w, which is evident from the oscillatory behavior near the boundaries of K_h. However, the flow equations are being satisfied in some sense, and so the relevant physics are being represented. Further, information from outside K_h is being introduced into the interior of K_h, which is preferable to no information inside K_h at all.

Intuitively, the two types of dynamics are fighting against each other. The advective portion of the model equations is attempting to only propagate solutions along characteristic curves, while the elliptic portion is attempting to spread information in a physically homogeneous manner. The relative sizes of these terms determine which effect is dominant, and when they have compa-

rable sizes, the effect is a mixture of the two. For grid points that are within some critical neighborhood of an observation, the diffusive part of the dynamics is able to propagate information from that observation to the gridpoint. The other points, near the middle of K_h, are not within this critical radius, and so do not feel the impact of these observations as much. This is evident when we compare the streamfucntion solutions before and after smoothing, with the portions of the boundary that have larger streamfunction values being surrounded by larger values in the smoothed solution, and similarly for the smaller values.

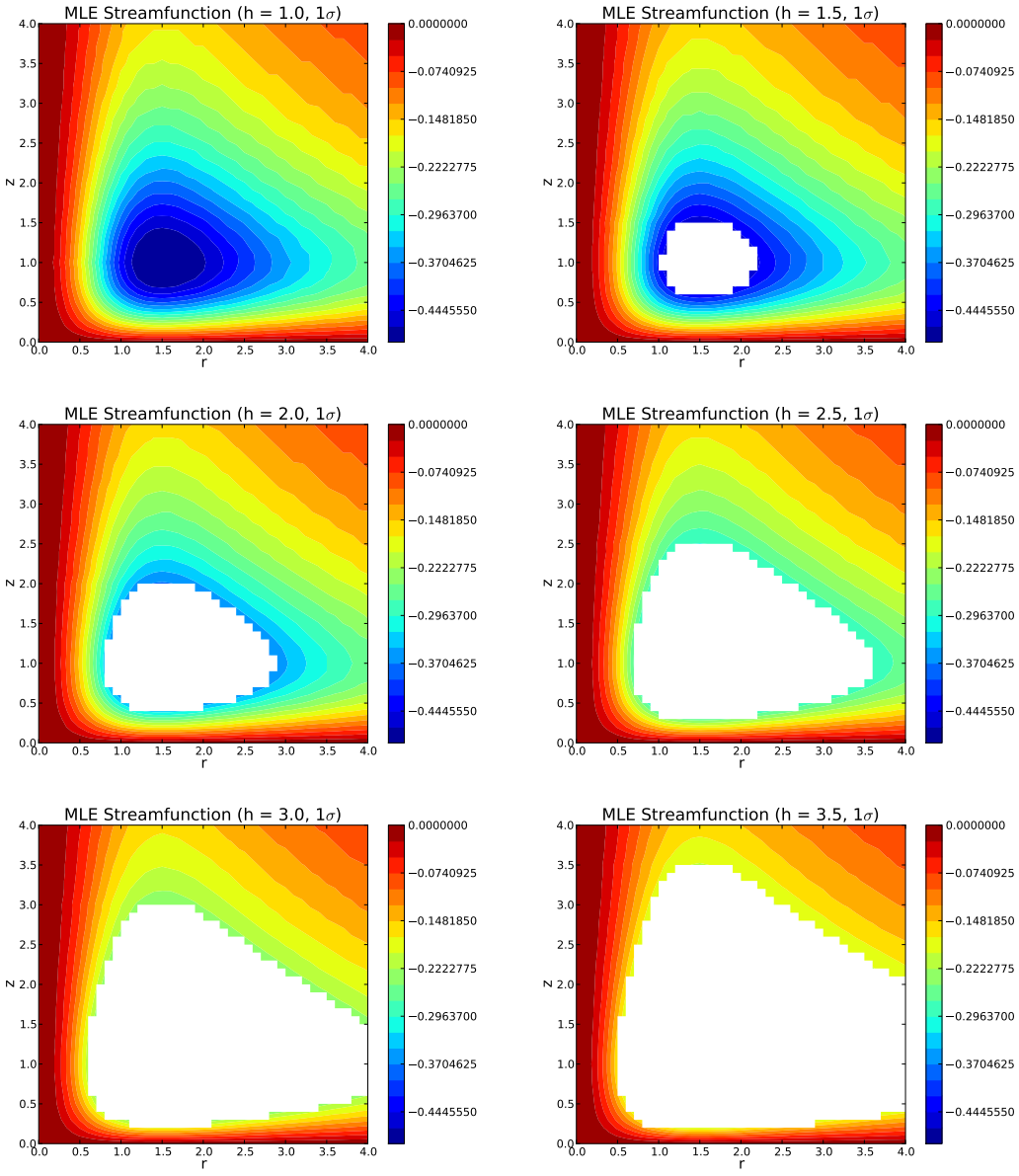


Figure 8.5: Retrieved Streamfunction Fields Using the MLE Tangential Velocity for Different Values of h and Error Σ.

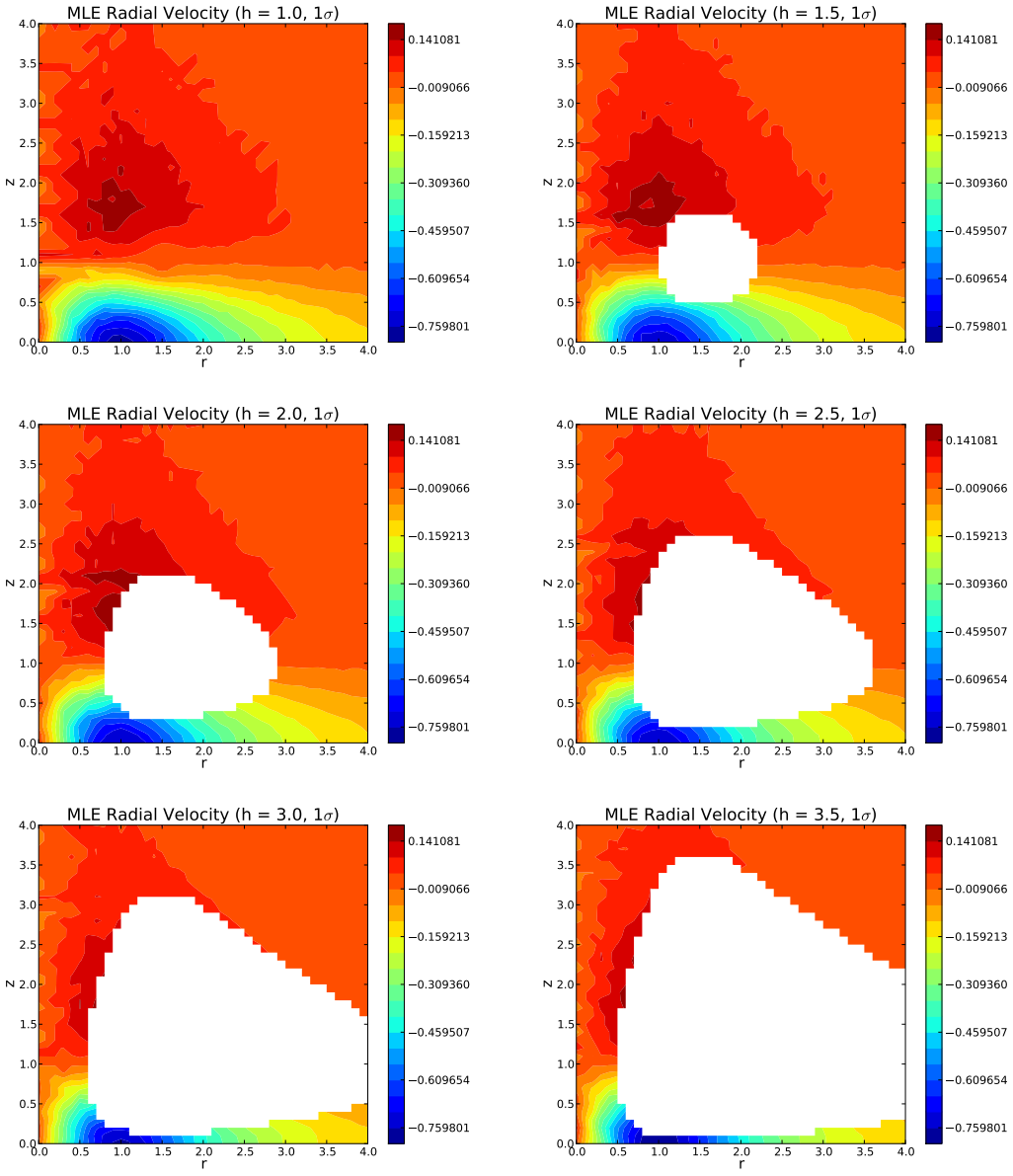


Figure 8.6: Retrieved Radial Velocity Fields Using the MLE Tangential Velocity for Different Values of h and Error Σ.

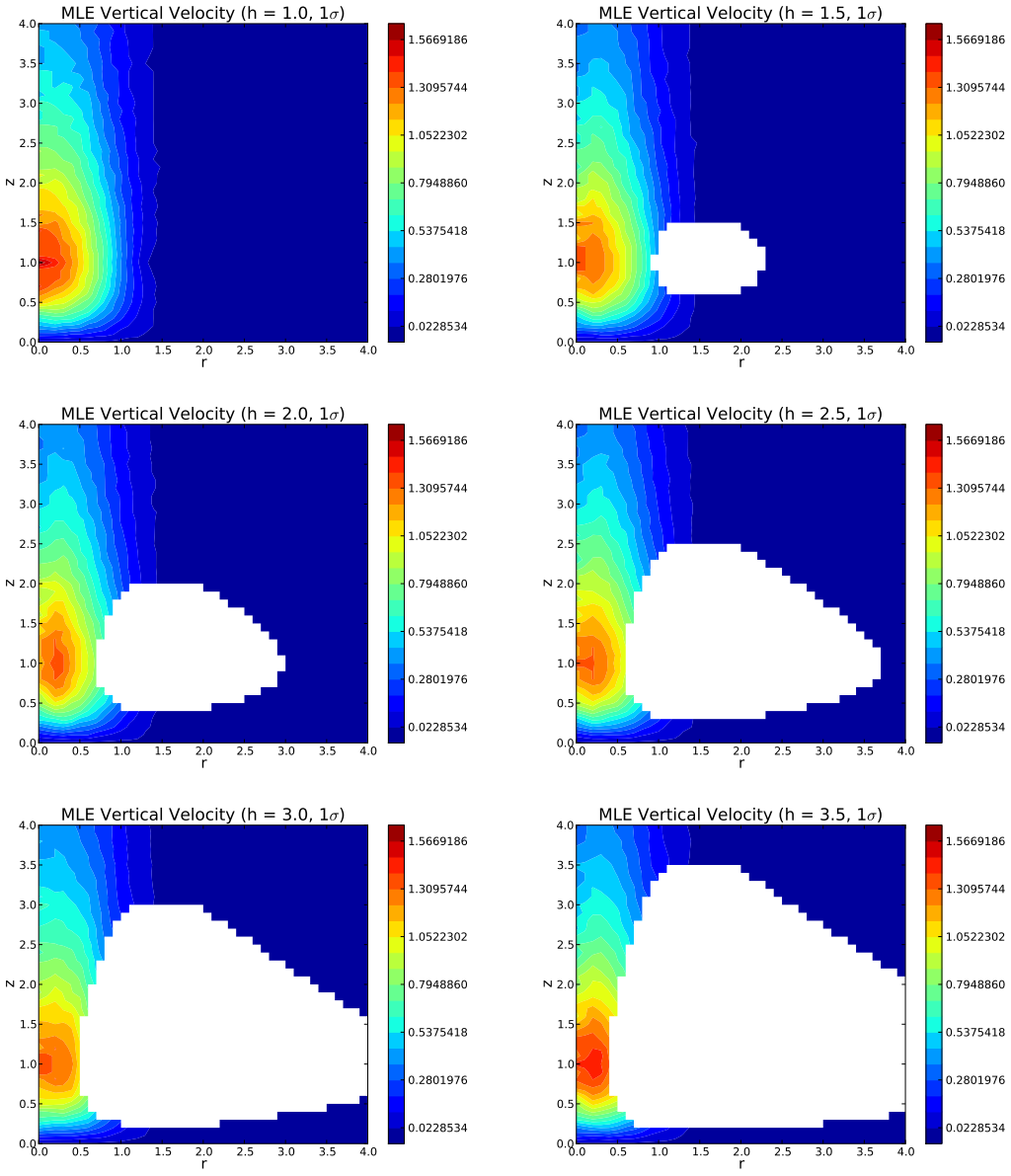


Figure 8.7: Retrieved Vertical Velocity Fields Using the MLE Tangential Velocity for Different Values of h and Error Σ.

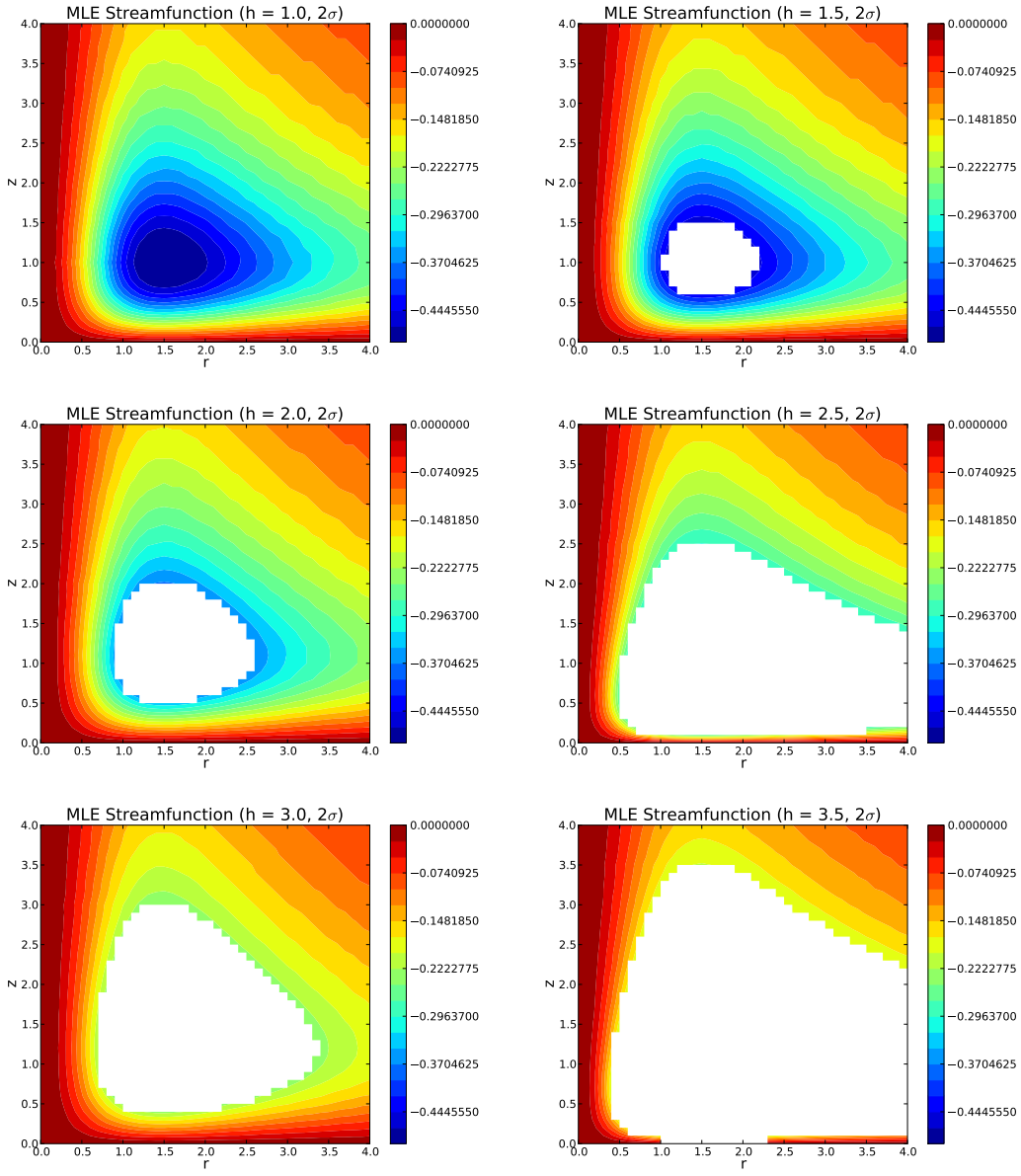


Figure 8.8: Retrieved Streamfunction Fields Using the MLE Tangential Velocity for Different Values of h and Error 2Σ.

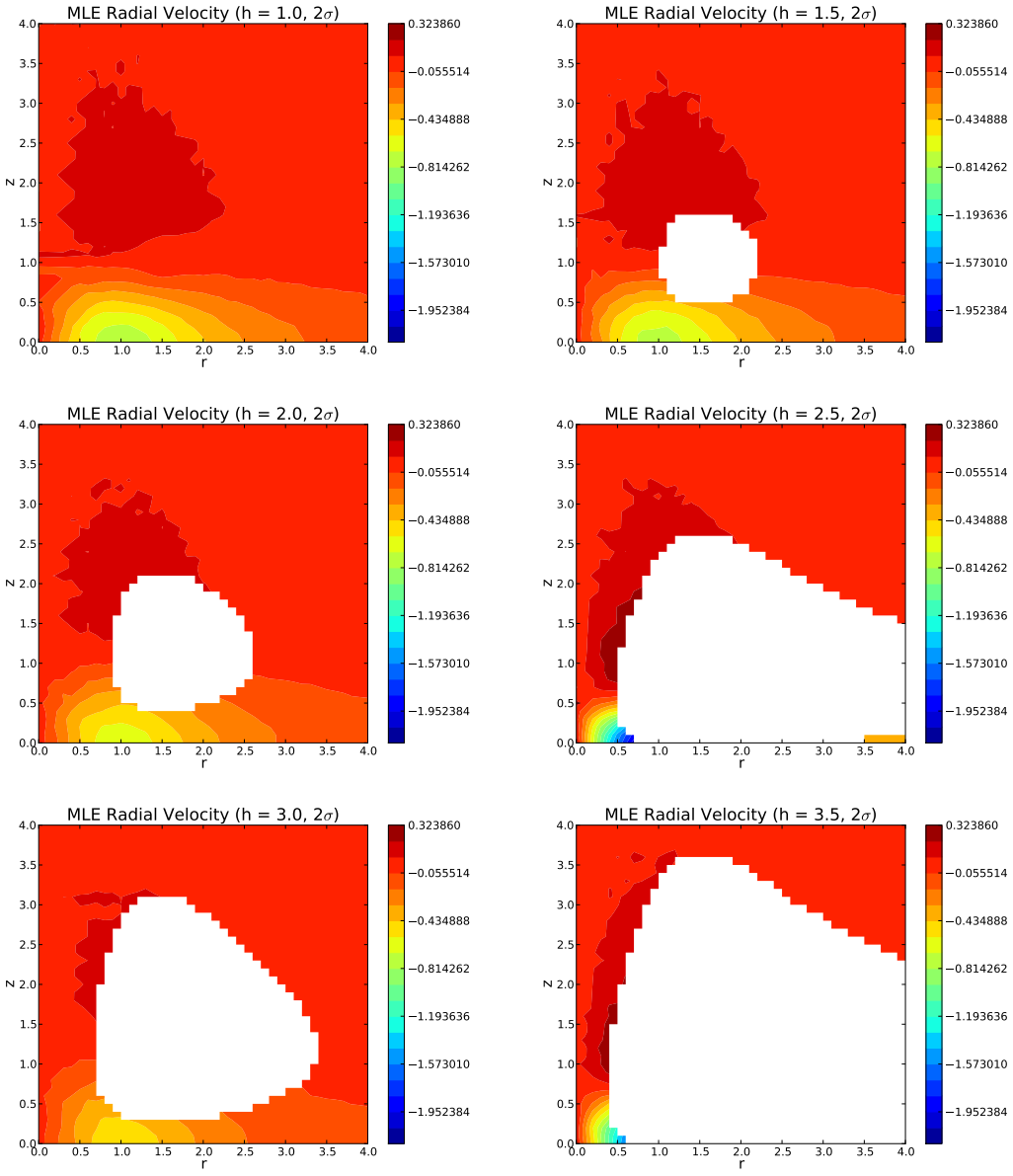


Figure 8.9: Retrieved Radial Velocity Fields Using the MLE Tangential Velocity for Different Values of h and Error 2Σ.

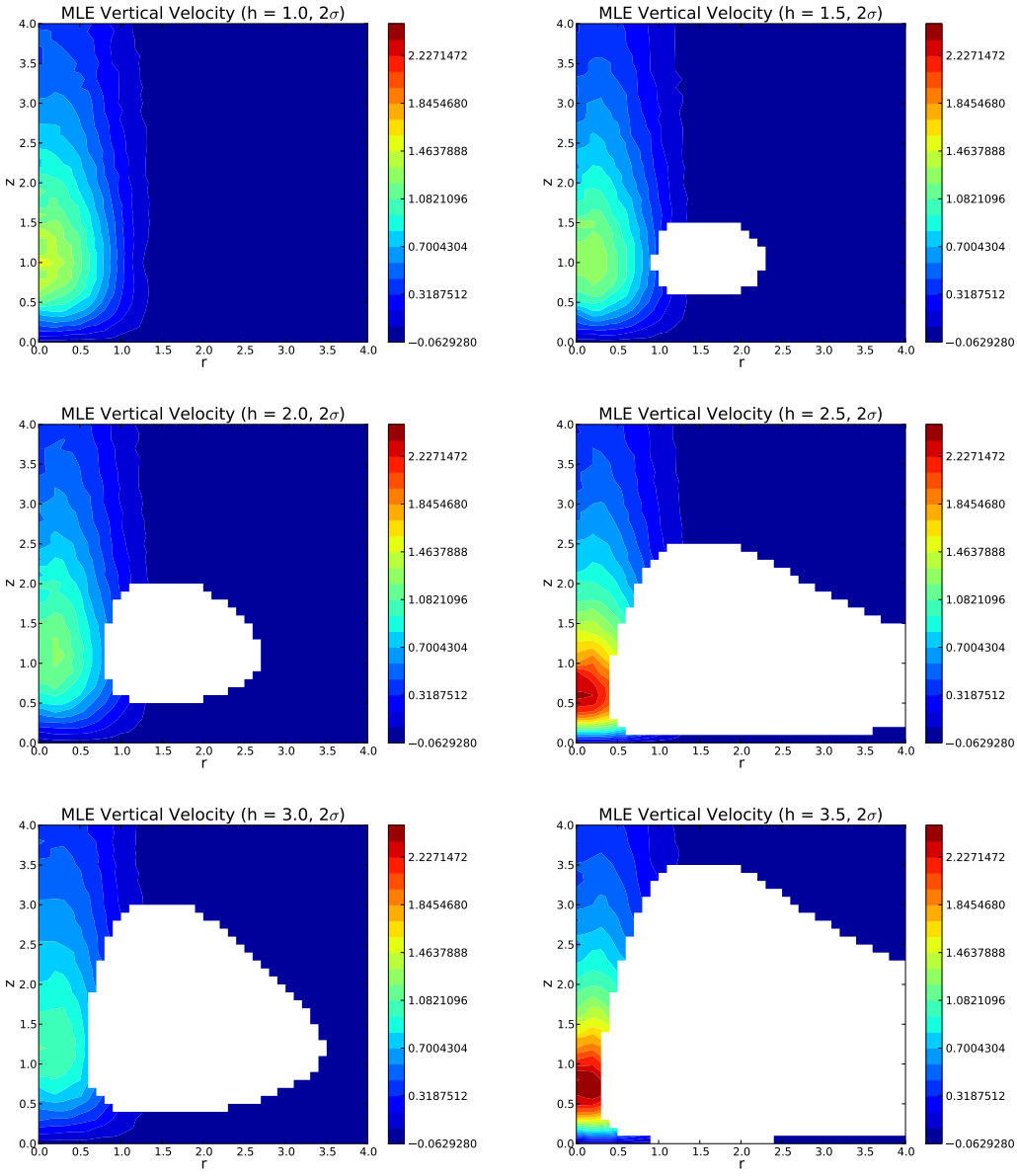


Figure 8.10: Retrieved Vertical Velocity Fields Using the MLE Tangential Velocity for Different Values of h and Error 2Σ.

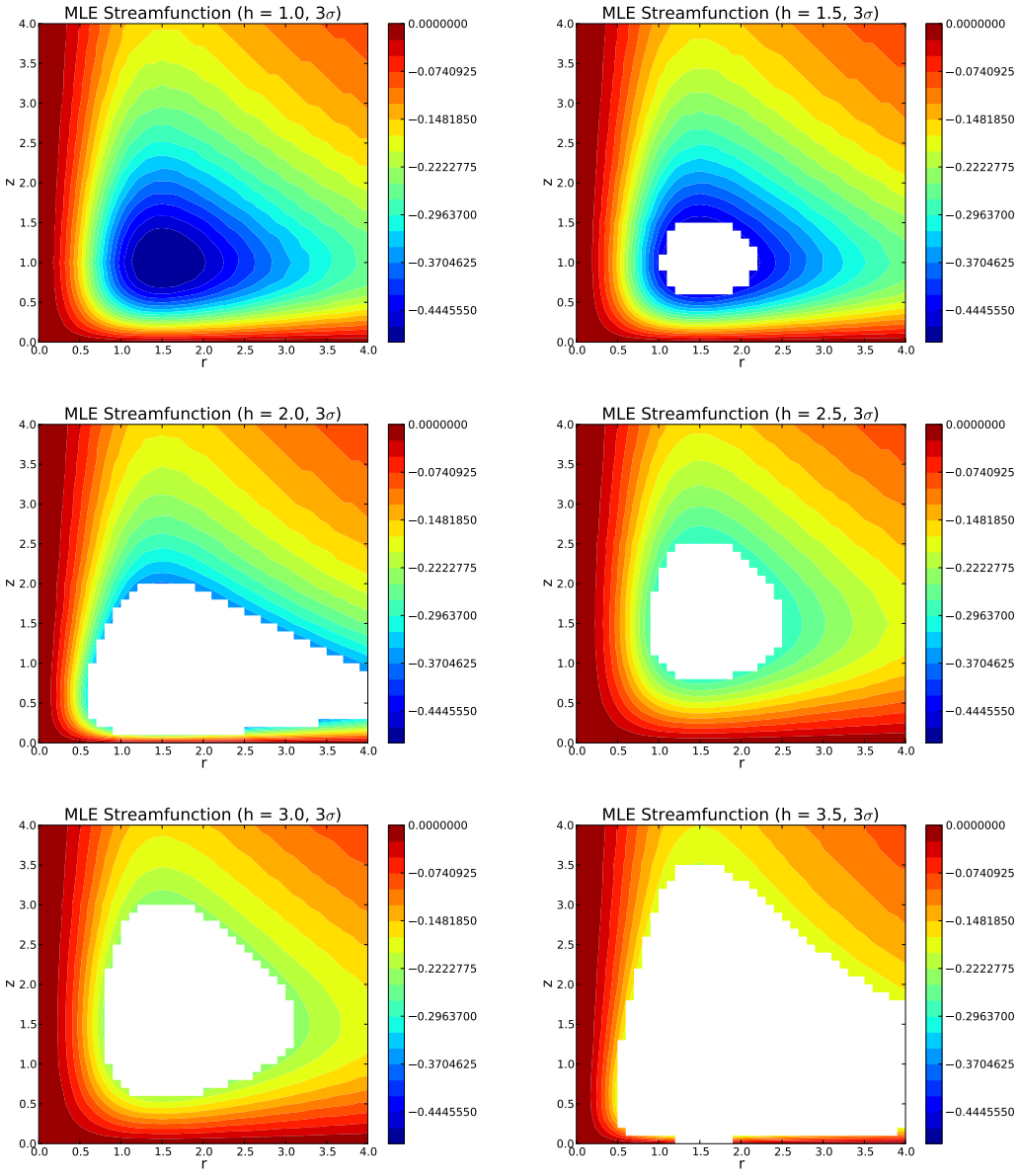


Figure 8.11: Retrieved Streamfunction Fields Using the MLE Tangential Velocity for Different Values of h and Error 3Σ.

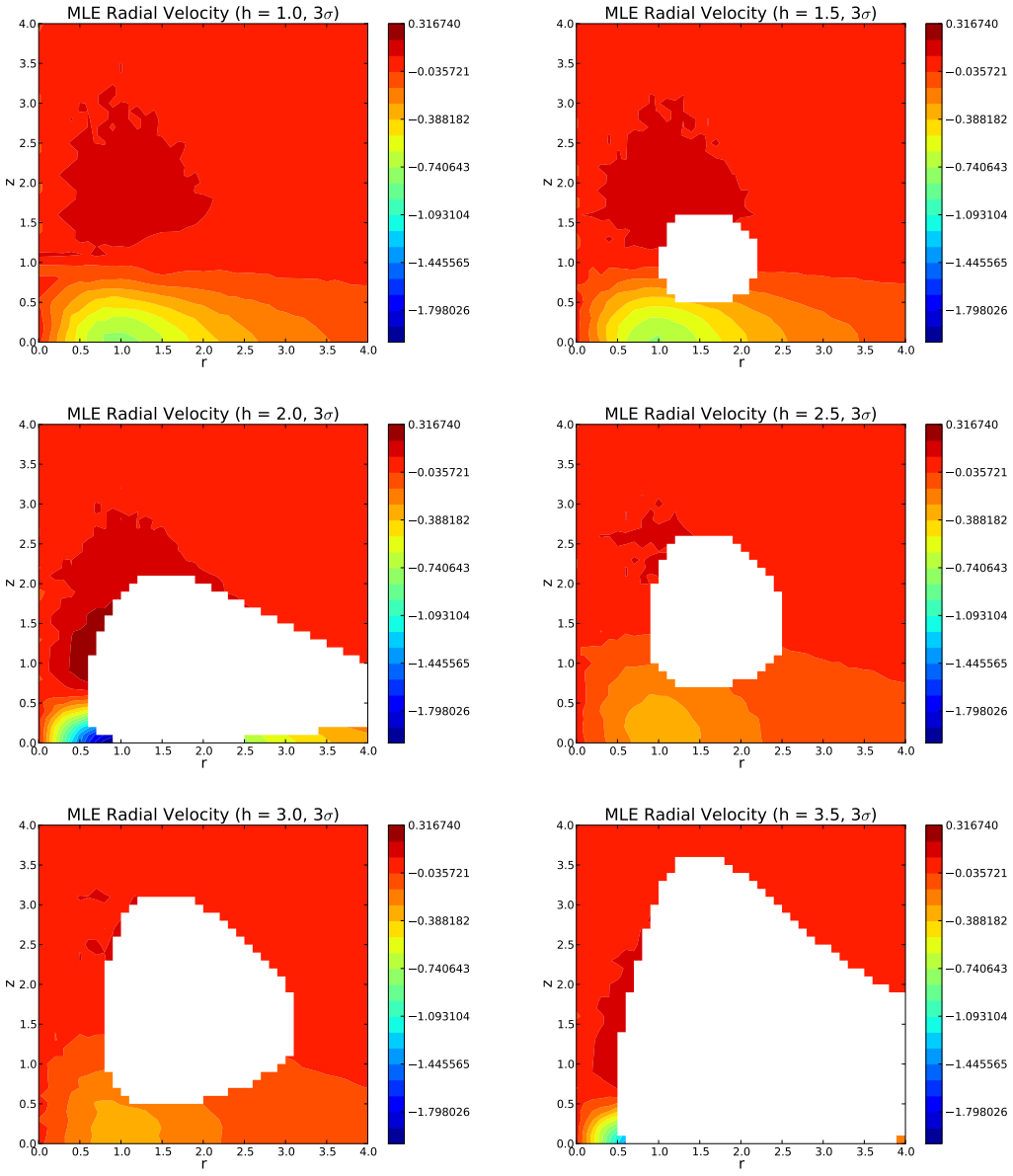


Figure 8.12: Retrieved Radial Velocity Fields Using the MLE Tangential Velocity for Different Values of h and Error 3Σ.

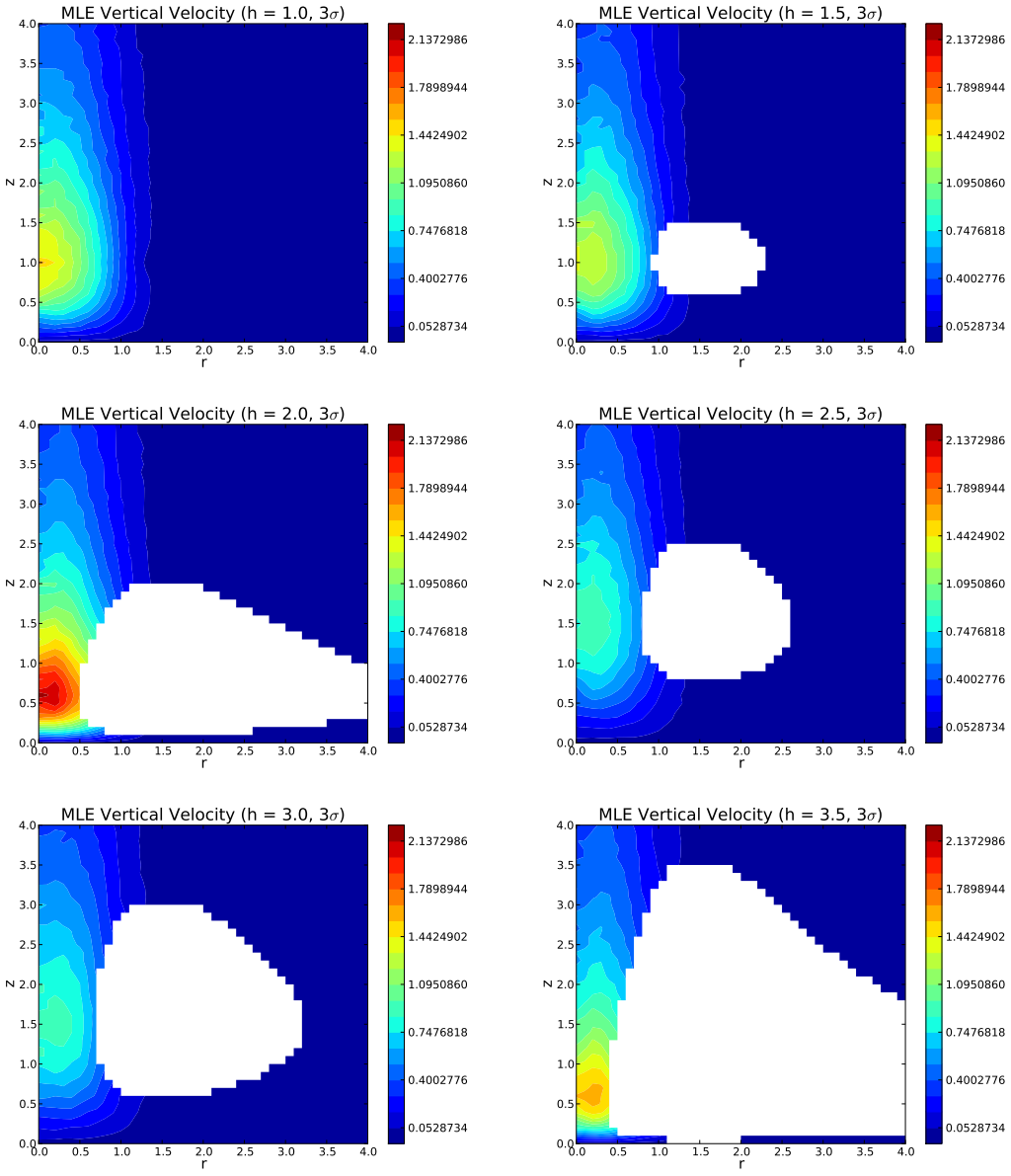


Figure 8.13: Retrieved Vertical Velocity Fields Using the MLE Tangential Velocity for Different Values of h and Error 3Σ.

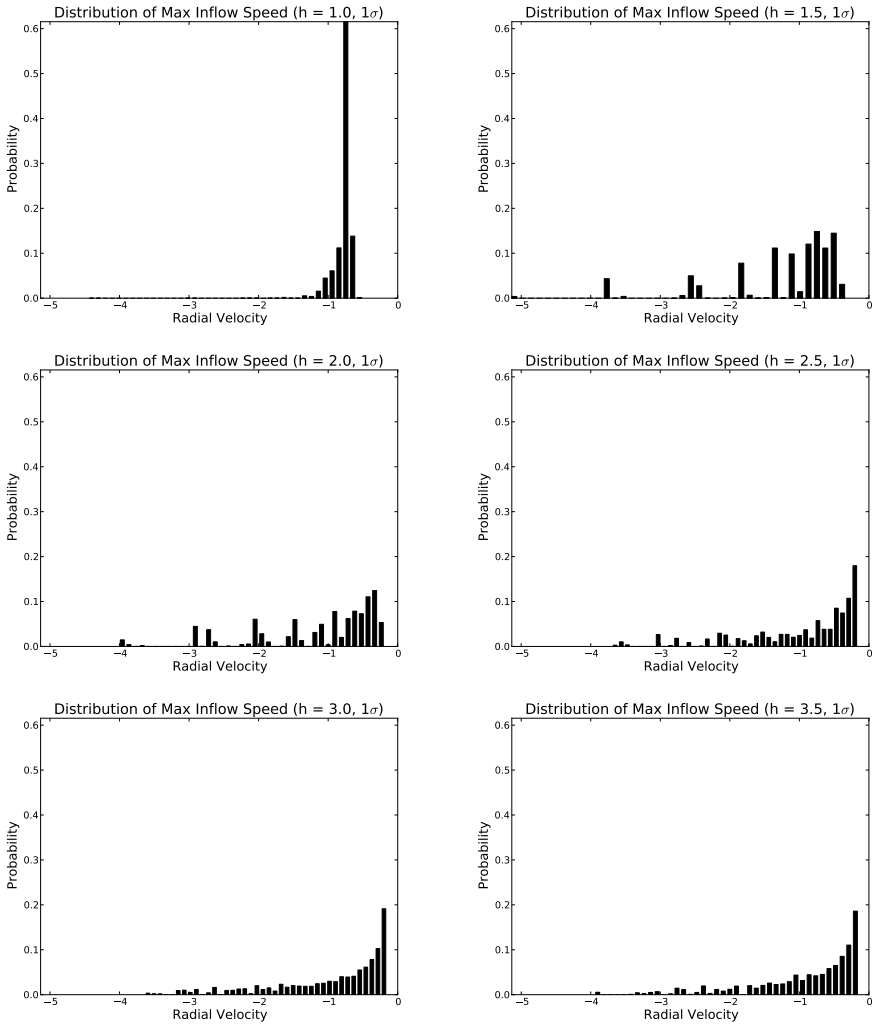


Figure 8.14: Conditional Distributions of 1000 Most Likely Values of u^+ for Different Values of h and Error Σ.

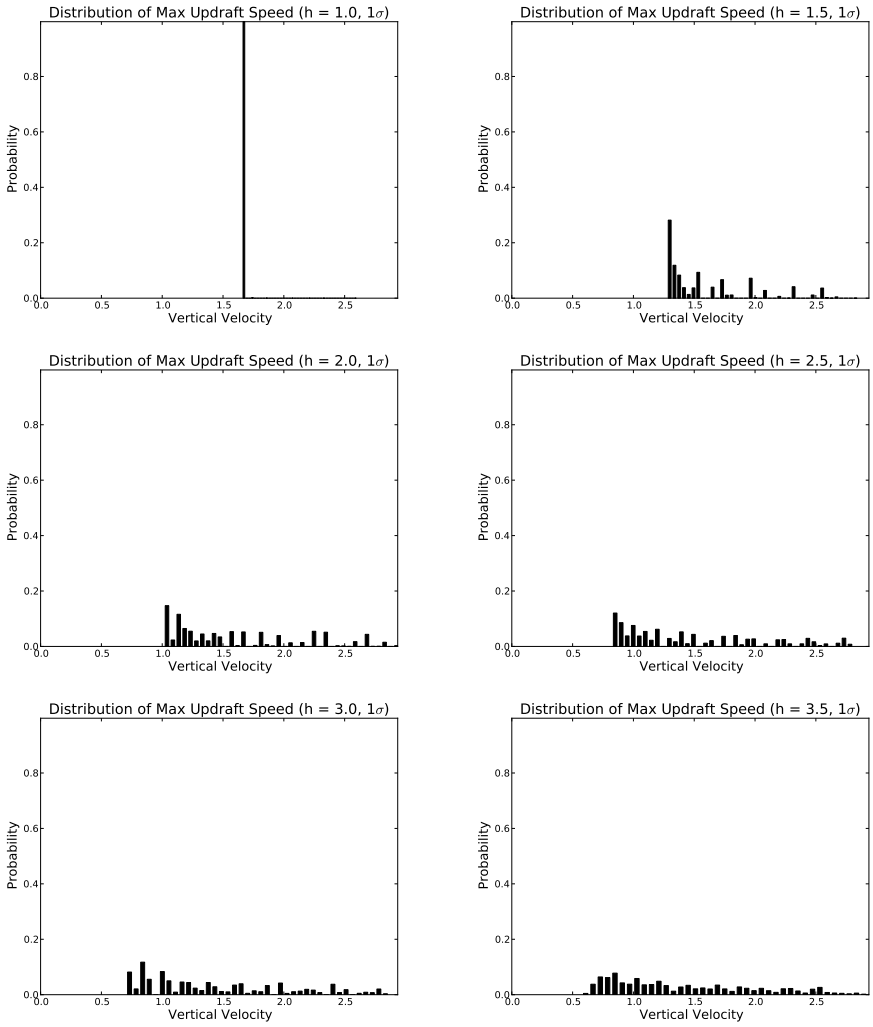


Figure 8.15: Conditional Distributions of 1000 Most Likely Values of w^+ for Different Values of h and Error Σ.

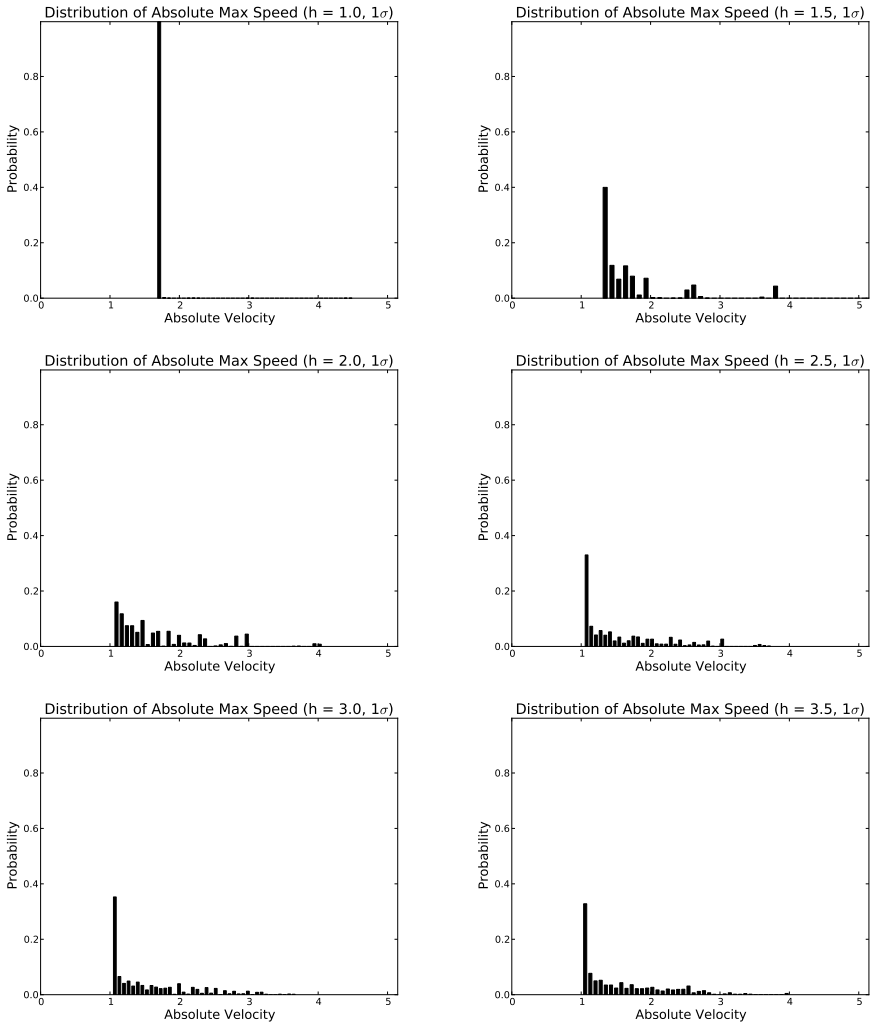


Figure 8.16: Conditional Distributions of 1000 Most Likely Values of $|\vec{v}|_{\max}$ for Different Values of h and Error Σ.

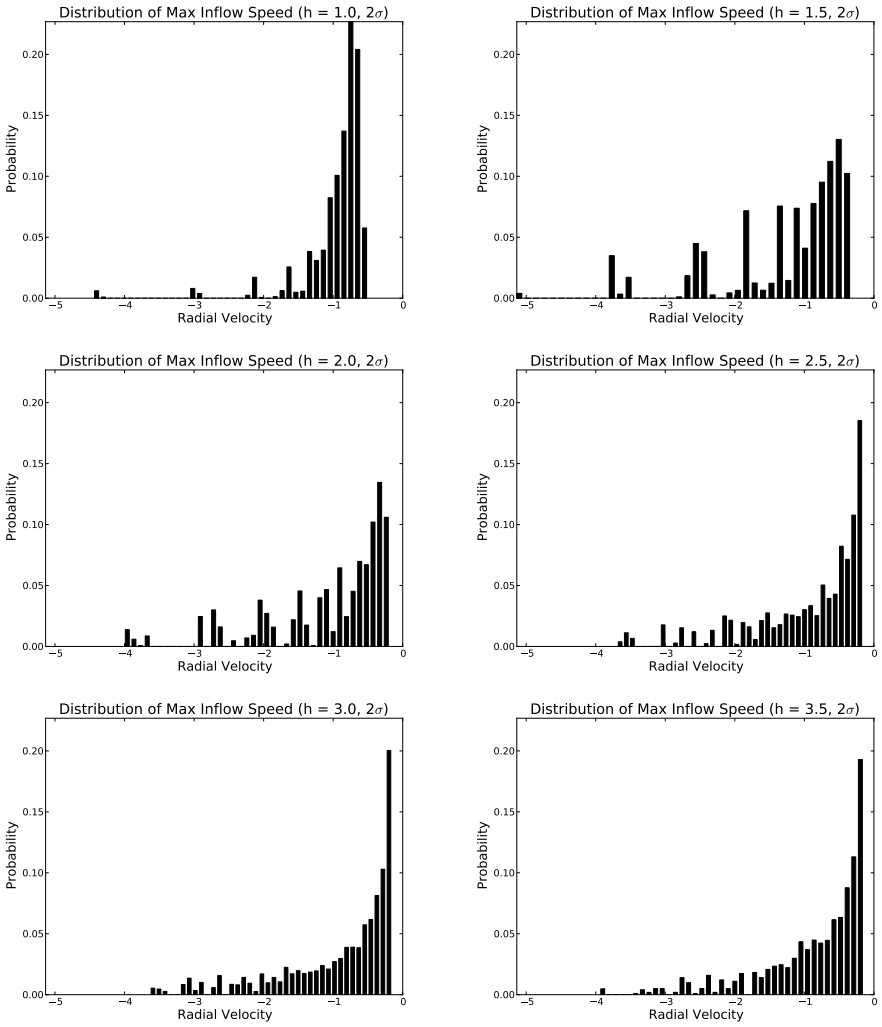


Figure 8.17: Conditional Distributions of 1000 Most Likely Values of u^+ for Different Values of h and Error 2Σ.

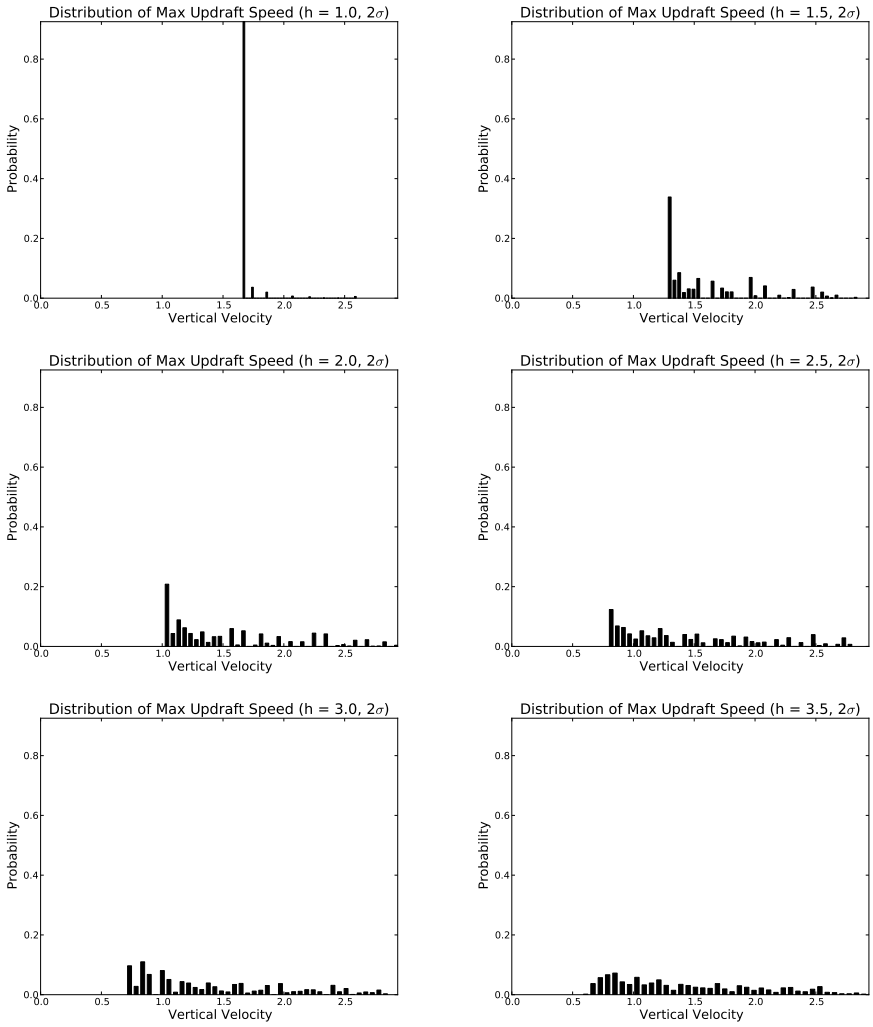


Figure 8.18: Conditional Distributions of 1000 Most Likely Values of w^+ for Different Values of h and Error 2Σ.

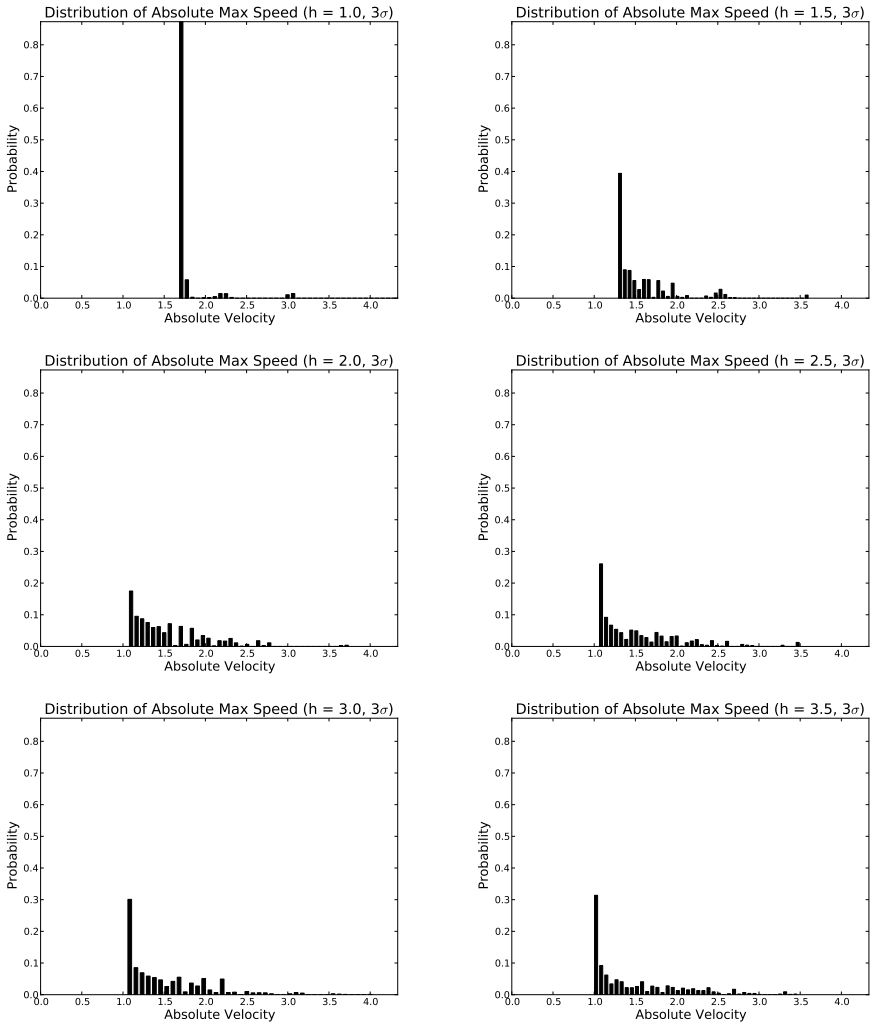


Figure 8.19: Conditional Distributions of 1000 Most Likely Values of $|\vec{v}|_{\max}$ for Different Values of h and Error 2Σ.

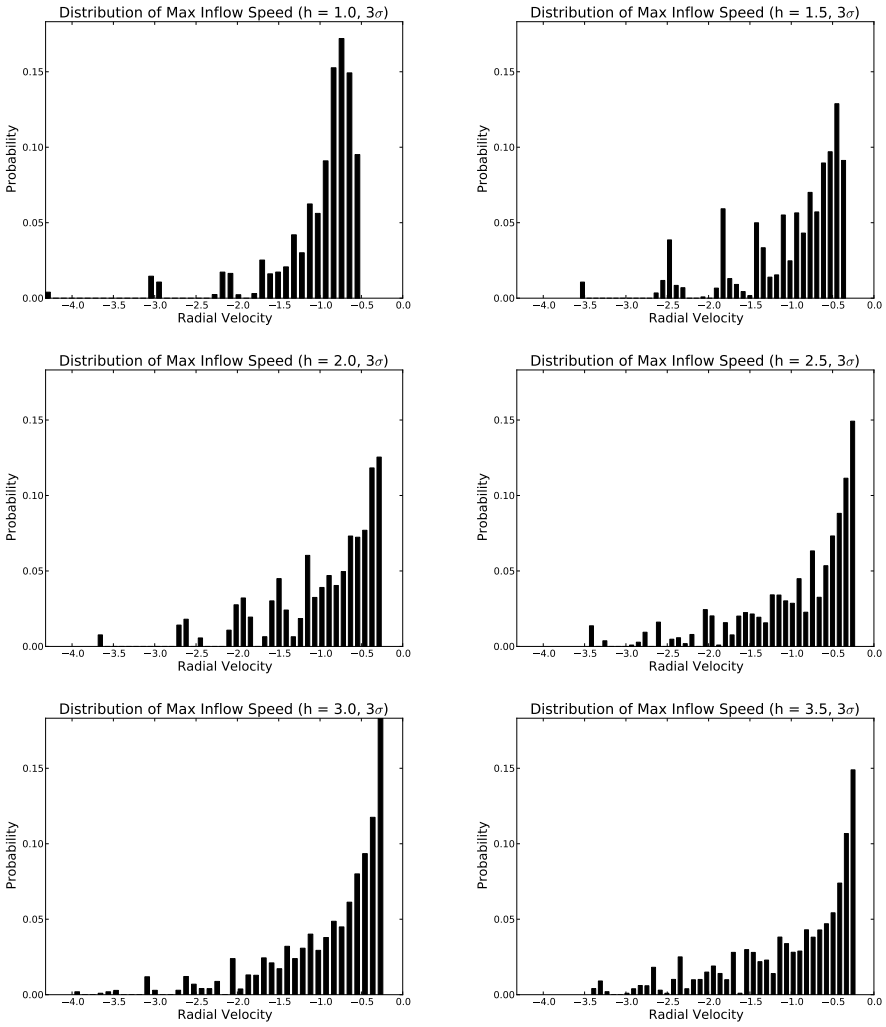


Figure 8.20: Conditional Distributions of 1000 Most Likely Values of u^+ for Different Values of h and Error 3Σ.

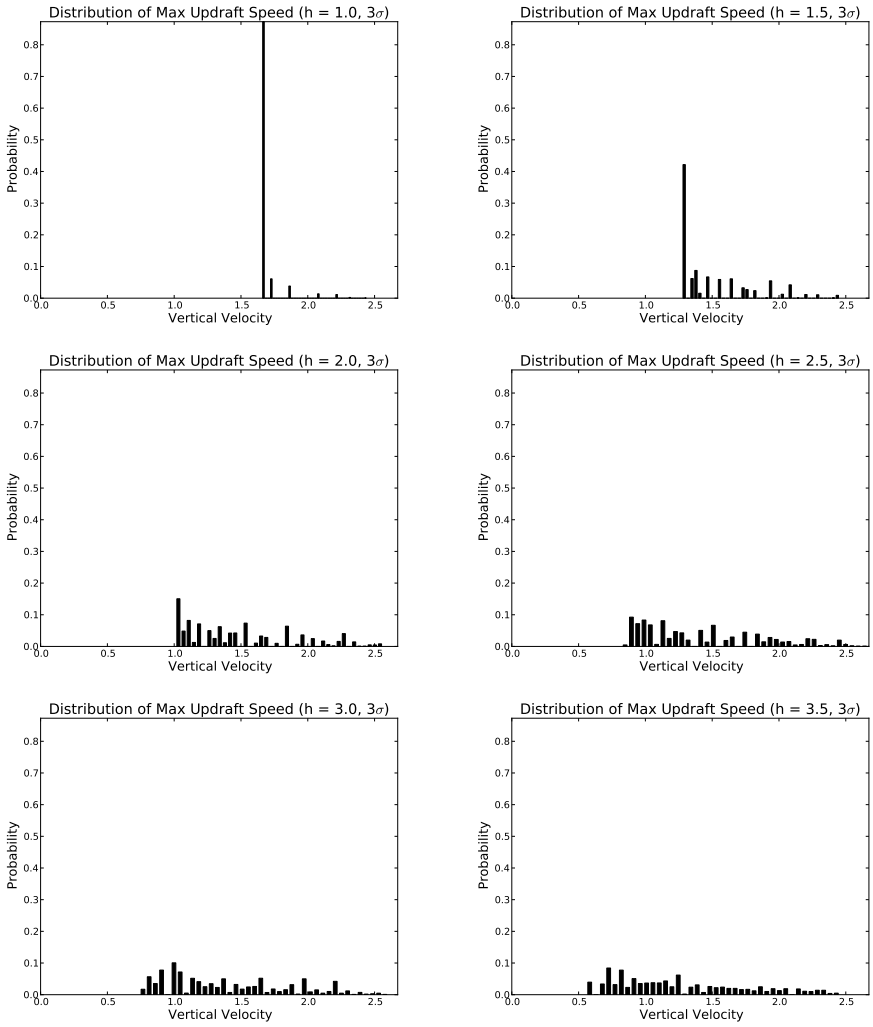


Figure 8.21: Conditional Distributions of 1000 Most Likely Values of w^+ for Different Values of h and Error 3Σ.

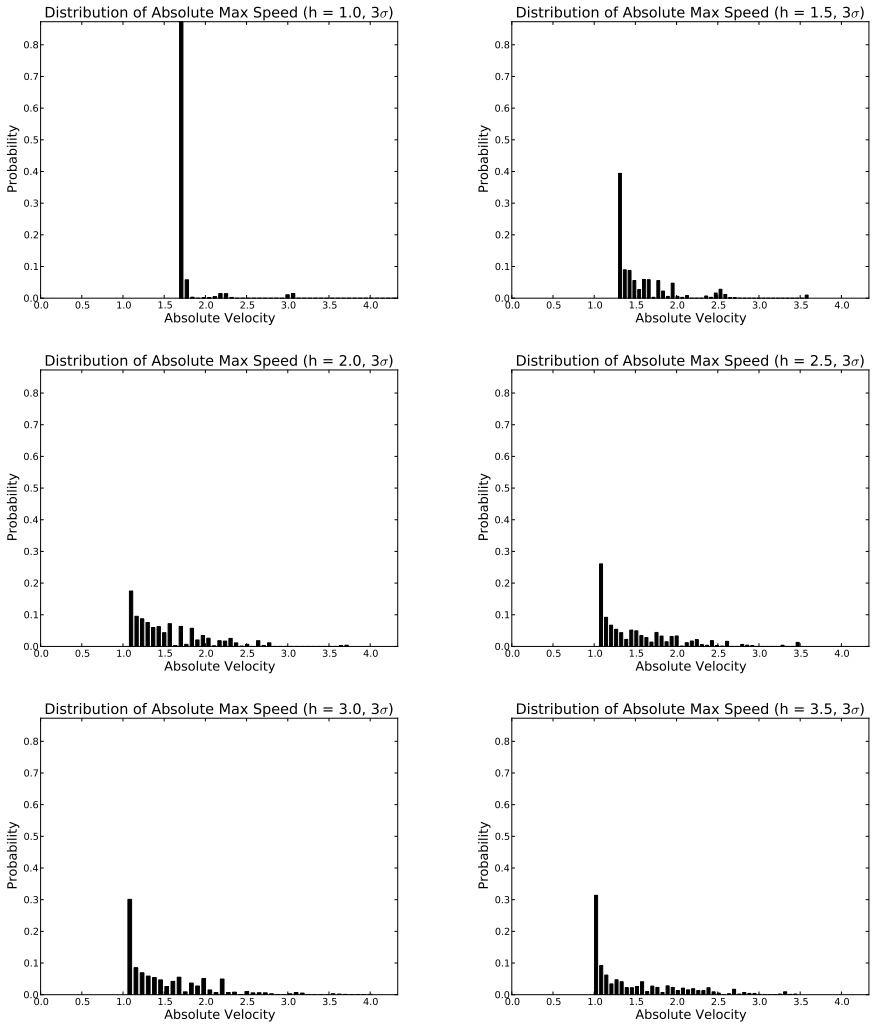


Figure 8.22: Conditional Distributions of 1000 Most Likely Values of $|\vec{v}|_{\max}$ for Different Values of h and Error 3Σ.

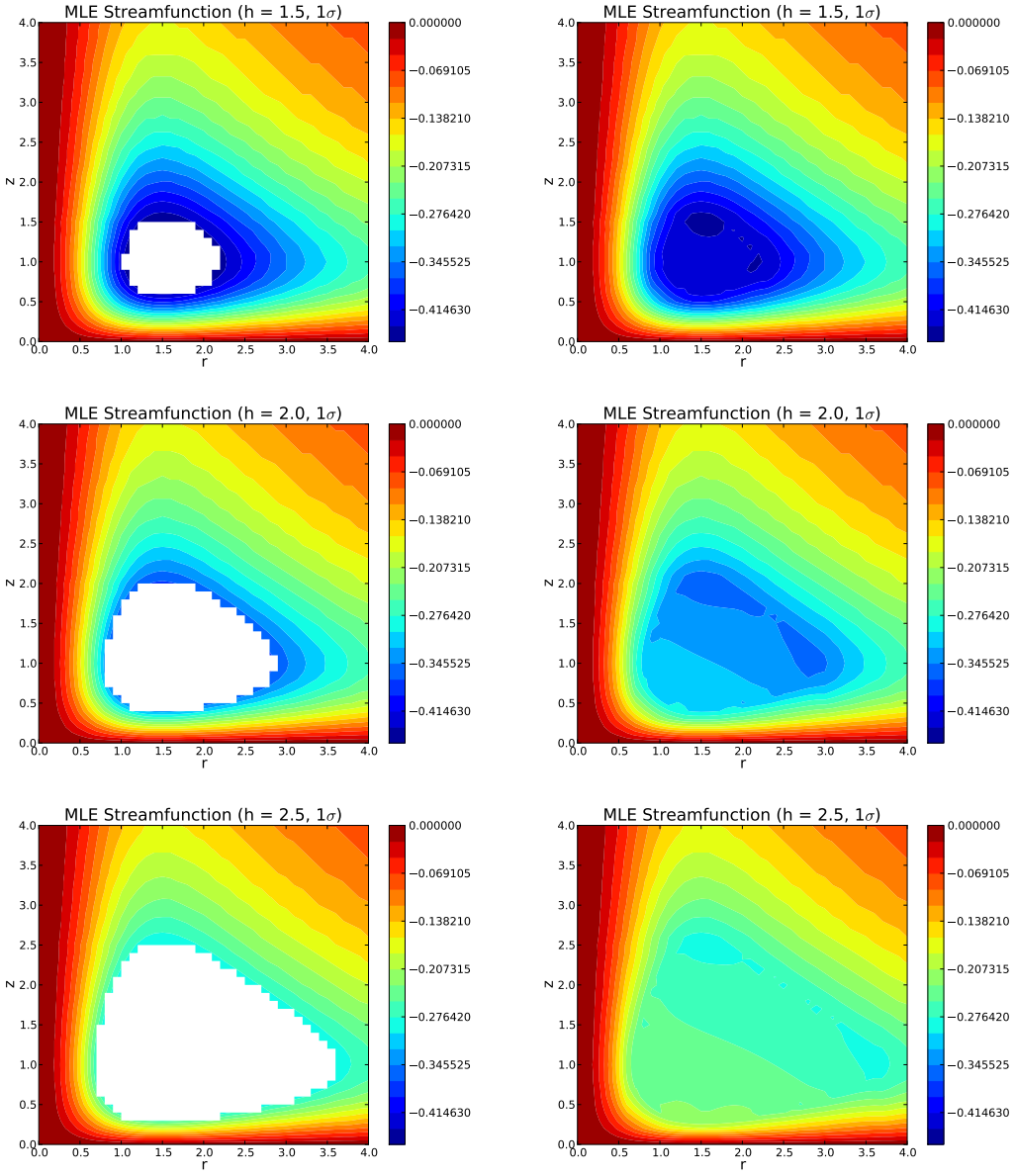


Figure 8.23: MLE characteristic streamfunction solutions (left) and elliptic BVP solutions (right) for error 1σ for $h = 1.5$ (top), $h = 2$ (middle) and $h = 2.5$ (bottom).

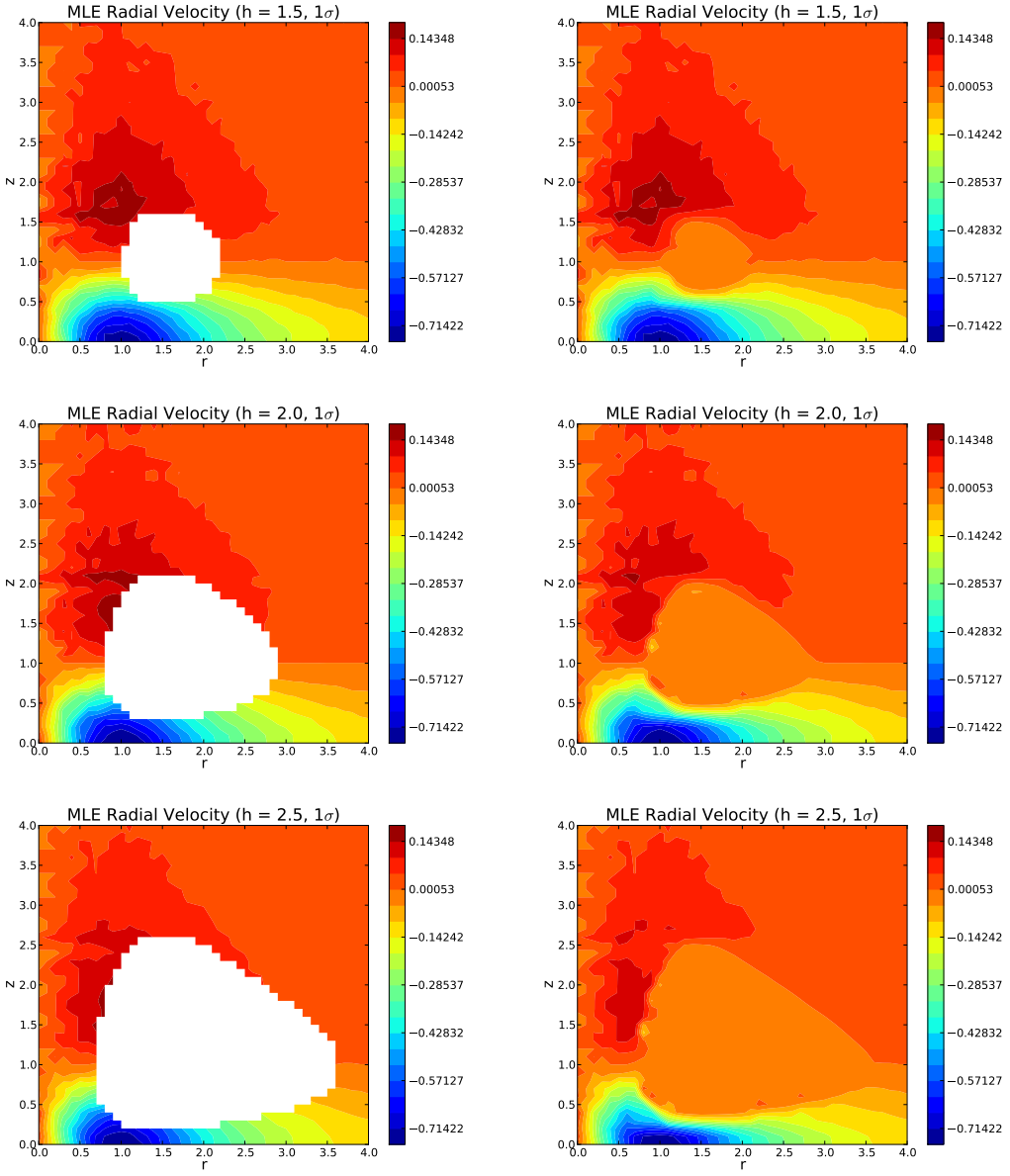


Figure 8.24: MLE characteristic radial velocity solutions (left) and elliptic BVP solutions (right) for error 1σ for $h = 1.5$ (top), $h = 2$ (middle) and $h = 2.5$ (bottom).

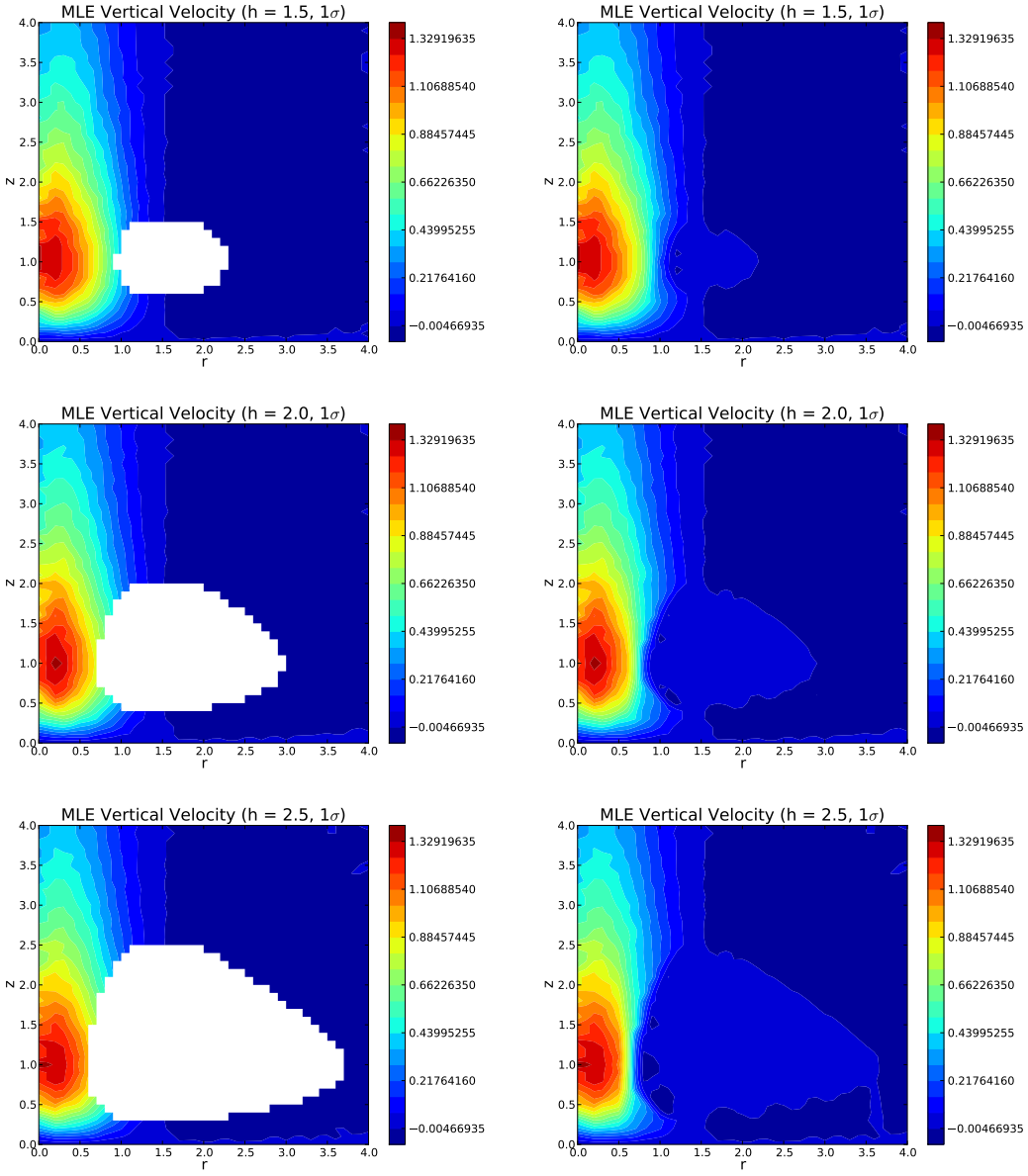


Figure 8.25: MLE characteristic vertical velocity solutions (left) and elliptic BVP solutions (right) for error 1σ for $h = 1.5$ (top), $h = 2$ (middle) and $h = 2.5$ (bottom).

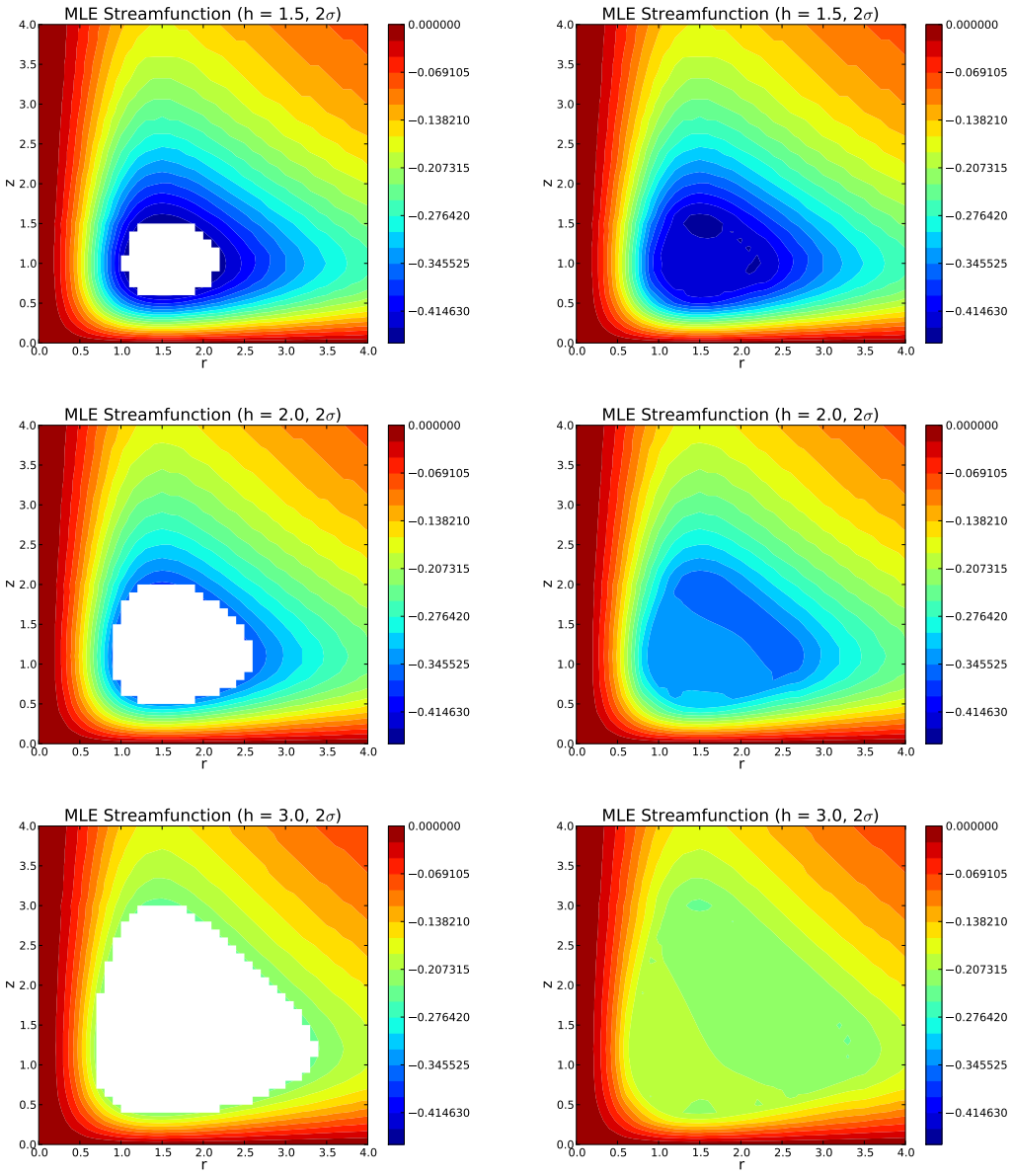


Figure 8.26: MLE characteristic streamfunction solutions (left) and elliptic BVP solutions (right) for error 1σ for $h = 1.5$ (top), $h = 2$ (middle) and $h = 3$ (bottom).

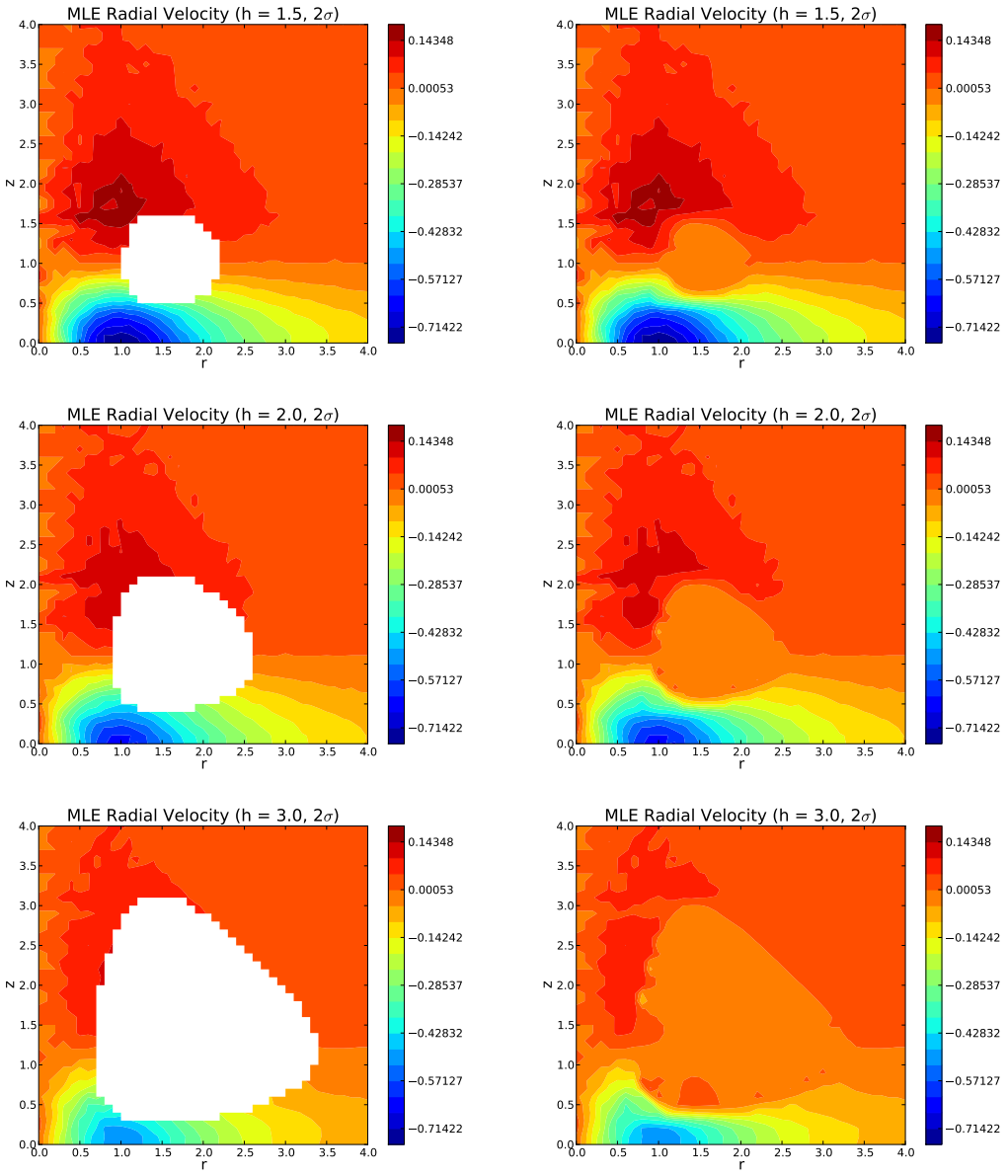


Figure 8.27: MLE characteristic radial solutions (left) and elliptic BVP solutions (right) for error 1σ for $h = 1.5$ (top), $h = 2$ (middle) and $h = 3$ (bottom).

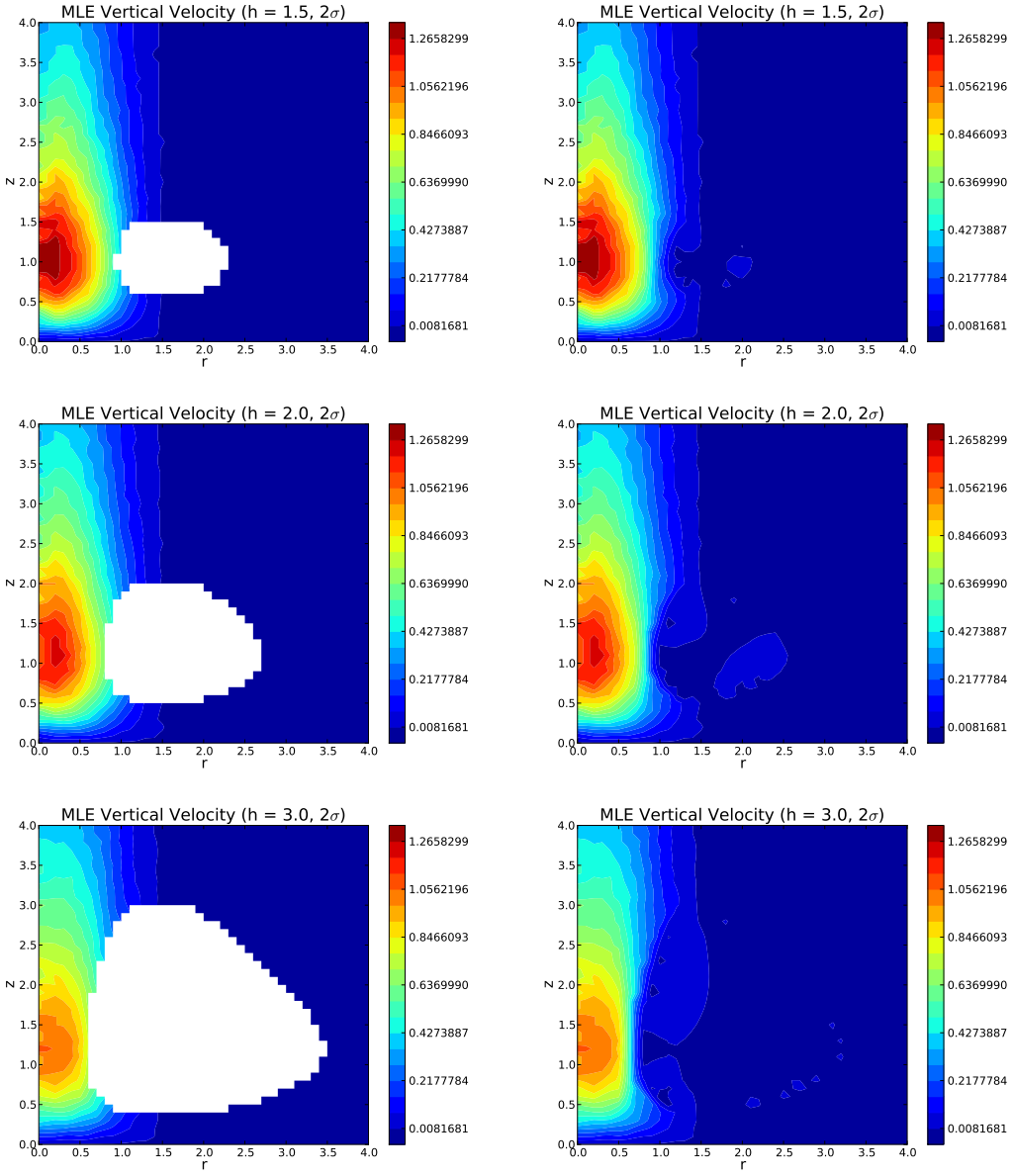


Figure 8.28: MLE characteristic vertical velocity solutions (left) and elliptic BVP solutions (right) for error 1σ for $h = 1.5$ (top), $h = 2$ (middle) and $h = 3$ (bottom).

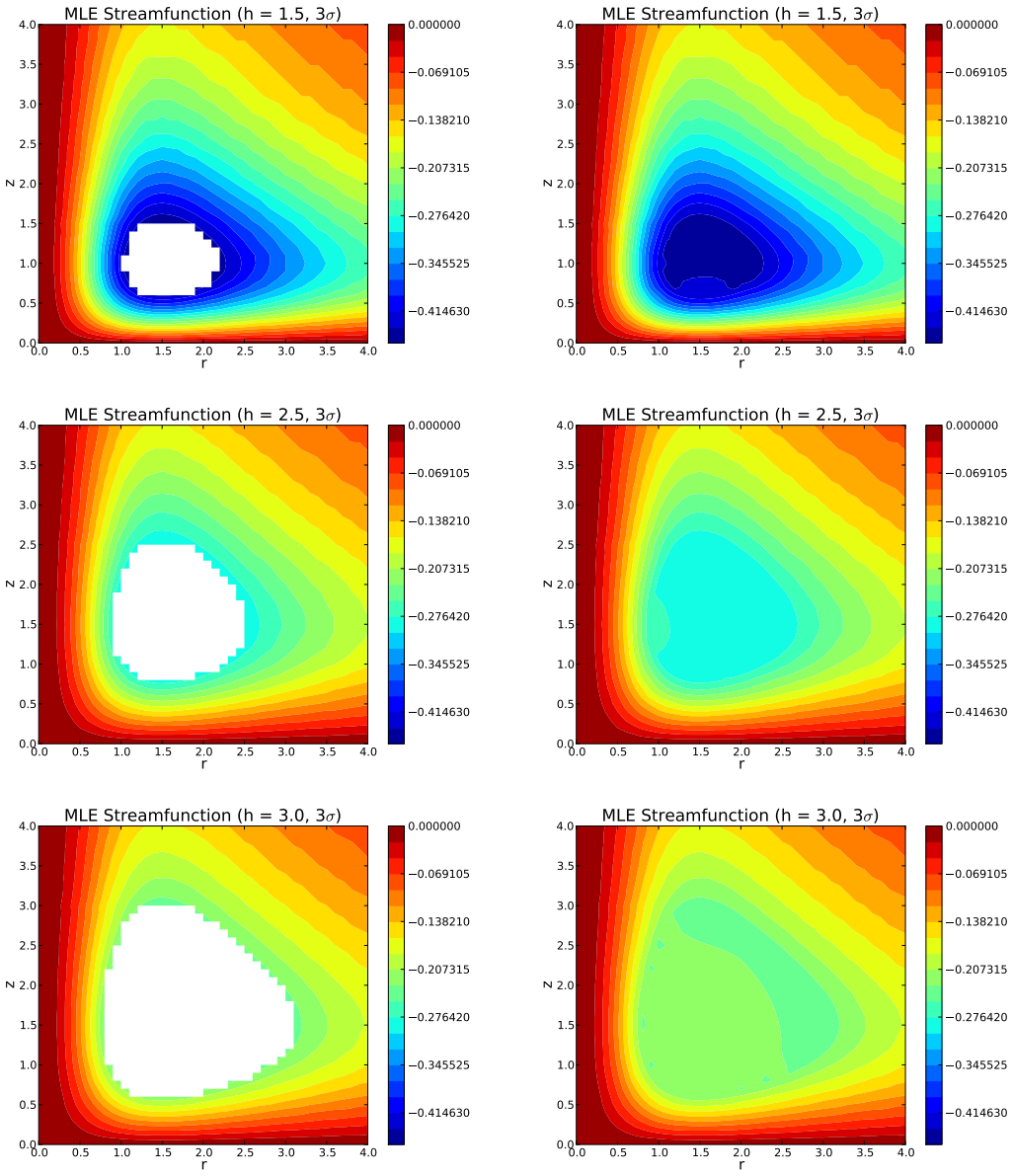


Figure 8.29: MLE characteristic streamfunction solutions (left) and elliptic BVP solutions (right) for error 1σ for $h = 1.5$ (top), $h = 2.5$ (middle) and $h = 3$ (bottom).

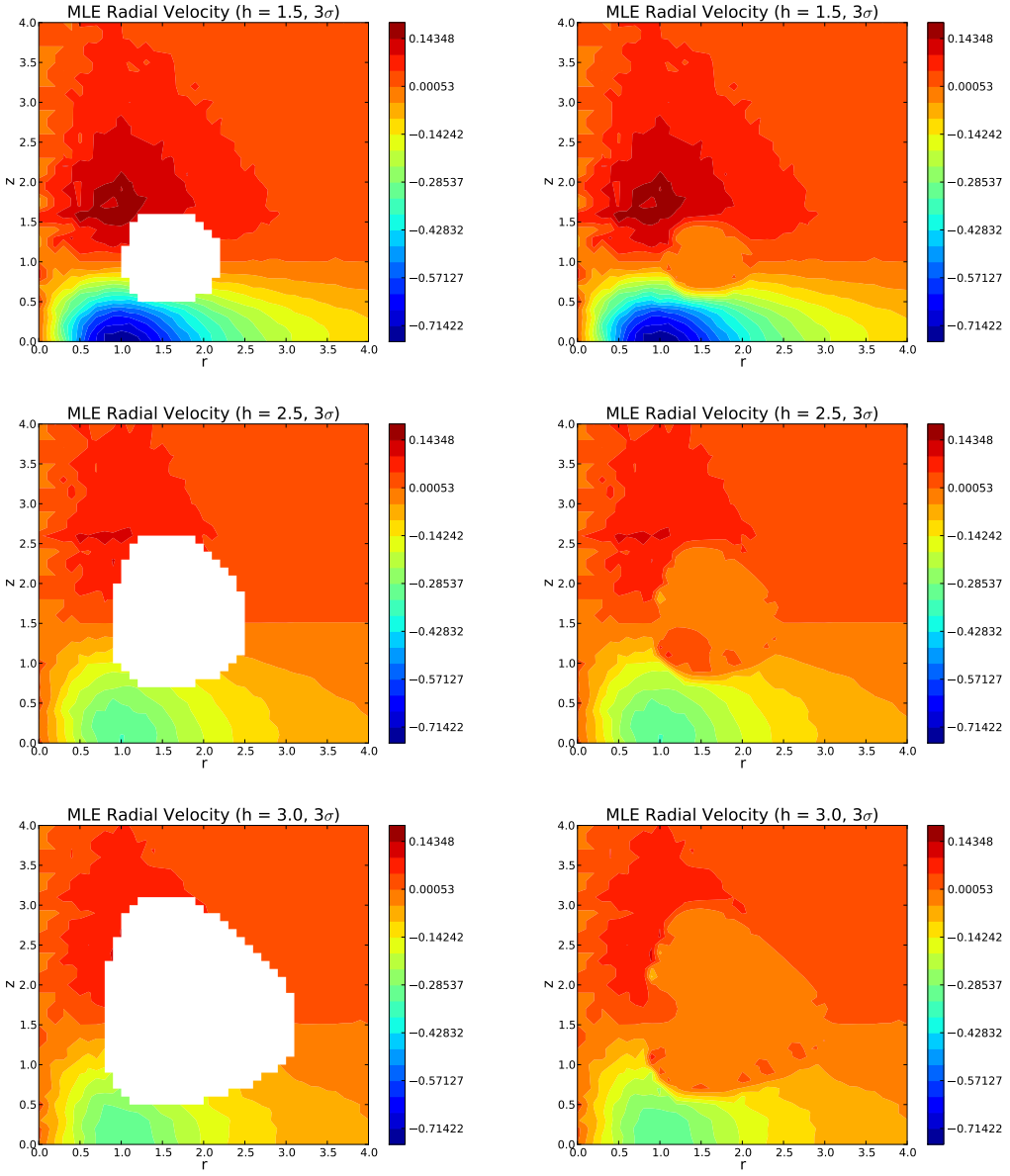


Figure 8.30: MLE characteristic radial velocity solutions (left) and elliptic BVP solutions (right) for error 1σ for $h = 1.5$ (top), $h = 2.5$ (middle) and $h = 3$ (bottom).

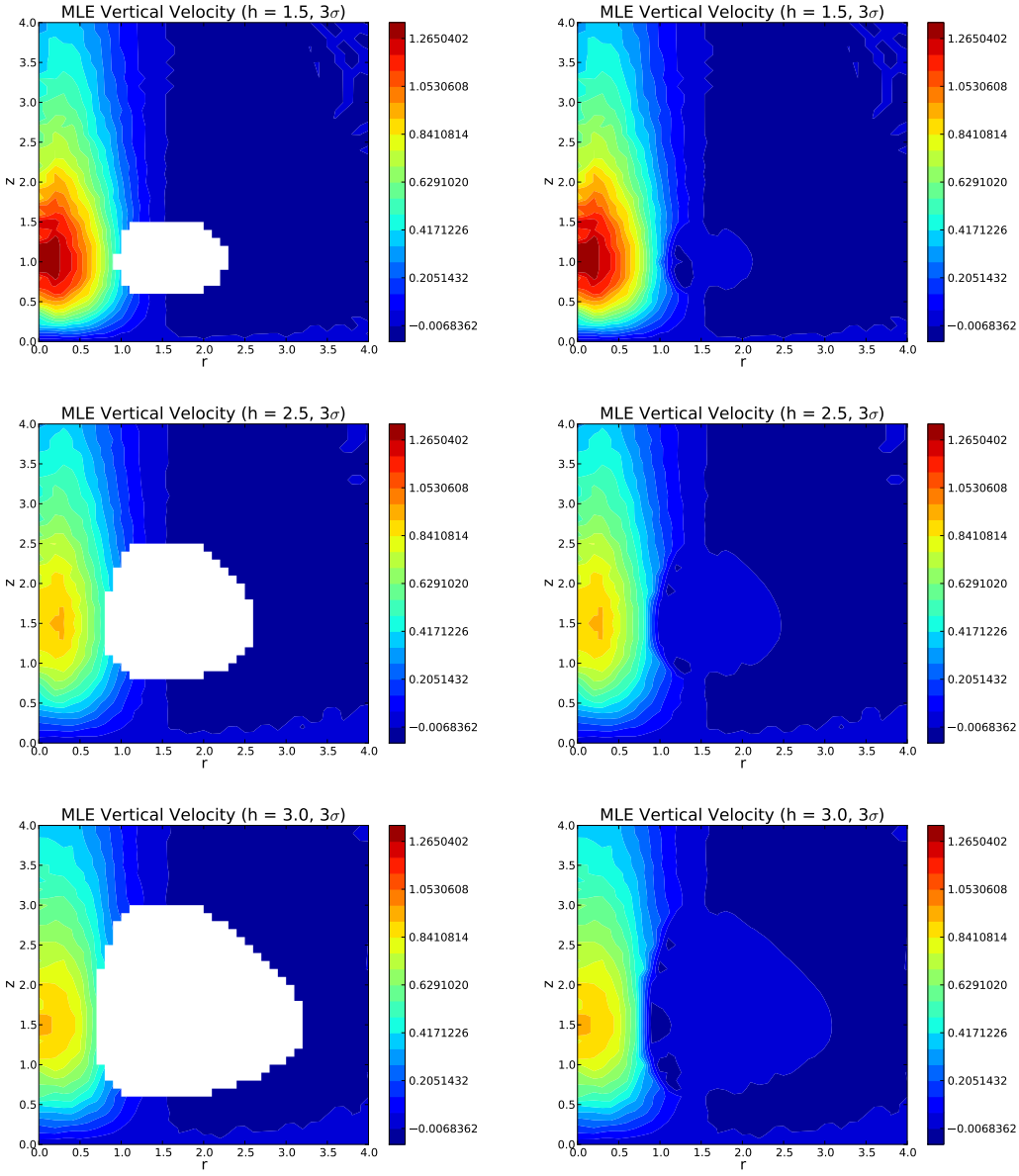


Figure 8.31: MLE characteristic vertical velocity solutions (left) and elliptic BVP solutions (right) for error 1σ for $h = 1.5$ (top), $h = 2.5$ (middle) and $h = 3$ (bottom).

Chapter 9

Summary and Discussion

At the outset of this work, we asked whether it was possible to utilize measurements of wind velocities from a few hundred meters above the surface to estimate the character of the wind velocities near the surface in a tornadic flow. Several approaches presented themselves. We chose a simple set of dynamics, coupled with an empirical parametric model for the tangential velocity, in order to (1) allow for a complete mathematical analysis of theoretical issues like existence and uniqueness and to (2) facilitate a careful analysis of the propagation of uncertainty in the form of measurement error through the retrieval process.

The first insight we drew on was the modeling of the tangential wind component using empirical models. These functions represent our best guess about the behavior of the tangential velocity near the surface, where the interaction with the surface causes v to weaken, thus allowing air to penetrate into the core of the vortex. In the same chapter, we discussed how uncertainty in the model and the data could be represented as probability density functions, and how these densities could be combined to get a posterior density, from which we could draw samples and attempt to understand the impact of errors on the retrieved radial and vertical velocities.

We addressed the theoretical questions of finding strong solutions u and w to our model equations in Chapter 5. We found that there is always a nontrivial region near the surface that can be directly estimated from data aloft. We also discovered that the combination of our observations and model constraints were not always enough to obtain a unique solution over the entire unobservable domain, flowing directly from the mathematical formulation of our problem as a first order hyperbolic equation. For a particular class of tangential velocity models, namely the tensor product of two functions satisfying certain conditions, we classified sets we called *information voids* where the strong solutions fail to be uniquely defined, and showed that for more general tangential velocity models, this classification no longer holds, since there are counterexamples.

In Chapter 6, we explored three methodologies for specifying a unique solution on information voids, and showed how do so with minimal departure from the strong solutions by choosing a diffusivity constant ϵ which is no larger than necessary to satisfy the requirements of the Lax-Milgram theorem.

For a deeper look at investigating the effects of uncertainty, Chapter 7 initially reviewed a few theorems that gave assurance that the solution map $v \mapsto u, w$ is continuous for our set of equations, and so small errors or perturbations in v should not concern us too much. A few simple results show how we can specify values of the velocities along the boundary of Ω_h which ensure maximum agreement of the characteristic solutions with observations in $\Omega \backslash \Omega_h$. Finally, we explicitly discuss how sampling the parameter space $\mathcal{Q}$ and computing the forward solutions corresponding to each parameter vector leads to a probability distribution for the velocity components. Using this distribution, we can calculate moments and other statistics, and perform hypothesis tests,

which are far more useful than a single "optimal" answer.

We implemented these ideas in Chapter 8 using a set of pseudo-observations generated in part from an idealized thunderstorm/tornadogenesis model written by Robert Davies-Jones, a research meteorologist with a distinguished career studying, among other things, tornado dynamics. The numerical tests indicated that for our idealized problem, the methodology performs well when the model parameters are estimated accurately, indicating the need for ensembles to average out parameter estimate errors. Since the collections of strong solutions were not all defined on the entire physical domain, random variables defined on the velocities were calculated, and the propagation of uncertainty from the observations to these variables was also investigated numerically.

To recap, the initial question we asked was answered in the affirmative, and along the way we developed mathematical theory to address the difficulties we encountered. There are a few open questions to answer. The first is how to best estimate the streamfunction from observations of u and v alone. In our tests we used measurements of w to initialize Ψ, and using a real dual Doppler data set, we would not have access to the vertical velocity. The second is how to choose an appropriate tangential model for a collection of radar data. This question is best addressed in the realm of model selection, using one or more of the various information criteria. Finally, a real data set is going to have nontrivial, possibly correlated random error in it, and before we are able to apply this methodology, we will need to find an appropriate method to preprocess observations so as to end up with useful results. These are all appropriate topics for future work.

Bibliography

M. Bebendorf. A Note on the Poincarè Inequality for Convex Domains. *Zeitschrift f ur Analysis ihre Anwendungen*, 22(4):751–756, 2003.

C. Church, J. Snow, and E. Agee. Tornado Vortex Simulation at Purdue University. *Bull. Am. Met. Soc.*, 58(9):900–908, September 1977.

C. Church, J. Snow, G. Baker, and E. Agee. Characteristics of Tornado-Like Vortices as a Function of Swirl Ratio: A Laboratory Investigation. *J Atmos Sci*, 36:1755–1776, September 1979.

R. Davies-Jones. Can a descending rain curtain in a supercell instigate tornadogenesis barotropically? *J. Atmos Sci*, 65:2469–2497, 2008.

J. Dieudonne. *Foundations of Modern Analysis*. Number 10 in Pure and Applied Mathematics. Academic Press, New York, 1960.

L. Evans. *Partial Differential Equations*, volume 19 of *Graduate Studies in Mathematics*. American Mathematical Society, 1998.

B. Fiedler. The thermodynamic speed limit and its violation in axisymmetric numerical simulations of tornado-like vortices. *Atmos-Ocean*, 32(2):335–359, 1994.

B. Fiedler and R. Rotunno. A theory for the maximum windspeeds in tornado-like vortices. *J. Atmos Sci*, 43(21):2328–2340, 1986.

P. Kundu and I. Cohen. *Fluid Mechanics*. Academic Press, 4 edition, 2008.

H. L. Kuo. Note on the similarity solutions of the vortex equations in an unstably stratified atmosphere. *J Atmos Sci*, 24:95–97, 1967.

S. Lakshmivarahan, J. Lewis, and S. K. Dhall. *Dynamic Data Assimilation: A least squares approach*. Cambridge University Press, 2006.

D. C. Lewellen, W. S. Lewellen, and J. Xia. The influence of local swirl ratio on tornado intensification near the surface. *J Atmos Sci*, 57:527–544, 2000.

W.S. Lewellen. Tornado vortex theory. In C. Church, D. Burgess, C. Doswell, and R. Davies-Jones, editors, *The Tornado: Its Structure, Dynamics, Prediction, and Hazards.*, number 79 in Geophysical Monograph, pages 19–39. American Geophysical Union, 1993.

W.S. Lewellen and Y.P. Sheng. Modeling Tornado Dynamics. Contract Rpt. NUREG/CR-1585. ARAP Report 421, U.S. Nucl. Regul. Comm., 1980.

R. Long. Vortex motion in a viscous fluid. *J Meteo*, 15:108–112, 1958.

Nicholas Rott. On the viscous core of a line vortex. *Zeitschrift f ur Angewandte Mathematik und Physik*, 9(5-6):543–553, March 1958.

R. Rotunno. A Study in Tornado-Like Vortex Dynamics. *J Atmos Sci*, 36: 140–155, 1979.

J.T. Snow. A Review of Recent Advances in Tornado Vortex Dynamics. *Reviews of Geophysics and Space Physics*, 20(4):953–964, 1982.

RD Sullivan. A two-cell vortex solution of the navier-stokes equations. *J Aerosp Sci*, 26:767–768, 1959.

A. Tarantola. *Inverse Problem Theory and Methods for Model Parameter Estimation*. SIAM, 2005.

V. Wood and L. White. A new parametric model of vortex tangential wind-profile: Development, testing and verification. *J. Atmos Sci*, 68:990–1006, 2011.